Modeling and Control of VSC-HVDC Connected Offshore Wind Farms

Von der Fakultät für Ingenieurwissenschaften,
Abteilung Elektrotechnik und Informationstechnik
der Universität Duisburg-Essen

zur Erlangung des akademischen Grades

Doktors der Ingenieurwissenschaften (Dr.-Ing.)

vorgelegte Dissertation

von

Mohammad Suwan
aus
Amman, Jordanien

1. Gutachter: Univ.-Prof. Dr.-Ing. habil. Istvan Erlich
2. Gutachter: Univ.-Prof. Dr.-Ing. Dirk Westermann

Tag der Einreichung: 18.01.2017
Tag der mündlichen Prüfung: 27.06.2017

Abstract

In Europe, large offshore wind farms are installed in the North Sea area using modern multi-megawatt wind turbines. Voltage source converter - high voltage direct current (VSC-HVDC) technology has proved to be a promising solution for offshore wind power grid access. The importance of grid impact studies of wind power integration rises with the rapid increase in the installed wind power capacity.

This thesis explores the main technical challenges and features associated with integrating large offshore wind farms into the onshore grid via VSC-HVDC systems. For this purpose, dynamic models of wind turbines and VSC-HVDC are developed and control requirements are analyzed with the aid of a simulation software environment. Enhancements in the controller design are afterwards proposed for the VSC-HVDC converters to improve steady-state and dynamic behavior with a special focus on the offshore grid side converter.

The primary frequency control by the VSC-HVDC connected offshore wind farm is investigated, where enhancements for existing kinetic energy control strategies are proposed and verified by simulation results. Additionally, a novel overfrequency-limiting method is developed by utilizing the HVDC chopper.

Zusammenfassung

In Europa werden große Offshore-Windparks mit Windenergieanlagen der Megawatt-Klasse im Nordseeraum errichtet. Die Hochspannungsgleichstromübertragung auf Basis spannungsgeführter Umrichter (VSC-HGÜ) hat sich als vielversprechende Lösung für die Netzanbindung von Offshore-Windparks erwiesen. Mit dem rasanten Anstieg der installierten Windenergieanlagen steigt der Bedarf nach genauen Studien über deren Auswirkungen auf das elektrische Netz.

Diese Arbeit untersucht die wichtigsten technischen Herausforderungen und Merkmale, die bei der Netzintegration der Offshore-Windparks über VSC-HGÜ zu berücksichtigen sind. Zu diesem Zweck werden dynamische Modelle von Windenergieanlagen und VSC-HGÜs entwickelt und deren Regelungsanforderungen mit Hilfe einer Simulationssoftware analysiert. Für den Offshore-seitigen HGÜ-Umrichter werden Verbesserungen der Regelungskonzepte vorgestellt, um das stationäre und dynamische Verhalten zu optimieren. Außerdem wird die kurzfristige Frequenzstützung durch den über eine VSC-HGÜ-angeschlossenen Offshore-Windpark untersucht. Hierbei werden Erweiterungen von existierenden Strategien der Frequenzstützung aus den rotierenden Massen (kinetic energy control, KEC) vorgestellt und durch Simulationsergebnisse verifiziert. Zusätzlich wurde ein neuartiges Verfahren zur Begrenzung der Überfrequenz unter Verwendung des HGÜ-Bremswiderstandes entwickelt.

Acknowledgements

This thesis was written during my time as a research and technical assistance at the institute of Electrical Power Systems (EAN) of the University Duisburg-Essen between 2012 and 2016.
Foremost, I would like to express my sincere gratitude to my supervisor Prof. Dr. Istvan Erlich. I had the great fortune to be part of his small but highly productive research team. Not only his encouragement and enlightenment, but also his extreme professionalism and constructive critic had a significant impact on the quality of my contribution in this thesis.

Special thanks go to the second reviewer of my Thesis, Prof. Dr.-Ing. Dirk Westermann, for his engagement and thorough assessment. I would like as well to thank Dr. Christian Feltes and Dr. Lijun Cai for their support as supervisors of my research projects with RWE and Senvion. My acknowledgement goes to my colleagues in the EAN institute in Duisburg who directly or indirectly contributed to this work by their good suggestions and their kind help. In particular, my sincere thankfulness goes to Dr. Fekadu Shewarega for his advices and proofreading of my papers published during this time. I am also very thankful for the fruitful discussions on a daily basis with my dear colleague Tobias Neumann which inspired me and encouraged me through hard times.

Finally I would like to thank my wife Maya for her unconditional support and for her patience during the last phases of writing and reviewing this thesis.

Erlangen, September 2017 Mohammad Suwan

Contents

Figures

Nomenclature

Notation

$u(t)$	Time dependent quantity
$\underline{u}^{\angle}$	Space vector
$\underline{u}$	Complex quantity
$\underline{u}_1^{\angle}$	Positive sequence
$\underline{u}_2^{\angle}$	Negative sequence
$\underline{u}^{\angle\omega_S}$	Space vector aligned to the rotating reference frame of positive sequence stator frequency
$\underline{u}^{\angle-\omega_S}$	Space vector aligned to the rotating reference frame of negative sequence stator frequency
$\underline{u}^{\angle u_{G1}}$	Space vector aligned to the rotating reference frame of positive sequence grid voltage
$\underline{u}^{\angle u_{G2}}$	Space vector aligned to the rotating reference frame of negative sequence grid voltage

Symbols

E	Energy in [J=W.s]
P	Active power in [W]
Q	Reactive power in [var]
$\underline{s}$	Complex power in [p.u.]
f	Frequency in [Hz]
ω	Angular frequency in [rad/s]
t	Time in [s]
β	Pitch angle in [°]
u	Instantaneous voltage in [p.u.]
i	Instantaneous current in [p.u.]
H	Inertia time constant in [p.u.]
ψ	Instantaneous flux in [p.u.]
T	Time constant in [s]
l	Inductance in [p.u.]
x	Reactance in [p.u.]

z	Impedance in [p.u.]
s_G	Generator slip
t	Torque in [p.u.]
τ	Time constant [s]
φ	Phase angle in [rad]

Abbreviations

AC	Alternating current
DC	Direct current
WT	Wind turbine
WF	Wind farm
HVDC	High voltage direct current
LLC	Line commutated converter
VSC	Voltage source converter
MMC	Multi-level modular converter
HV	High voltage
MV	Medium voltage
LV	Low voltage
PCC	Point of common coupling
DFIG	Doubly fed induction generator
FSCG	Full scale converter generator
PMSG	Permanent magnet synchronous generator
FOM	Full order model
EMT	Electromagnetic transient
RMS	Root mean square
FRT	Fault ride though
LSC	Line side converter
MSC	Machine side converter

SEC	Sending end converter
REC	Receiving end converter
PWM	Pulse width modulation
PT1	First order delay
IGBT	Insulated gate bipolar transistor
OFLC	Overfrequency limiting by DC chopper
FSPC	Frequency support by pitch control
RoCoF	Rate of change of frequency
KEC	Kinetic energy control

1 Introduction

In recent years the renewable energy sector has enjoyed a rapid growth of capacity worldwide. Being by far one of the most promising and technically advanced renewable power sources, wind energy generation related projects and research studies have scaled up significantly. A worldwide trend has been set in the last years to adopt long term alternatives for the shortage of fossil based energy resources. Besides this, depending mainly on nuclear power plants is not an appealing solution when considering its ecological impacts and safety risks. In Germany a major energy transition, known in German as the Energiewende, from fossil based energy sources to renewable energy sources is taking place. Such a significant energy transition is facing different kind of challenges; along with numerous technical issues that should be handled, the political will and public acceptance will play a decisive role in realizing the planned energy transition successfully. Public acceptance is a corner stone when considering the potential increase in electricity bill prices, increased number of installed photovoltaic (PV) solar and wind power plants on land, as well as the required extensions and enforcements of the existing electrical grid.

Offshore wind power technology offers concentrated high wind power generation in high wind speed regions away from residential areas and land restrictions. In Europe, large offshore wind farms (WFs) are installed in the North Sea area using modern multi-megawatt (multi-MW) wind turbines (WTs). The doubly-fed induction generator (DFIG) based WT is currently the most installed technology worldwide in multi-MW WFs. Nowadays, however, full scale converter generator (FSCG) based WT technology is becoming the favorable choice for multi-MW WF projects.

With the increasing share of grid integrated wind power generation plants, the impact on the existing grid must be studied carefully. This is due to the fact that the characteristics of the conventional generation plants differ from both DFIG and FSCG based WFs. In a conventional plant, the direct grid connection of the synchronous generator will couple the generator speed to the grid frequency. Modern multi-MW WTs, on the other hand, are equipped with frequency converters which allow fast decoupled control of active and reactive power. The frequency converter achieves a decoupling from the grid frequency and allows variable speed operation to optimize the output power for varying wind speeds under consideration of the rotor blade characteristics. Thus unlike the synchronous generators in conventional plants, the WTs do not possess an inertia response, leading to lower total grid inertia as the wind power share increases. Besides this, the future grid will have more and

more power converter interfaces; this fact creates the need for detailed analysis of the possible impact on the small signal stability, harmonics, and voltage and frequency stability.

Transferring a high amount of power for long distances requires a robust transmission system which can ensure stable operation with minimal possible losses. Voltage source converter – high voltage direct current (VSC-HVDC) technology has proved to be a promising solution for the connection of large offshore WFs as an alternative to an AC connection. The capability to cover long transmission distances, for example of 100 km and more is one of the decisive advantages of VSC-HVDC over high voltage AC (HVAC) transmission technology. The VSC-HVDC technology features modern insulated gate bipolar transistor (IGBT) valves and offers a decoupled control of active and reactive power with bidirectional power flow, black start capability and the ability of interconnecting passive grids by establishing the required voltage magnitude and frequency. Furthermore, for the case of offshore WFs connection via HVDC and a careful control design is required to avoid undesired control interactions between the converters of the HVDC and the connected WFs, due to the converter line connection at both ends. Such interactions may lead to increased harmonic levels or grid instability and possible total outage in the offshore grid.

A central aspect in the grid integration of large WFs is the recently introduced grid code requirements. The technical requirements include steady-state and dynamic or fault ride through (FRT) requirements. Additional requirements regarding frequency-dependent active power reduction control are introduced to support the grid frequency stability. Despite these new technical regulations, the following open questions have to be answered before moving towards an electrical grid with 100% renewable energy sources: Do renewable energy sources and namely wind and PV solar power have the ability to replace large conventional plants while keeping a secure and stable operation of the electrical grid? How can the frequency stability in weak inertia grids be guaranteed? Can near future developments in energy storage technologies provide practical solutions for unpredictable wind and solar power generation? Can the VSC-HVDC transmission system for connecting offshore WFs contribute to the grid stability and how?

1.1 Objectives of the thesis

The newly introduced configuration to integrate large offshore WFs via VSC-HVDC connections unleashed several technical challenges to fulfill the current grid code requirements and guarantee undisturbed and secure transmission of a high amount of power. The new features that this configuration offers will be explored in detail in this thesis. The

objectives of this thesis are:

- Design, development and analysis of the VSC-HVDC transmission system for connecting mainly DFIG based WTs.
- Testing and evaluation of the existing methods and development of enhanced control strategies for the offshore-side converter of the VSC-HVDC.
- Investigating symmetrical and unsymmetrical AC offshore grid faults for the proposed control strategies and assess the possibility of FRT scenarios. The overall protection philosophy in the AC offshore grid will be discussed, considering mainly offshore WF configurations with DFIG based WTs. The influence of the HVDC control strategies on the short-circuit current contribution in the offshore grid will be studied as well.
- Comparison, analysis and enhancement of the existing inertia emulation control strategies by the offshore WFs for primary frequency control during under-frequency events
- Analysis of over-frequency scenarios in a grid with different wind share levels, while investigating the application of kinetic energy control (KEC) methods to limit the transient frequency overshoot during overfrequency events.
- Development of new overfrequency limiting control strategy for VSC-HVDC connected offshore WFs. The new method offers an enhanced performance regarding the overfrequency limitation in comparison with the existing methods.

1.2 Outline of the thesis

A general introduction to modern state-of-the-art WT systems is given in ***Chapter 2*** where the classification of the four main WT types is introduced. The modeling concept of the DFIG system with its main electrical and mechanical components and the related equivalent circuits and control systems are introduced briefly in this chapter. A simplified model of FSCG based WTs is afterwards presented for the grid integration studies conducted in this thesis.

In the first section of ***Chapter 3*** the VSC-HVDC technology with its different configurations and network topologies is presented. The focus in this chapter is on offshore WFs integration via VSC-HVDC where the special characteristics of the offshore grid in such applications are discussed. Afterwards, the mathematical model of the equivalent circuit of the VSC is derived. The control concepts for the onshore receiving-end converter (REC) and the offshore sending-end converter (SEC) of the VSC-HVDC system are presented in the last part of this chapter. This includes introducing new control strategies for the offshore HVDC-SEC to enhance the overall system performance during transients.

Chapter 4 focuses on FRT operation for VSC-HVDC connected offshore WFs consisting of

DFIG based WTs. The chapter starts with a brief overview of the offshore grid connection requirements in Germany with a focus on FRT requirements. Different dynamic simulation studies are performed in this chapter to evaluate the performance of the VSC-HVDC control concepts developed in chapter 3. For this purpose, a test network is developed in an EMT-type simulation which includes an aggregated representation of two offshore WFs connected via VSC-HVDC system. Symmetrical and unsymmetrical onshore and offshore grid faults are carried out to analyze the short-circuit contribution of both the DFIG based WFs and the VSC-SEC. Special emphasis is given to the offshore grid faults and possible FRT scenarios with different HVDC-SEC current limitation concepts.

Chapter 5 deals with the contribution of the VSC-HVDC connected offshore WFs to the primary frequency control. After introducing the basic response characteristics of the grid frequency and the corresponding control concepts, a two-area, weakly coupled AC test network is introduced to perform primary frequency studies. The influence of the wind share in the provided test network is analyzed throughout several simulation tests. Existing methods to enable WTs to participate in the primary frequency control are analyzed by applying different operation scenarios in order to identify advantages and drawbacks of the existing methods. Several controller improvements are proposed to enhance the performance of the primary frequency response during underfrequency events.

Chapter 6 discusses potential overfrequency events, which is an issue that has been recently given more attention with the high penetration of offshore wind power production in the northern part of Germany. A scenario where a sudden loss of a main transmission line between the northern part with concentrated wind power production and the center loads in the southern part of Germany will cause an overfrequency in the isolated northern part of the grid due the energy surplus coming from the offshore WFs. This situation requires a fast power reduction by the WTs to limit the frequency overshoot in the transient period of the primary frequency response. This chapter discusses the existing strategies that can be utilized to limit the overfrequency by the WTs. A new method to utilize the DC braking choppers in VSC-HVDC and the WTs is proposed. The introduced method targets fast and robust energy dissipation for a defined period of time to limit the frequency overshoot. Several simulation studies are carried out to demonstrate and validate the proposed solution.

A summary of the main results and conclusions from this work is given in ***Chapter 7***, where an overview of related future research topics is provided.

1.3 Simulation software tools

The time-domain simulations in this thesis have been carried out using the software package DIgSILENT PowerFactory. DIgSILENT offer a graphical user interface to build electrical power systems using built-in defined components as electrical machines, transformers, converters and cables. Beside static load flow and short-circuit analysis, user-defined dynamic controllers can be implemented to simulate the dynamic behavior of generation, transmission and load systems during transients. Both root means square (RMS) and electromagnetic transients (EMT) simulation types have been carried out for this thesis using this software tool.

2 Modeling of modern multi-MW wind turbines

Since 2010 several large offshore WFs were taken successfully into operation in the North Sea of Germany. In 2015, the SylWin1 offshore WF became the largest offshore WF in operation with an 864 MW capacity [1]. The recent trend in the rapid development in number and size of the offshore WFs increased significantly the importance of studying the impact of increasing share of wind power generation in the electrical grid.

2.1 Classification of modern WT systems

Modern WTs are divided into four main types [2] as illustrated in Figure 2-1:

- Type 1: Fixed speed induction generator (FSIG) based WTs.
- Type 2: Slip ring induction generator (SRIG) with variable rotor resistance based WTs.
- Type 3: Doubly-fed induction generator (DFIG) based WTs.
- Type 4: Full-scale converter generator (FSCG) based WTs.

The overall efficiency of type 1 is lower than the others due to its inability to optimally utilize the wind power by varying the rotor speed. Moreover, FSIG based WTs are reactive power consumer and thus cannot be installed without static synchronous compensator (STATCOM) according to many grid codes including Germany, which makes it as a result an expensive and unattractive solution [4]. Type 2 has a slightly higher efficiency in comparison to type 1, due to the variability of its generator rotor speed up to 10%; nevertheless, it has the same drawback of being a reactive power consumer and requires compensation devices. Type 3 and Type 4 offers both a wider range of rotor speed variability featuring fully controllable 4-quadrant frequency converter and offering decoupled active and reactive power control capability. In most countries type 1 and type 2 concepts have been replaced by type 3 and type 4 for modern grid-connected WTs. The main focus in this thesis will be on type 3 DFIG based WT system.

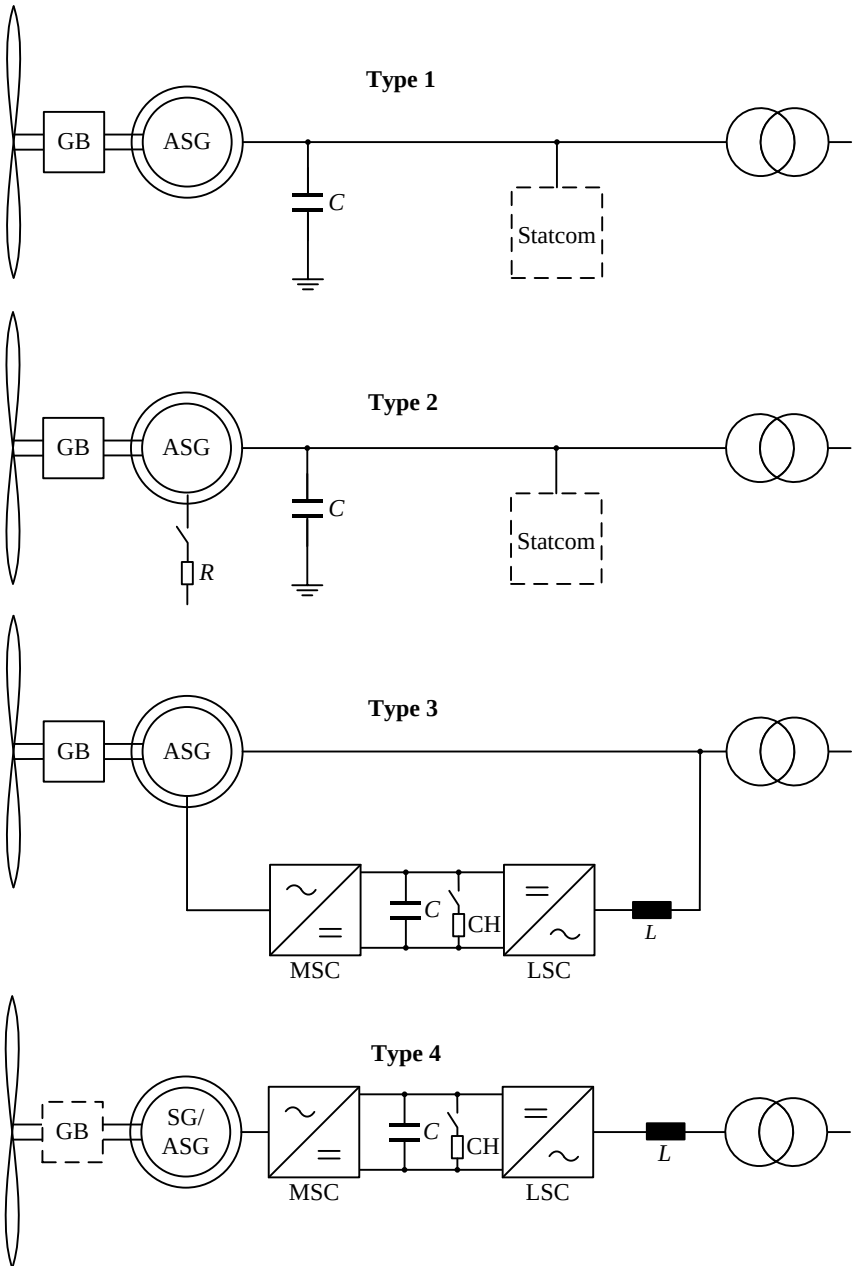

Figure 2-1: Basic configuration of the four WT types

2.2 Doubly fed induction generator (DFIG) based WTs – Type 3

The doubly-fed term comes from the fact that the electrical power flow is divided between the stator and rotor circuits. Thanks to the rapid developments in IGBT technology and the practical know-how acquired from small scale WTs, multi-MW DFIG based WTs were successfully installed worldwide in the last couple of years.

The extracted wind power by the WT blades is mechanically transmitted through a gear box to the induction generator. The stator side is directly connected to the low or medium voltage level of the AC grid, while the rotor side is connected typically to the low voltage level through a back-to-back IGBT-based frequency converter system. The converter is designed

for 30-40% rated system power where a DC link with a constant voltage separates the machine-side converter (MSC) from the line side converter (LSC) as shown in Figure 2-2.

The MSC controls the active and reactive power flow of the generator, while the LSC maintains the DC voltage level to allow a stable flow of the rotor power and can additionally be utilized for reactive power or AC voltage control according to the grid requirements at the connection point. Despite the direct connection of the stator circuit to the grid terminal through a transformer in DFIG systems, the grid frequency is nearly decoupled from the induction generator mechanical frequency through the frequency converter in the rotor circuit.

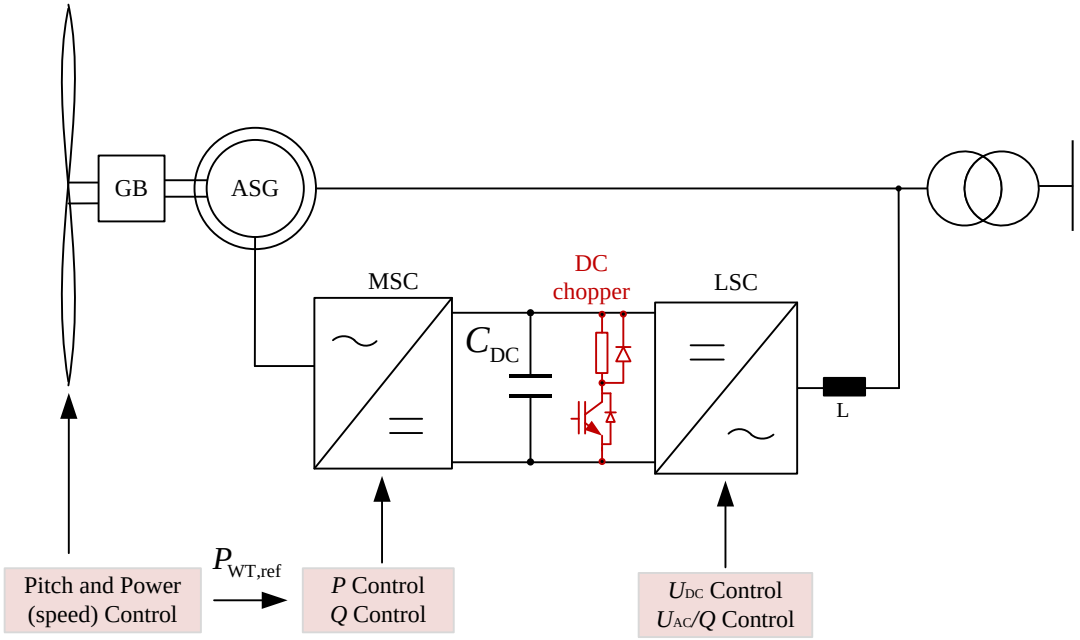

Figure 2-2: Basic Design of DFIG based WT – Type 3

The DC chopper (CH) limits the DC link voltage following grid faults as it must not exceed a certain limit with respect to the IGBT modules ratings. In consequence the converter will not be forced to stop operating due to over-voltages and will continue to inject active and reactive current to the grid without interruption. The DC chopper is realized as IGBT module switch connected in series to a resistor. The resistor is responsible for dissipating the surplus energy supplied into the DC link. The chopper is switching on and off by a simple hysteresis characteristic depending on the DC voltage level.

2.2.1 Generator model

The full-order model (FOM) of the DFIG is mathematically presented in space vector form by the system of equations (2.1)-(2.8). The per-unit (p.u.) system is adopted as a unit of measurement for all quantities and the generator sign convention is used.

Voltage equations:

$$\underline{u}_{\mathrm{S}}^{\angle} = -r_{\mathrm{S}}\underline{i}_{\mathrm{S}}^{\angle} - \frac{\mathrm{d}\underline{\psi}_{\mathrm{S}}^{\angle}}{\mathrm{d}t} - \mathrm{j}\omega_{\angle}\underline{\psi}_{\mathrm{S}}^{\angle} \tag{2.1}$$

$$\underline{u}_{\mathrm{R}}^{\angle} = -r_{\mathrm{R}}\underline{i}_{\mathrm{R}}^{\angle} - \frac{\mathrm{d}\underline{\psi}_{\mathrm{R}}^{\angle}}{\mathrm{d}t} - \mathrm{j}\left(\omega_{\angle} - \omega_{\mathrm{R}}\right)\underline{\psi}_{\mathrm{R}}^{\angle} \tag{2.2}$$

Flux linkages:

$$\underline{\psi}_{\mathrm{S}}^{\angle} = l_{\mathrm{S}}\underline{i}_{\mathrm{S}}^{\angle} + l_{\mathrm{M}}\underline{i}_{\mathrm{R}}^{\angle} \tag{2.3}$$

$$\underline{\psi}_{\mathrm{R}}^{\angle} = l_{\mathrm{M}}\,\underline{i}_{\mathrm{S}}^{\angle} + l_{\mathrm{R}}\,\underline{i}_{\mathrm{R}}^{\angle} \tag{2.4}$$

Where $l_{\mathrm{S}} = l_{\mathrm{M}} + l_{\sigma\mathrm{S}}$ and $l_{\mathrm{R}} = l_{\mathrm{M}} + l_{\sigma\mathrm{R}}$

Equation of motion:

$$\frac{\mathrm{d}\omega_{\mathrm{R}}}{\mathrm{d}t} = \frac{1}{2H_{\mathrm{G}}}\left(\mathrm{Im}\left\{\underline{\psi}_{\mathrm{R}}^{\angle}\underline{i}_{\mathrm{S}}^{*\angle}\right\} + t_{\mathrm{W}}\right) \tag{2.5}$$

The quasi-stationary model is obtained by neglecting the stator flux derivative term in the stator voltage [3]. The DFIG positive sequence model can be derived now in the synchronous reference frame ω_{S}. From equation (2.1) the stator flux linkage can be expressed in the positive sequence synchronous reference frame (denoted by $\angle\omega_{\mathrm{S}}$) as:

$$\underline{\psi}_{\mathrm{S}}^{\angle\omega_{\mathrm{s}}} = \frac{-\underline{u}_{\mathrm{S1}}^{\angle\omega_{\mathrm{s}}} - r_{\mathrm{S}}\underline{i}_{\mathrm{S1}}^{\angle\omega_{\mathrm{s}}}}{\mathrm{j}\omega_{\mathrm{S}}} \tag{2.6}$$

By combining equations (2.3) and (2.4) to eliminate the rotor current and substituting in equation (2.6), the following generator equations are obtained:

$$\underline{u}_{\mathrm{S}}^{\angle\omega_{\mathrm{s}}} = -r_{\mathrm{S}}\underline{i}_{\mathrm{S}}^{\angle\omega_{\mathrm{s}}} - \mathrm{j}\omega_{\mathrm{S}}\left(l_{\mathrm{S}}\underline{i}_{\mathrm{S}}^{\angle\omega_{\mathrm{s}}} + \frac{l_{\mathrm{M}}}{l_{\mathrm{R}}}\left(\underline{\psi}_{\mathrm{R}}^{\angle\omega_{\mathrm{s}}} - l_{\mathrm{M}}\underline{i}_{\mathrm{S}}^{\angle\omega_{\mathrm{s}}}\right)\right) = -\left(r_{\mathrm{S}} + \mathrm{j}\omega_{\mathrm{S}}l'\right)\underline{i}_{\mathrm{S}}^{\angle\omega_{\mathrm{s}}} - \mathrm{j}\omega_{\mathrm{S}}k_{\mathrm{R}}\underline{\psi}_{\mathrm{R}}^{\angle\omega_{\mathrm{s}}} \tag{2.7}$$

where $l' = \sigma l_{\mathrm{S}}$ is the transient inductance and $k_{\mathrm{R}} = \frac{l_{\mathrm{M}}}{l_{\mathrm{R}}}$ is the coupling factor. By substituting equation (2.4) in (2.2), the rotor flux can be expressed as:

$$\frac{\mathrm{d}\underline{\psi}_{\mathrm{R}}^{\angle\omega_{\mathrm{s}}}}{\mathrm{d}t} = \left(\frac{-r_{\mathrm{R}}}{l_{\mathrm{R}}} + \mathrm{j}\left(\omega_{\mathrm{S}} - \omega_{\mathrm{R}}\right)\right)\underline{\psi}_{\mathrm{R}}^{\angle\omega_{\mathrm{s}}} + k_{\mathrm{R}}r_{\mathrm{R}}l_{\mathrm{M}}\,\underline{i}_{\mathrm{S}}^{\angle\omega_{\mathrm{s}}} - \underline{v}_{\mathrm{R}}^{\angle\omega_{\mathrm{s}}} \tag{2.8}$$

Equation (2.7) represents the quasi-stationary circuit shown in Figure 2-3. The superscripts of the synchronous reference frame are removed for simplicity.

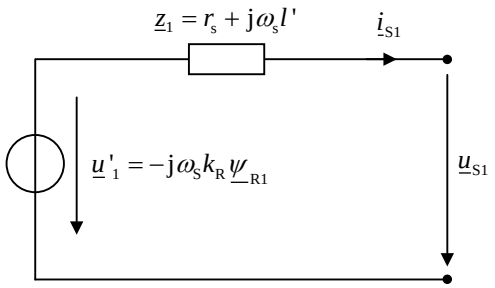

Figure 2-3: Quasi-stationary equivalent circuit of the Asynchronous machine

The steady-state DFIG model can be obtained by setting all derivatives in the system equations to zero ($\frac{dx}{dt} = 0$). The steady-state model cannot be used to model the induction machine for network studies, since no generator dynamics are considered in the model. However, the calculation of the steady-state model is necessary to calculate the initial conditions required of the correct initialization of the state variables of the system equations. Additionally, the design of MSC control is based on the steady state equations without considering the derivative terms. From equations (2.1) and (2.2) the positive sequence voltage equations are expressed in the steady-state as:

$$\underline{u}_{S1}^{\angle\omega_s} = -r_S \underline{i}_{S1}^{\angle\omega_s} - j\omega_S \underline{\psi}_{S1}^{\angle\omega_s} \tag{2.9}$$

$$\underline{u}_{R1}^{\angle\omega_s} = -r_R \underline{i}_{R1}^{\angle\omega_s} - j(\omega_S - \omega_R) \underline{\psi}_{R1}^{\angle\omega_s} \tag{2.10}$$

By substituting equations (2.3) and (2.4) in equations (2.9) and (2.10) respectively to eliminate the flux linkages, the following equations are be obtained:

$$\underline{u}_{S1}^{\angle\omega_s} = -r_S \underline{i}_{S1}^{\angle\omega_s} - jx_S \underline{i}_{S1}^{\angle\omega_s} - jx_M \underline{i}_{R1}^{\angle\omega_s} \tag{2.11}$$

$$\frac{\underline{u}_{R1}^{\angle\omega_s}}{s_{G1}} = -\frac{r_R}{s_{G1}} \underline{i}_{R1}^{\angle\omega_s} - jx_M \underline{i}_{S1}^{\angle\omega_s} - jx_R \underline{i}_{R1}^{\angle\omega_s} \tag{2.12}$$

With the positive sequence slip $s_{G1} = \frac{\omega_S - \omega_R}{\omega_S}$.

The steady-state negative sequence voltage equations of the DFIG can be expressed in the negative sequence rotating synchronous reference frame $\angle -\omega_S$ as:

$$\underline{u}_{S2}^{\angle-\omega_s} = -r_S \underline{i}_{S2}^{\angle-\omega_s} - j\omega_S \underline{\psi}_{S2}^{\angle-\omega_s} \tag{2.13}$$

$$\underline{u}_{R2}^{\angle-\omega_s} = -r_R \underline{i}_{R2}^{\angle-\omega_s} - j(\omega_S + \omega_R) \underline{\psi}_{R2}^{\angle-\omega_s} \tag{2.14}$$

Similar to the positive sequence, the flux dependencies in the negative sequence equations (2.13) and (2.14) can be eliminated resulting in the following expressions:

$$\underline{u}_{S2}^{\angle-\omega_s} = -r_S \underline{i}_{S2}^{\angle-\omega_s} - jx_S \underline{i}_{S2}^{\angle-\omega_s} - jx_M \underline{i}_{R2}^{\angle-\omega_s} \tag{2.15}$$

$$\frac{\underline{u}_{R2}^{\angle-\omega_s}}{2-s_{G1}} = -\frac{r_R}{2-s_{G1}}\underline{i}_{R2}^{\angle-\omega_s} - \mathrm{j}x_M\underline{i}_{S2}^{\angle-\omega_s} - \mathrm{j}x_R\underline{i}_{R2}^{\angle-\omega_s} \tag{2.16}$$

The resulting induction generator steady-state equivalent circuits in the positive and negative sequence are illustrated in Figure 2-4 and Figure 2-5 respectively. The superscripts of the reference systems $\angle\omega_S$ and $\angle-\omega_S$ are removed for simplicity.

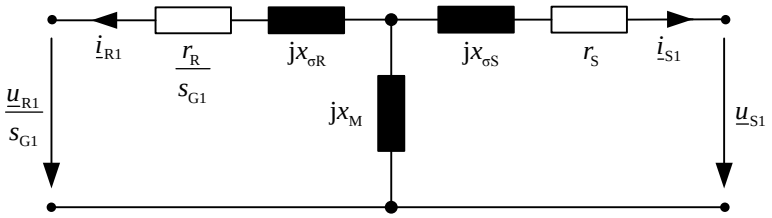

Figure 2-4: Steady-state equivalent circuit of the Asynchronous machine in the positive sequence

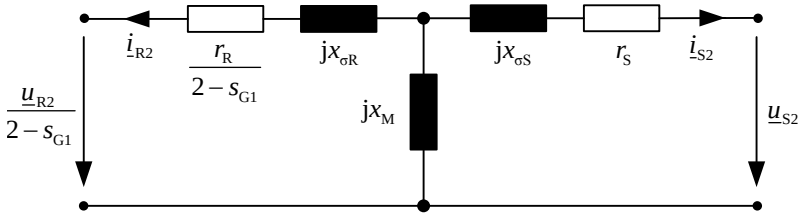

Figure 2-5: Steady-state equivalent circuit of the Asynchronous machine in the negative sequence

2.2.2 Converter-Generator control

The converter control design of the DFIG based WT was handled in details in [1], [4].and [5] Since the focus of this thesis is on the VSC-HVDC control and its interactions with the offshore WF, the WT converter control is described only briefly in this section.

2.2.2.1 Machine-side converter control

The MSC control is based on a vector control approach where the controller quantities are aligned to the stator voltage oriented reference frame (denoted by $\angle u_S$) as shown in Figure 2-6. The MSC control contains an outer and inner control loops. The outer active and reactive power control loop generates the reference rotor current components for the inner control current loop.

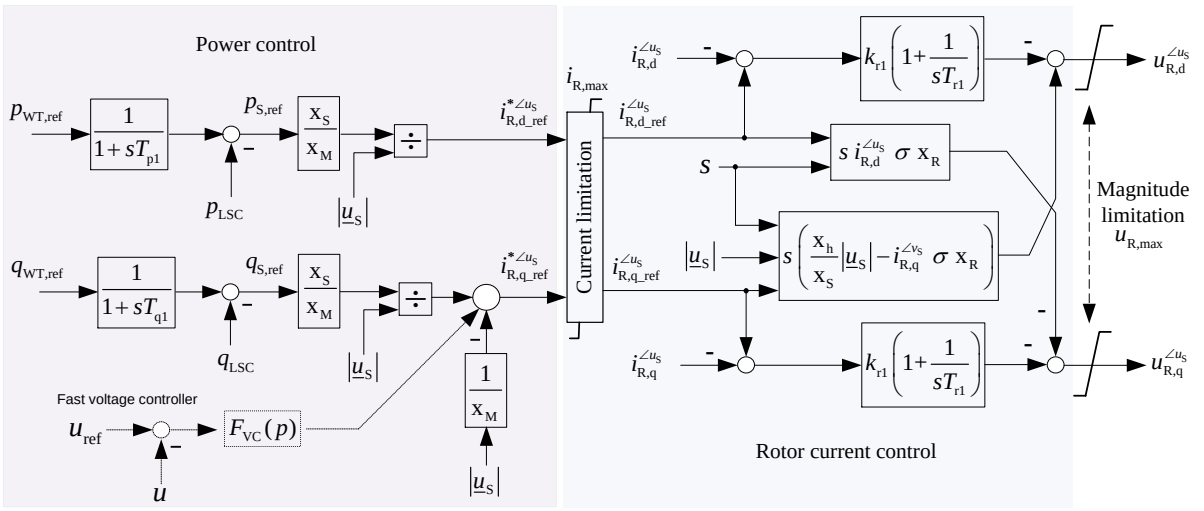

Figure 2-6: MSC control for the DFIG based WT

The controller outputs $u_{R,d}^{\angle u_S}$ and $u_{R,q}^{\angle u_S}$ should be transformed into the rotor reference frame. This will require the knowledge of the rotor (position) angle. The rotor angle can be obtained by measuring the rotor position using a position encoder sensor. Alternatively the rotor transformation angle and the slip transformation angle are obtained mathematically using the measured stator and rotor currents [5].

2.2.2.2 Line-side converter control

The LSC control is based as well on a voltage oriented vector control approach and consists similarly of an outer and inner control loops as illustrated in Figure 2-7. In the outer control loop, the main task of the LSC is to maintain the DC voltage level through adjusting the active current component. The LSC can be assigned to control the terminal voltage or the reactive power. The fast inner current control loop allows a fast dynamic response and ensures an effective current limitation.

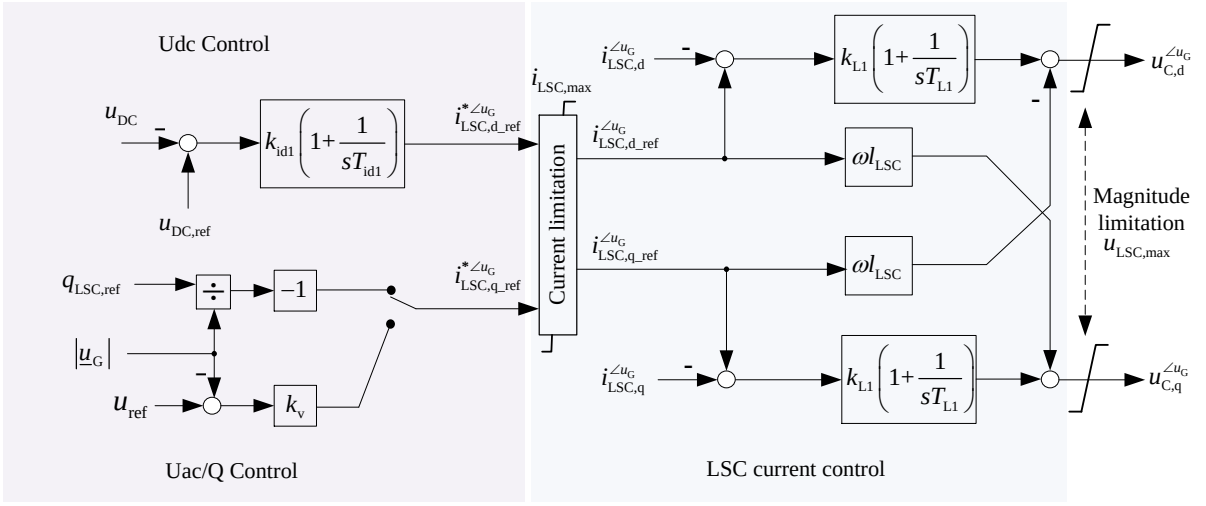

Figure 2-7: LSC control for the DFIG based WT

2.2.3 WT aerodynamic model

The mechanical power extracted from the wind can be calculated as:

$$P_{\mathrm{W}} = \frac{1}{2}\rho\, A_{\mathrm{rot}} c_{\mathrm{p}}(\lambda,\beta) v_{\mathrm{w}}^3 \tag{2.17}$$

Where ρ is the air density, A_{rot} is the cross-section through which the air mass is streaming, c_{p} is the power coefficient and v_{w} is the wind speed. The tip-speed ratio is defined as:

$$\lambda = \omega_{\mathrm{W}} R / v_{\mathrm{w}} \tag{2.18}$$

Where R is the radius of rotor blade and ω_{W} is the speed of the turbine. WT manufacturers specify the power coefficient for the rotor blades which is defined as:

$$c_{\mathrm{p}}(\lambda,\beta) = \frac{P_{\mathrm{W}}(\lambda,\beta)}{P_{\mathrm{wind}}} \tag{2.19}$$

Figure 2 -8 shows power coefficient curves of a multi-MW pitch controlled WT. The pitch actuators can limit the generated power at high wind speed conditions by increasing the pitch angle β.

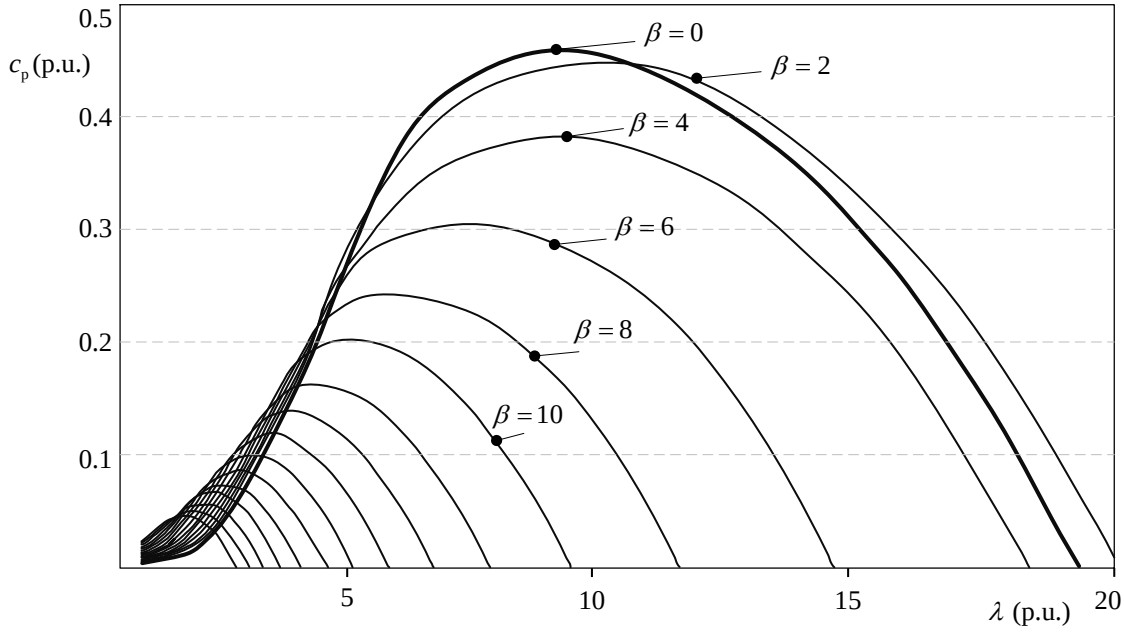

Figure 2 -8: Typical power coefficient curves for a DFIG based WT

The drive train of the WT differs from type to type mainly by the choice of a gearbox or a direct drive (gearless) system. The two-mass model with the dominant two masses of the wind rotor and the generator offers a better approximation in comparison to the one-mass model [4]. Figure 2 -9 shows the structure of the two-mass model.

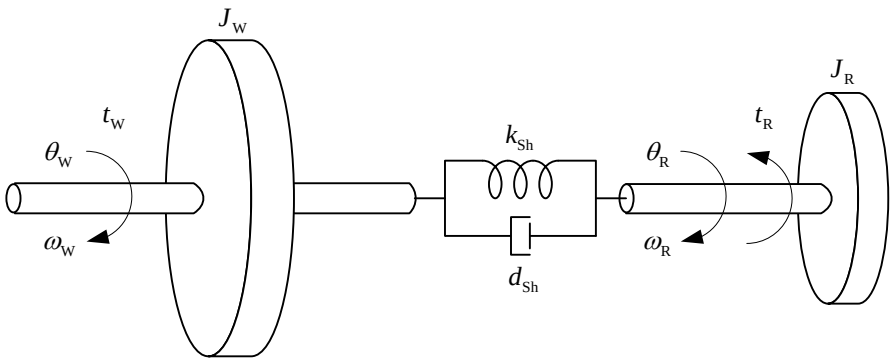

Figure 2 -9: Two-mass model of the WT drive train

The two-mass model can be described by the following equations:

$$J_W \frac{d\omega_W}{dt} = t_W - k_{Sh}\Delta\theta - d_{Sh}\Delta\omega \tag{2.20}$$

$$J_G \frac{d\omega_R}{dt} = -t_R + k_{Sh}\Delta\theta + d_{Sh}\Delta\omega \tag{2.21}$$

With the mechanical speed and angle difference:

$$\Delta\omega = \omega_W - \omega_R = \frac{d\Delta\theta}{dt} = \frac{d(\theta_W - \theta_R)}{dt} \tag{2.22}$$

All quantities are related to the high-speed side of the gearbox.

2.2.4 Pitch and speed control

The WT speed control targets maximizing the generated power of the WT across a defined range of wind speeds by adjusting the turbine rotational speed according to optimal tracking characteristics based on the manufacturer design of the rotor blades. The speed control generates the active power set-point that is passed to the MSC which controls the electrical power of the DFIG. The typical chosen nominal speed for the generator is around 1.2 p.u.. Figure 2 -10 shows a typical power curve of a WT.

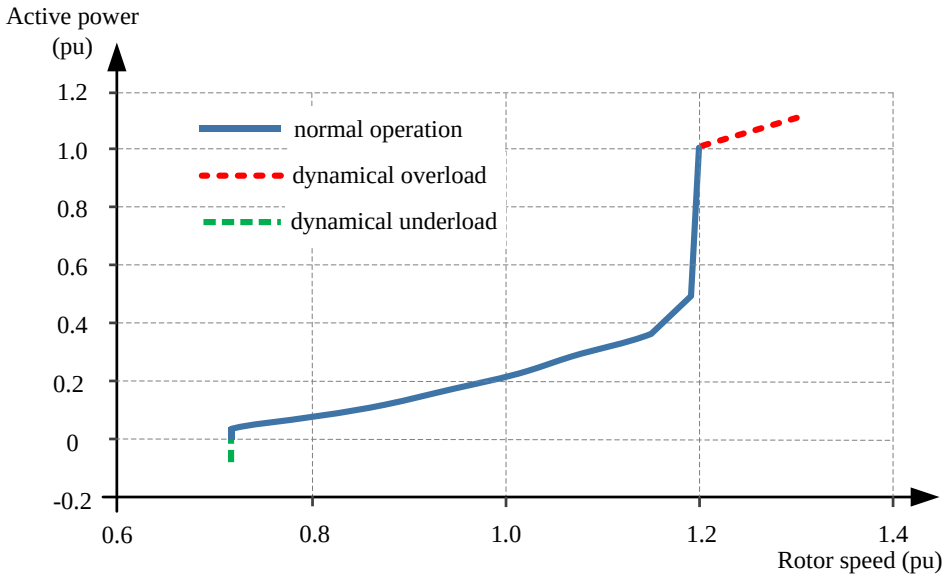

Figure 2 -10: Typical WT Power-speed characteristics

The speed control concept is shown in Figure 2 -11 with two layouts: torque controller or direct power controller. The direct power controller approach is preferred in real applications to avoid unnecessary deviations of the power setpoint caused by the rotor speed multiplication [7]. The direct power controller is used for all studies conducted in the next chapters of this thesis.

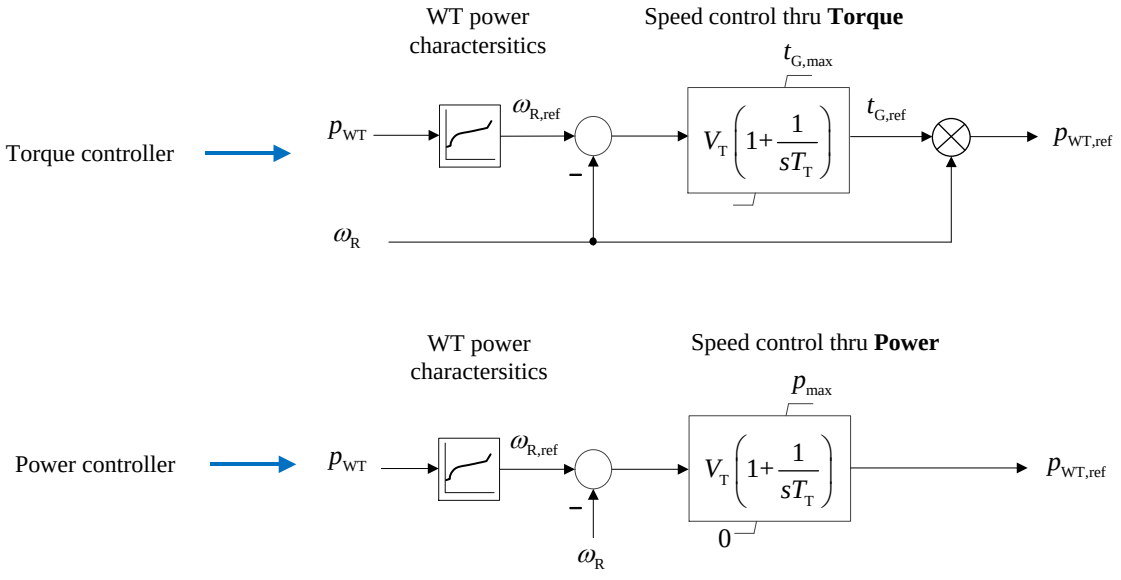

Figure 2 -11: Layouts for the WT Speed controller

The main task of pitch (rotor blade) control is to limit the WT mechanical power (torque) at high wind speeds to the nominal value and to keep the rotor speed inside the desired range. After exceeding the nominal rotor speed, a PI-controller is activated to maintain the rotor speed through adjusting the pitch angle as shown in Figure 2 -12. The pitch booster provides a fast reaction of the pitch actuators in case of dynamic speed changes during strong wind gusts

or during electrical grid transients. Additionally it increases the damping of the pitch controller. The pitch booster is not deactivated through certain limits during partial load operation. The pitch actuator can be modeled as a simple first order lag (PT1) element with a response time in the range of tens of milliseconds. The power conversion model is based on equation (2.17). The high frequency of wind speed fluctuations is usually very local and is smoothed over the large area of the rotor blades surface [8]. Therefore the measured wind speed is smoothed using a low-pass PT1 filter to emulate this effect.

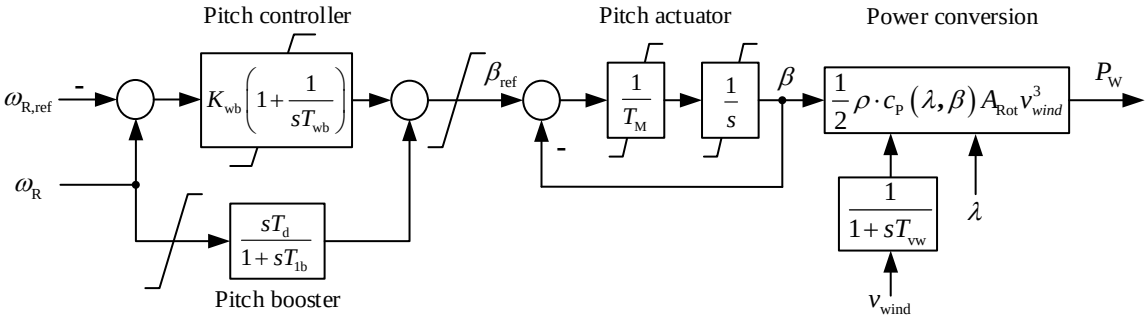

Figure 2 -12: Pitch control with power conversion model

2.3 Full-scale converter generator (FSCG) based WTs – Type 4

The basic layout and control concept for the FSCG based WT is shown in Figure 2-13. The generator can be either an induction machine or synchronous machine. Due to its technical advantages, the direct drive permanent magnet synchronous generator (PMSG) is commonly used for this WT type. The frequency converters in this type are fully-rated to the nominal generator power. The LSC control objective and structure are similar to the LSC of the DFIG, while the MSC controllers of both types have several differences.

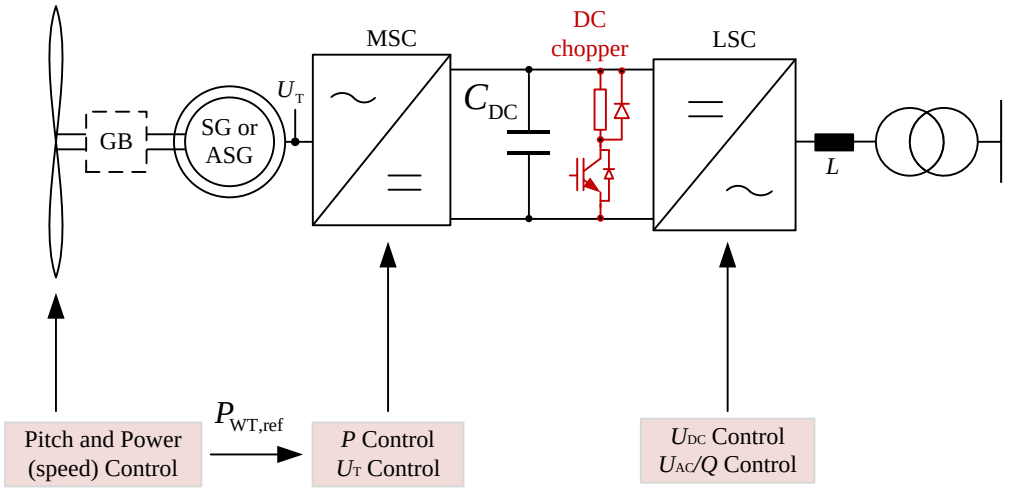

Figure 2-13: Basic layout of FSCG based WT – Type 4

From a grid connection point of view, the selection of the generator and the MSC does not influence the behavior towards the grid since the DC-link decouples the Generator and MSC

from the LSC. In general, the response to grid faults are determined by the LSC, thus detailed modeling of the generator and MSC is usually not necessary [6].

Based on the above, the generator and MSC models can be simplified by an active power reference with a simple first order delay equivalent to the time constants of the MSC current controllers (typically 0.5 to 5 ms). The DC-link model is considered in grid integration studies when the DC chopper performance is part of the study. Figure 2-14 shows the simplified layout of the FSCG-based WT. The LSC control structure is similar to the one shown in Figure 2-7.

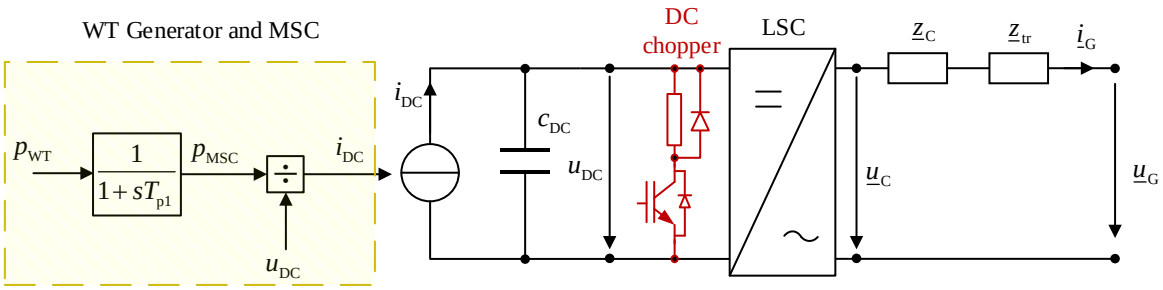

Figure 2-14: Simplified Model of FSCG based WT – Type 4 for grid integration studies

3 Modeling of VSC-HVDC with offshore WF connection

The HVAC cable transmission solution (50 Hz system) for large offshore grids is technically limited to short distances (up to 100 km). The reason behind this limitation is the high charging currents that will flow in long HVAC cables due to its large electrical capacitance; this charging current is proportional to the transmission voltage level and reaches at a certain distance the level of nominal currents. Thus parallel reactance compensation must be installed at both cable ends to compensate this effect to minimize the transmission losses. Since the offshore WFs can be geographically located hundreds kilometers from the onshore connection point, an AC cable solution would feature several AC cable sections with a number of offshore compensation points. This solution is obviously not economical and can be technically challenging. Skin effect phenomenon is an important issue that must be taken into consideration in the HVAC cable design; this effect is negligible in HVDC cables since it takes place only during fast current transients. Additionally dielectric losses and insulation material aging due to constant polarity change are phenomena that can occur only in HVAC cables [9]. The HVDC transmission solution offers therefore much lower transmission losses and is economically a favorable solution for offshore WF integration with long cable distances (above 100 km).

Two options for HVDC transmission solutions are currently available: the classical HVDC system featuring line-commutated converter (LCC) equipped with thyristor valves and the VSC-HVDC. The LCC-HVDC technology offers a high ‘bulk’ power transmission capability with relatively low losses. The main drawback of this technology is the minimum short-circuit level required for the interconnected AC networks which is mainly related to the reactive power consumption and harmonics generation of the LCC-HVDC system. This means weak or islanded systems as in the case of offshore WF cannot be interconnected via the LCC-HVDC technology without extra equipment [10].

VSC-HVDC technology offers currently lower power transmission capability in comparison to LCC-HVDC, but overcomes the main drawbacks of the latter technology. The self-commutated valves (mainly IGBTs) in the VSC allow bidirectional power flow and fast independent active and reactive power control. A decisive feature of VSC-HVDC is the black start capability and ability to interconnect weak and passive networks. These significant features make VSC-HVDC technology the suitable solution for grid integration of the offshore WFs. This chapter deals with modeling the VSC-HVDC system for offshore WF applications. A special emphasis is given to the control design of the offshore HVDC-SEC

considering the special characteristics and requirements of the offshore WF grid.

3.1 VSC-HVDC technology

VSC-HVDC technology has proved to be a promising solution for grid connection of large offshore WFs. VSCs for HVDC applications featured in the past two-level IGBT based converters. Cascaded two-level converters [11] or multi-level modular converter (MMC) [12] topologies are used in modern VSC-HVDC applications due to their technical advantages over the two-level concept.

Two basic configurations are typically used in modern VSC-HVDC projects: symmetrical monopole and bipolar system as shown in Figure 3-1. The symmetrical monopole features two high ± DC voltage cable conductors with one VSC at each end. The bipolar system features two converters at each end with earth return installed at each end [15].

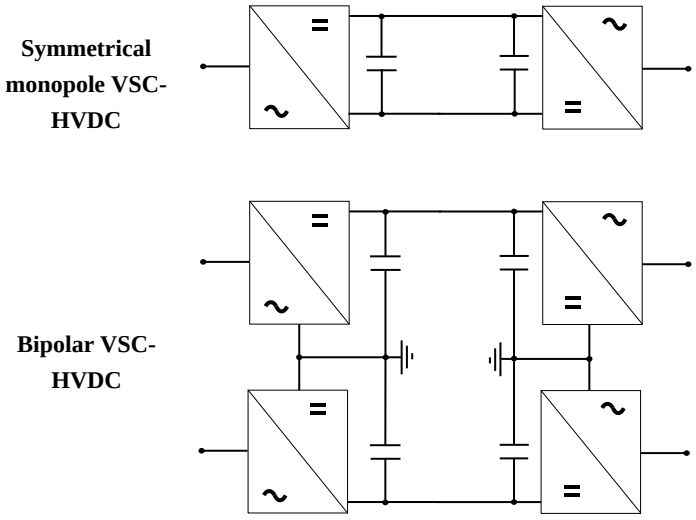

Figure 3-1: Typical basic configurations for VSC-HVDC

The main advantage of the bipolar system over the symmetrical monopole is the redundancy concept that allows the operation in a monopole mode upon the loss of one of the DC transmission line. However, due to the high costs, symmetrical monopole seems to be the preferred solution for connecting offshore WFs. Since the detailed DC circuit modeling is not the focus of this thesis, only simple symmetrical monopole arrangement is considered in the modeling the VSC-HVDC in this chapter.

Beside the symmetrical and monopole configurations, VSC-HVDC systems are typically classified according to the DC interconnection topology as illustrated in Figure 3-2.

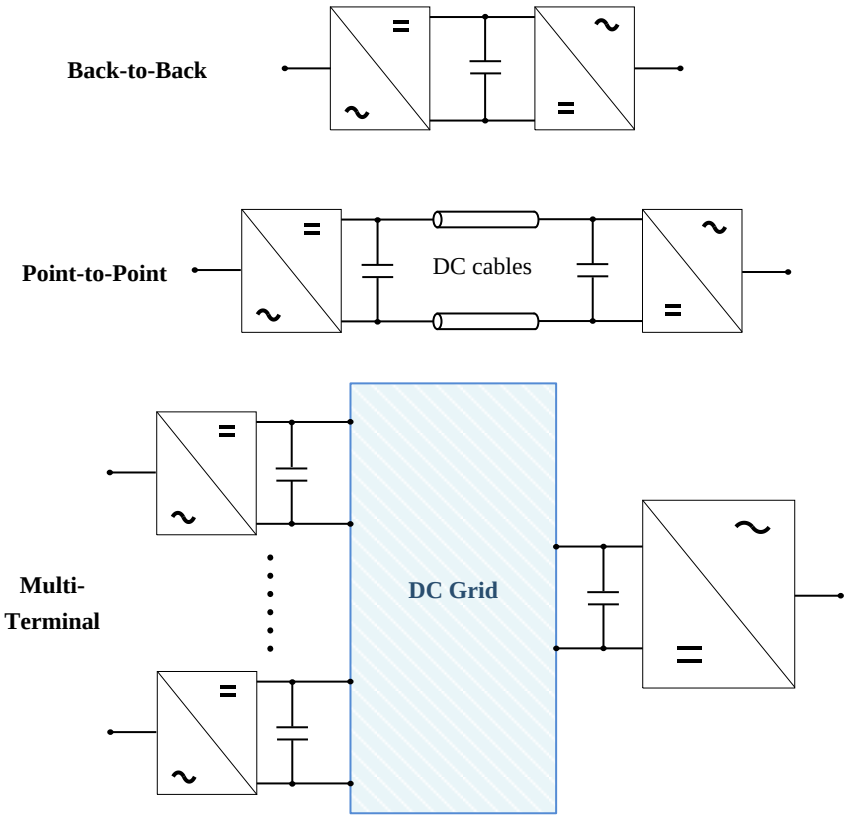

Figure 3-2: Different DC interconnection concepts for VSC-HVDC

In the back-to-back topology no HVDC cables exist in the DC-link and both converters are located in one station. VSC-HVDC back-to-back can be used to: a) interconnect two AC Networks with different frequencies as connecting a 50 Hz AC network to a 60 Hz AC network or b) interconnect two asynchronous independent (50 Hz or 60 Hz) AC networks to allow the exchange of active power flow between them. For offshore WFs application, the point-to-point VSC-HVDC topology includes two converter stations connected by DC sea cables. Multi-terminal HVDC grid concepts are introduced to reduce the number of the required converter stations and improve the power flow control and energy trading between the interconnection points, such concepts are still however in the research phase [19].

3.2 VSC-HVDC topologies

The first generation of the VSC-HVDC was based on two-level 6-IGBT valves topology as illustrated in Figure 3-3. Each IGBT valve is equipped with a freewheeling diode in an anti-parallel connection. Two modulation voltage levels can be achieved in this topology, which results in a high harmonic distortion that must be treated by an AC filter. Additionally the required high switching frequency generates considerable losses for the converter. Another important point is that this topology is not appropriate for MV or HV levels due to the limited voltage rating of the commercially available IGBT-valves. Three-level neutral-point clamped

(NPC) converters are the most common converter topology in MV applications. The NPC converter includes additional diodes to connect the taps between the IGBT in one bridge arm to the neutral point of the converter. This provides a third modulation level of the output voltage, which allows the reduction of the switching frequency of the AC filter size.

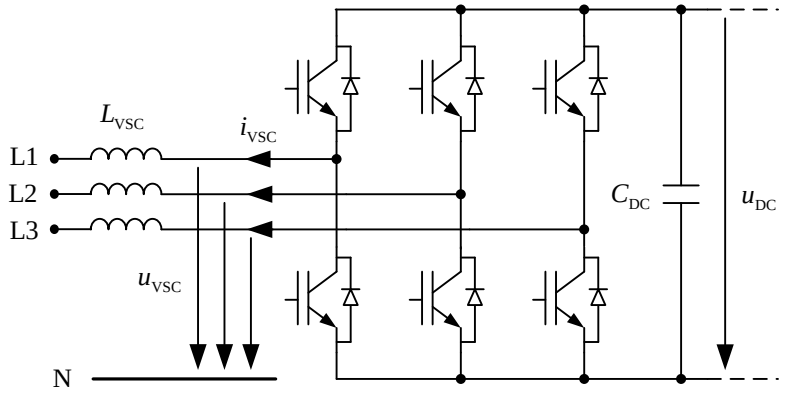

Figure 3-3: Basic configuration of two-level VSC

For HV applications as VSC-HVDC, higher-level topologies are the preferred solution. The modular multi-level converter (MMC) or HVDC plus is considered nowadays the state-of-art of VSC-HVDC. A high numbers of independently controlled IGBT sub-modules (up to 200 hundred per converter arm or more) are connected in series to generate very small steps in the output voltage. The MMC-HVDC basic configuration with half-bridge modules is shown in Figure 3-4. The MMC has lower losses due to the low switching frequency in the IGBT sub-modules in comparison to two-level or NPC converter topologies. As the voltage output of the MMC is nearly sinusoidal an AC filter is typically not required [16].

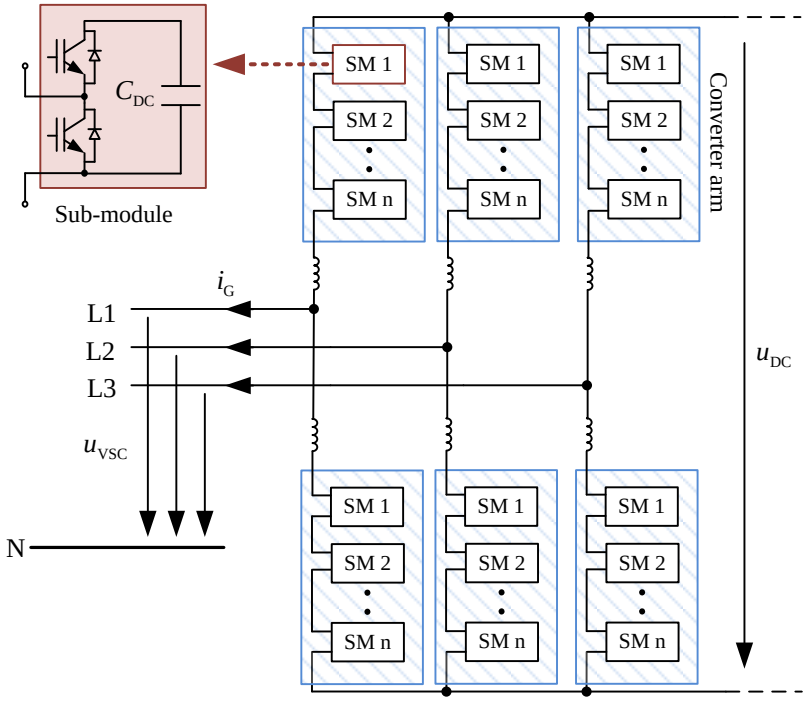

Figure 3-4: Basic configuration of MMC-HVDC Plus with half-Bridge

In the MMC-HVDC, the total voltage of the two arms in each phase determines the DC voltage level, while the ratio of the converter arm voltages in one phase determines the AC voltage level [16]. The failure of a single or few modules will not lead to total shutdown of the system due to the redundancy concept developed in this topology. One limitation of the half bridge module is that it cannot block fault currents caused by short-circuit between the positive and negative DC terminals. In the full-bridge arrangement, the current fault can be blocked in both directions and the topology allows high over-modulation level with low DC voltage operation [17][18]. On the other hand, a full-bridge MMC suffers higher losses since more power electronics are involved in the switching, additionally, the production cost is significantly higher than the half-bridge MMC.

This thesis does not aim to go into details of the converter design and structure of the MMC topology, but rather to investigate the control concepts for integrating large offshore WF via VSC-HVDC and study the impact and contribution on the onshore AC grid considering technical and economic aspects of the proposed solutions.

3.3 VSC-HVDC for connecting offshore WFs

The basic configuration of the VSC-HVDC connected offshore WFs system is shown in Figure 3-5. The VSC-HVDC system consists of the offshore SEC and the onshore REC with HVDC symmetrical cables in between. In the following, a brief description of the main system components is presented.

3.3.1 Converter station components

The IGBT valves offer full controllability (turn-on and turn-off) over a wide range of switching frequency. In the MMC topology, each sub-module consists of an IGBT half bridge and a capacitor unit. In the real converter design, there is no common dc capacitors shared by all phases but rather a unit capacitor for each sub-module [20]. Since a simplified converter model is considered in this thesis, an equivalent DC capacitor is used as shown in Figure 3-5. The DC capacitors serve as energy storing units to improve the DC voltage quality by removing the ripple and limit to an extent the variations in the DC voltage during short-term grid faults.

The main purpose of the line reactors is to allow independent and fast active and reactive power, low-pass filtering the switching pattern to give the desired fundamental frequency voltage and to limit short-circuit currents [11].

In the simple two-level or three-level topology a number of harmonic filters (typically LCL

filter) are required to eliminate the harmonics resulting from the switching pattern in the converter voltage. The MMC technology obviates in principle the need for harmonic AC filters thanks to the nearly perfect sinusoidal converter voltage generated by the high number of IGBT submodules. In this thesis, the AC filter is not considered in the VSC modeling approach.

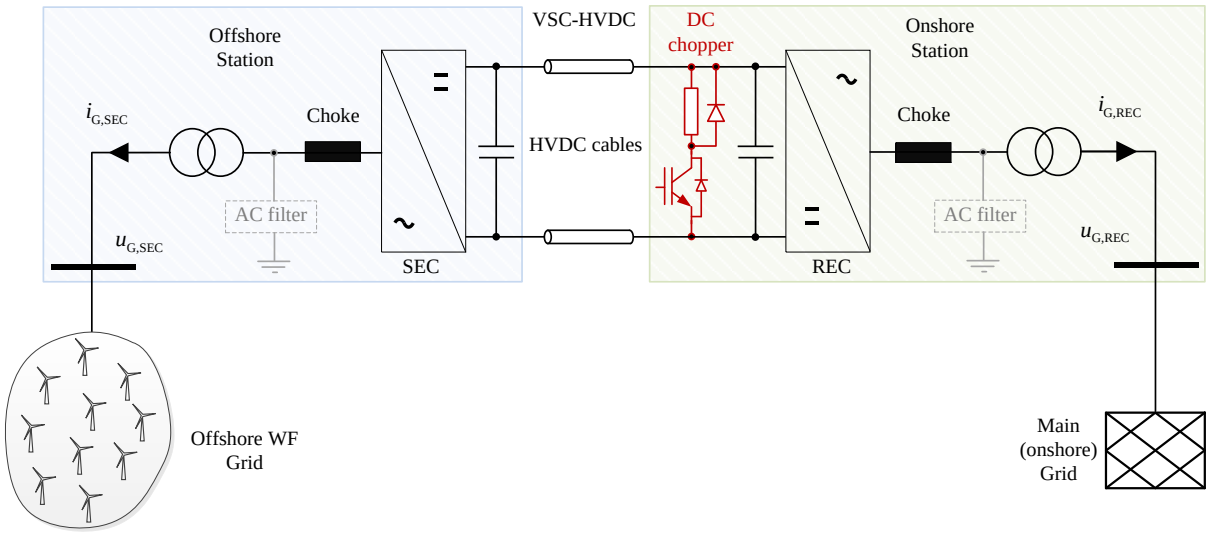

Figure 3-5: Basic configuration of VSC-HVDC connected offshore WFs

The converter transformer is a primary element of the converter station. The transformer tap changer controls the voltage level to optimize active and reactive power flow and the control capability of the VSC-HVDC. A third transformer winding can be used to energize some station equipment or supply a local load at low voltage level. In general, converter transformers in LCC-HVDC technology are subjected to higher harmonic components in comparison to standard applications and must be specifically designed to withstand vibration levels caused by the harmonic content. On the other hand, VSC-HVDC with MMC produce nearly no harmonics and can be equipped normally with standard transformers.

The DC chopper is typically [11][12] located at the onshore REC station. Similar to its functionality in DFIG and FSCG based WTs (described in section 2.2), the DC chopper in the VSC-HVDC dissipates the surplus energy during onshore grid faults to maintain the DC voltage within acceptable limits and allow undisturbed operation of the offshore WFs. The main disadvantage of using a DC chopper is the high cost, since it should be capable of dissipating the energy during nominal power operation. In [4] alternative methods were proposed based on coordinated control between the offshore WF and the VSC-HVDC to allow a safe FRT operation of the offshore WFs in the event of onshore-side grid faults.

3.4 Offshore WF grid characteristics

Large offshore WFs offer several advantages over onshore (on land) WFs. The higher average wind speeds and lower fluctuation makes the offshore WFs more efficient and productive. This feature is important since onshore projects faces big challenges for providing appropriate area for large scale projects, especially in countries with high population density as Western Europe. On the other hand, the installation costs which considers the extreme weather and environment conditions are much higher for offshore projects. Due to the high initial costs, only large scale multi-MW capacities are considered in offshore WFs projects. One important point that must be taken into account in designing the protection system in the offshore grid is the high costs, effort and duration required for accessing remote offshore stations. This means the offshore stations should be optimally designed in a way to operate 100% automatically without human presence.

3.4.1 Offshore WF configuration

In the upcoming studies, the focus will be mainly on DFIG based offshore WFs.

Figure 3-6 illustrates a simplified configuration of an offshore WF based on the Nordsee Ost offshore WF in Germany [29]. Typically, the MV-HV transformers have high impedances which weaken in case of faults in the MV cable the voltage drop at the other windings of the transformer located near the fault location.

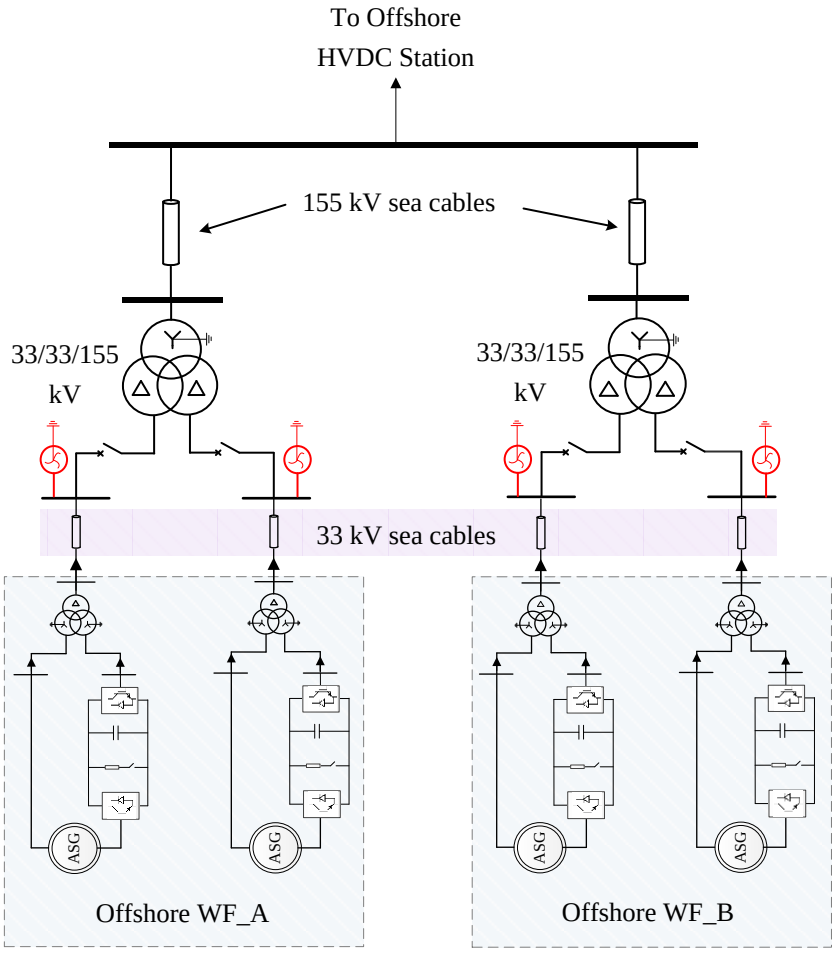

Figure 3-6: Typical Offshore WF configuration with DFIG based WTs

3.4.2 Grounding in MV offshore grid

The offshore grid code is provided in Germany by TenneT, which is one of the transmission system operators (TSOs) in Germany. According to these offshore grid requirements [25], the MV-HV offshore transformer must be implemented in the vector group Yn/d5 with all neutral points at the HV side solidly grounded. On the other hand, standard WT transformers (connecting the generator to the 33 kV grid) have the vector group Dyn5 or Dyn5yn5, offering thereby no grounding option at the 33 kV level. A single line to ground (SLG) fault current in this case may be too small to be detected, and, as a result, fast fault clearing is not possible. The over-voltages reaching nearly 1.73 p.u. during fault would pose a danger to the whole offshore grid. The transient voltage stress would also be relatively high.

As a result, additional grounding transformers are required in the offshore WF grid to allow a fast and reliable detection of single-line-to-ground faults and a selective tripping of the faulty elements. In this thesis, additional grounding transformers are considered in the MV offshore grid as recommenced in [26] to ensure that the fault currents during single-line-to-ground

faults are high enough for a reliable detection through the protection devices.

3.5 Modeling approach of the VSC

The MMC technology proved to be the state-of-the-art VSC-HVDC system which has successfully integrated several offshore WFs in the European North Sea [12]. For MMC modeling no AC filters are typically required. An average MMC model, proposed and validated in [26][27] in comparison to a detailed model, compromises six controlled voltage sources representing upper and lower converter arms. Since the focus in this thesis on the AC grid interactions with VSC-HVDC, the suppression control strategies for voltage unbalances and circulating currents between the converter arms are not considered; therefore a simpler approach that compromises a three-phase controlled voltage source is modeled and implemented as represented by the single line equivalent circuit in Figure 3-7.

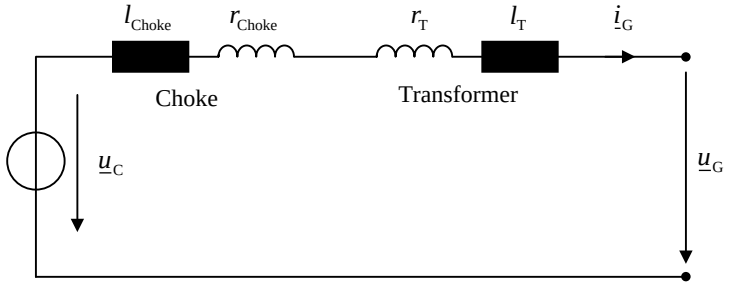

Figure 3-7: Thevenin equivalent circuit of the VSC

The grid voltage $\underline{u}_{\mathrm{G}}$ represents the point of common coupling (PCC) and is considered the measurement point for the VSC controller. Thus the transformer impedance must be considered in the modeling of the converter controller. In the stationary reference frame, the voltage equation is:

$$\underline{u}_{\mathrm{G}}^{\angle 0} = -r_{\mathrm{L}}\underline{i}_{\mathrm{G}}^{\angle 0} - l_{\mathrm{L}}\frac{\mathrm{d}\underline{i}_{\mathrm{G}}^{\angle 0}}{\mathrm{d}t} + \underline{u}_{\mathrm{C}}^{\angle 0} \tag{3.1}$$

Where $r_{\mathrm{L}} = r_{\mathrm{Choke}} + r_{\mathrm{T}}$ and $l_{\mathrm{L}} = l_{\mathrm{Choke}} + l_{\mathrm{T}}$. In the rotating reference frame of the PCC grid voltage denoted by the superscript $\angle u_{\mathrm{G}}$, the voltage equation becomes as follows:

$$\underline{u}_{\mathrm{G}}^{\angle u_{\mathrm{G}}} = -r_{\mathrm{L}}\underline{i}_{\mathrm{G}}^{\angle u_{\mathrm{G}}} - l_{\mathrm{L}}\frac{\mathrm{d}\underline{i}_{\mathrm{G}}^{\angle u_{\mathrm{G}}}}{\mathrm{d}t} - \mathrm{j}\omega_0 l_{\mathrm{L}}\underline{i}_{\mathrm{G}}^{\angle u_{\mathrm{G}}} + \underline{u}_{\mathrm{C}}^{\angle u_{\mathrm{G}}} \tag{3.2}$$

3.6 Onshore REC control

The HVDC converter control is based on a vector control approach in a rotating reference frame, aligned to the positive sequence grid voltage denoted by $\angle u_{\mathrm{G1}}$. A fast positive sequence separation is essential to guarantee a robust positive sequence voltage and current

control during unsymmetrical grid conditions. In this thesis, the phase shift based method developed by Le (1989) is applied for positive and negative sequence separation [4]. Considering the positive sequence current and voltage of equation (3.2), we obtain:

$$\underline{u}_{\mathrm{C1}}^{\angle u_{\mathrm{G1}}} = \underline{u}_{\mathrm{G1}}^{\angle u_{\mathrm{G1}}} + r_{\mathrm{L}}\,\underline{i}_{\mathrm{G1}}^{\angle u_{\mathrm{G1}}} + l_{\mathrm{L}}\,\frac{\mathrm{d}\underline{i}_{\mathrm{G1}}^{\angle u_{\mathrm{G1}}}}{\mathrm{d}t} + \mathrm{j}\omega_0 l_{\mathrm{L}}\,\underline{i}_{\mathrm{G1}}^{\angle u_{\mathrm{G1}}} \tag{3.3}$$

The positive sequence apparent power is expressed as (see appendix A.1):

$$\underline{s}_1 = \underline{u}_{\mathrm{G1}}^{\angle}.\,\underline{i}_{\mathrm{G1}}^{*\angle} = p_1 + \mathrm{j}q_1 \tag{3.4}$$

Where positive sequence active and reactive WT converter currents $i_{\mathrm{G1P}}, i_{\mathrm{G1Q}}$ are introduced:

$$\underline{i}_{\mathrm{G1}}^{\angle u_{\mathrm{G1}}} = i_{\mathrm{G1P}}^{\angle u_{\mathrm{G1}}} - \mathrm{j}i_{\mathrm{G1Q}}^{\angle u_{\mathrm{G1}}} \tag{3.5}$$

Standard PI-controller is applied for the VSC current:

$$\underline{u}_{\mathrm{C1,ref}}^{*\angle u_{\mathrm{G1}}} = k_1\left(1+\frac{1}{sT_1}\right)\left(\underline{i}_{\mathrm{G1,ref}}^{\angle u_{\mathrm{G1}}} - \underline{i}_{\mathrm{G1}}^{\angle u_{\mathrm{G1}}}\right) \tag{3.6}$$

The resulting current controller equation is:

$$\underline{u}_{\mathrm{C1}}^{\angle u_{\mathrm{G1}}} = \underline{u}_{\mathrm{G1}}^{\angle u_{\mathrm{G1}}} + \underline{u}_{\mathrm{C1,ref}}^{*\angle u_{\mathrm{G1}}} + (r_{\mathrm{L}} + \omega_0 l_{\mathrm{L}})\,i_{\mathrm{G1,ref}}^{\angle u_{\mathrm{G1}}} \tag{3.7}$$

Independent from the converter control objectives, the current controller represented by equation (3.7) is the same for both converter stations.

The REC outer control loop generates the reference active and reactive currents to maintain the DC voltage and to support the connected grid with a defined reactive current during steady-state and grid faults.

The derivation of the DC voltage controller is assuming symmetrical conditions considering therefore only the positive sequence components of the AC quantities. A simplified equivalent DC circuit which neglects the resistive losses of the DC cables is used to derive the DC voltage controller as shown in Figure 3-8. Additionally, the impact of the DC cables inductance on the rate of energy change (time constant) is neglected and will be compensated by the DC controller.

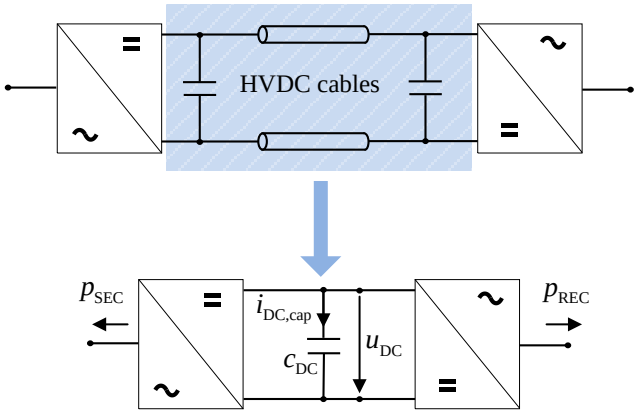

Figure 3-8: Simplified HVDC circuit for the design of the DC voltage controller

By neglecting the HVDC converters losses, the DC voltage equation based on Figure 3-8 can be expressed as:

$$u_{DC} = -\frac{p_{REC} + p_{SEC}}{i_{DC,cap}} \tag{3.8}$$

In a voltage oriented reference frame ($u_{G1} = u_{G1d}^{\angle u_{G1}}$ and $u_{G1q}^{\angle u_{G1}} = 0$) and by neglecting converter and resistive losses up to the measurement point, the power at the HVDC REC converter station is given as:

$$p_{REC} = u_{G1} i_{G1P}^{\angle u_{G1}} = p_{SEC} - u_{DC} i_{DC,cap} \tag{3.9}$$

It becomes obvious that the effective way to control the DC voltage by the REC is through the active current channel. The measurement of the DC current quantity $i_{DC,cap}$ is not required here since it is replaced by the output of the PI-controller as following:

$$p_{REC,ref} = p_{SEC} - k_{Pr}\left(1 + \frac{1}{sT_{Pr}}\right)\left(u_{DC,ref} - u_{DC}\right) \tag{3.10}$$

The SEC active power represents a feed-forward term that enhances the DC voltage controller. However, due to the long distance between the SEC offshore station and REC onshore station, a considerable communication delay of the measurement is expected. Therefore, this term can be neglected and the error will be compensated by the PI-controller.
For the reactive current channel, the reactive current reference can be directly expressed as:

$$i_{G1Q,ref}^{\angle u_{g1}} = \frac{q_{1REC,ref}}{u_{G1}} \tag{3.11}$$

The resulting REC control with outer and inner control loops is presented in Figure 3-9.

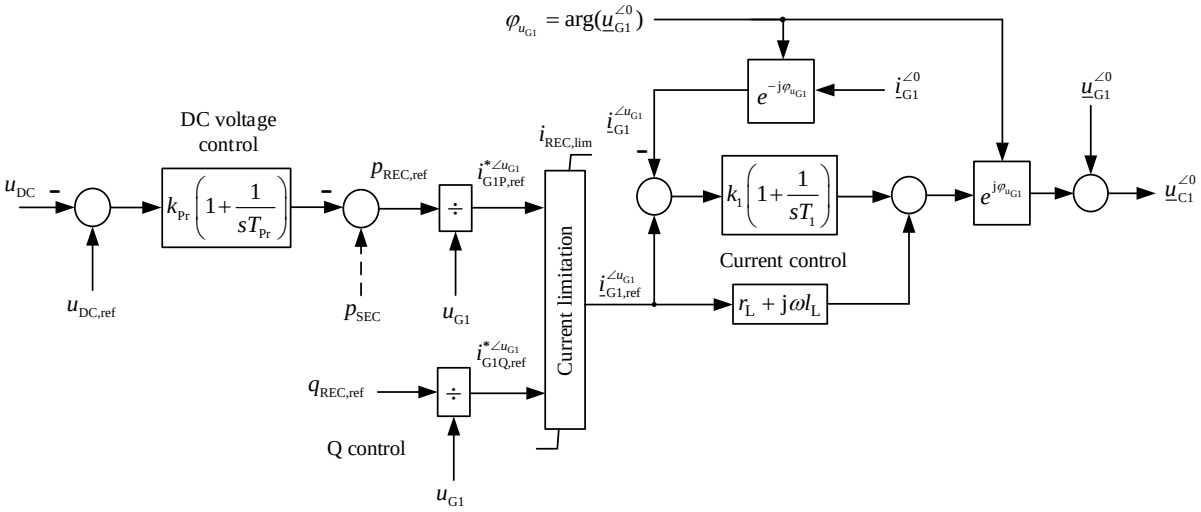

Figure 3-9: REC control with internal current control

The reactive current channels can be alternatively utilized to control the terminal AC voltage. Most of the European grid code requires providing a defined reactive current support through fast voltage control. A dead-band characteristics is not required if a continuous voltage control is implemented [30]. A simple proportional controller is shown in Figure 3-10 can basically fulfill the dynamic requirements regarding fast reactive power support.

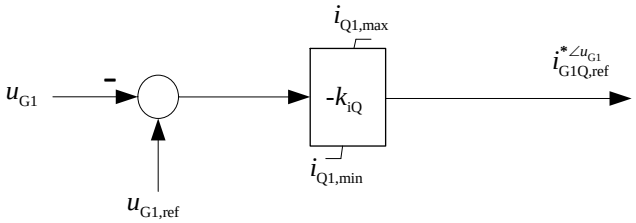

Figure 3-10: Fast local voltage control for HVDC converter

When the VSC-HVDC system is integrated to a large grid configuration, the HVDC is expected to adapt the steady-state reactive power flow in coordination with the grid operator which can in this case send direct set-points to the HVDC controller. The control layout in Figure 3-11 offers a hierarchical control which can fulfill both steady-state and dynamic requirements. The U-Q control consists of the primary controller which is the fast acting local voltage controller as in Figure 3-10. The secondary controller is a slow-acting reactive power tracking control which may receive its reference signal from the grid operator. The secondary controller is blocked when the voltage limits at the connection point reaches certain lower and upper limits. The U-Q control concept allows the HVDC to participate in the reactive power dispatch strategy of the whole interconnected AC network.

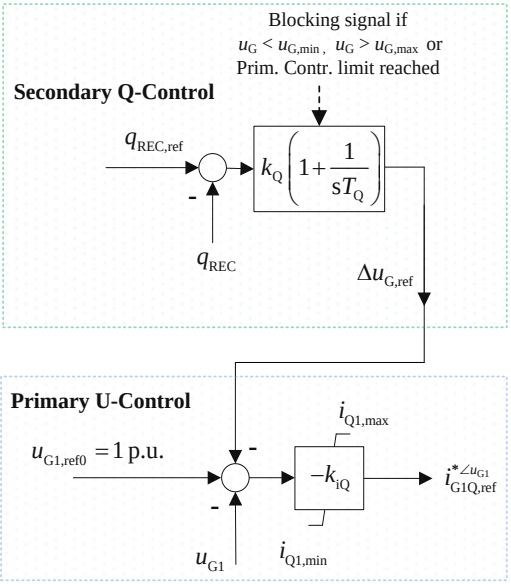

Figure 3-11: Hierarchical U-Q control concept for HVDC converter

3.7 Offshore SEC control

The main function of the offshore-side SEC is to establish and maintain the voltage magnitude and frequency of the offshore grid for insuring a stable power transmission. The control strategy must take into account several aspects regarding the characteristics of the offshore grid.

The short-circuit currents from the HVDC system depend on the implemented control and the protection schemes. In case of high short-circuit currents the converter is blocked by protection circuits to protect the IGBT valves. During the blocking period no short-circuit current will be contributed by the HVDC converter. The current level at which the IGBTs are blocked is specified usually by the manufacturer.

Faults in the offshore grid are mainly related to defects in a specific location in the AC sea cables which must be quickly isolated in order to allow the offshore WFs to continue feeding in power through the offshore SEC. This is however a challenging task, since the short-circuit current might not be high enough to be detected by simple over-current relays. In the other hand, if the SEC blocks during a fault event due to high short-circuit currents, the voltage at the HV side of the offshore grid will drop to nearly zero and a FRT will be a challenging task in this case.

3.7.1 SEC control without current limitation

A direct voltage magnitude and frequency control without current control is a simple straightforward control strategy. A direct stiff voltage reference is simply forwarded with a

PI-controller to compensate the steady-state error as illustrated in Figure 3-12.

In the absence of current limitation by the offshore SEC, any significant faults in the offshore grid with DFIG based WTs will lead to high short-circuit currents at the HVDC terminals. The SEC protection system will react upon a certain over-current level by blocking the IGBT valves to protect its power electronic components. As a result, the offshore WFs must be safely tripped due to the loss of the established reference voltage by the SEC. The offshore grid can be reenergized after replacing the defect cable part.

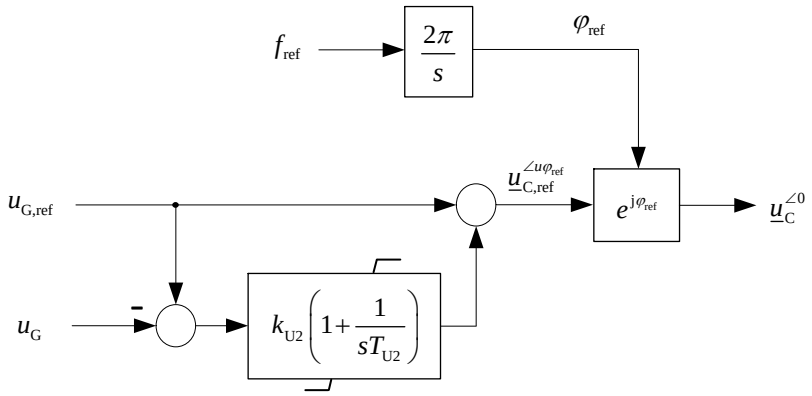

Figure 3-12: SEC direct voltage control without current limitation

3.7.2 SEC control with indirect current limitation

In this strategy it is proposed to utilize the reference voltage to limit the current during transients without the use of a current controller. At the event of an offshore fault, the voltage drops to a certain level and the current rises instantly, the SEC control will react fast by reducing the reference voltage in order to limit the HVDC short-circuit current contribution. One disadvantage of this method is that a peak current in the first milliseconds of the fault usually cannot be effectively limited. The required fast detection of the over-currents becomes a challenging task at very low impedance faults due to the fast rise and high peaks of the short-circuit currents that cannot be controlled. Since the IGBT valves are sensitive to over-currents, the valves will be blocked directly after exceeding a certain limit. The control strategy concept is illustrated in Figure 3-13. The PI-controller is acting slowly to eliminate steady-state deviations. Once the current magnitude exceeds a defined limit, a fast reduction of the reference voltage is initiated. If the fault is successfully isolated, the reference voltage can be restored to the nominal value.

In chapter 4, simulation studies are performed to validate and evaluate this control concept.

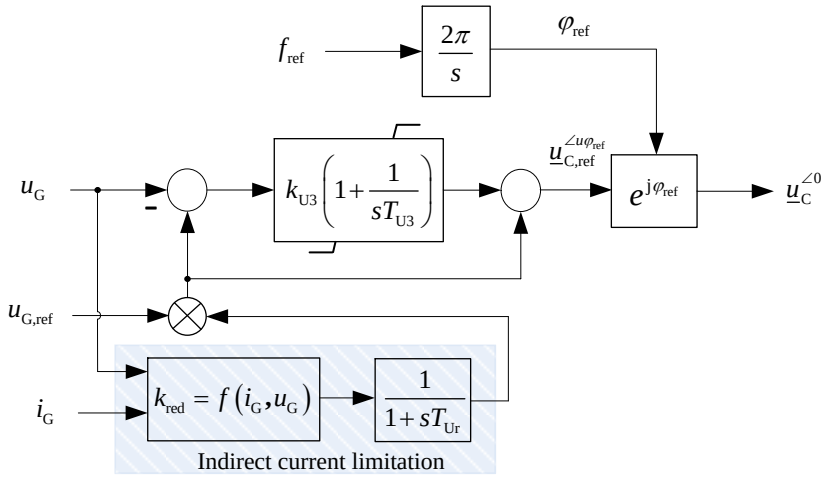

Figure 3-13: SEC voltage control with indirect current limitation

3.7.3 SEC control with direct current limitation

An inner current control loop can be implemented in the SEC control to ensure a controllable short-circuit current contribution from the HVDC. A separate positive sequence controller is considered here. Unlike the REC controller, the phase-locked loop (PLL) plays here an important role to compensate the phase deviations during variable frequency operation or grid faults. The SEC controller structure is based on the proposed method in [4] . In this thesis the validity of the presented control strategies is tested through simulation cases and the PLL is enhanced to ensure fast phase error compensation when changing the frequency setpoint during operation. The controller layout is shown in Figure 3-14. The frequency control is realized by a standard PI-controller according to the following equation:

$$\underline{i}_{G1P,ref}^{\angle u_{G1}} = k_{iP}\left(1+\frac{1}{sT_{iP}}\right)\left(f_{ref}-f_{SEC}\right) \tag{3.12}$$

Large offshore WFs with VSC-HVDC connection should be able to participate in the primary frequency control of the connected ‘onshore’ grid. Since the HVDC connection provides a complete decoupling between the main grid frequency and the offshore WF frequency, the frequency deviations must either be replicated in the offshore WF grid or the onshore frequency measurement be sent to the offshore WFs. If the robustness of the communication link between the onshore side and the offshore grid is questioned, the onshore grid frequency can be ‘artificially’ coupled to the offshore frequency through the VSC-HVDC controllers. This is realized as proposed in [4][38][39] using a dedicated droop control for the DC voltage control where the REC adjusts the DC voltage according to the onshore frequency deviation and the offshore SEC senses locally this DC voltage deviation and adjusts the reference offshore frequency to replicate the onshore grid frequency. The variable frequency operation

concept for DFIG based WTs proposed in [40] can be realized as well with this SEC control (Figure 3-14).

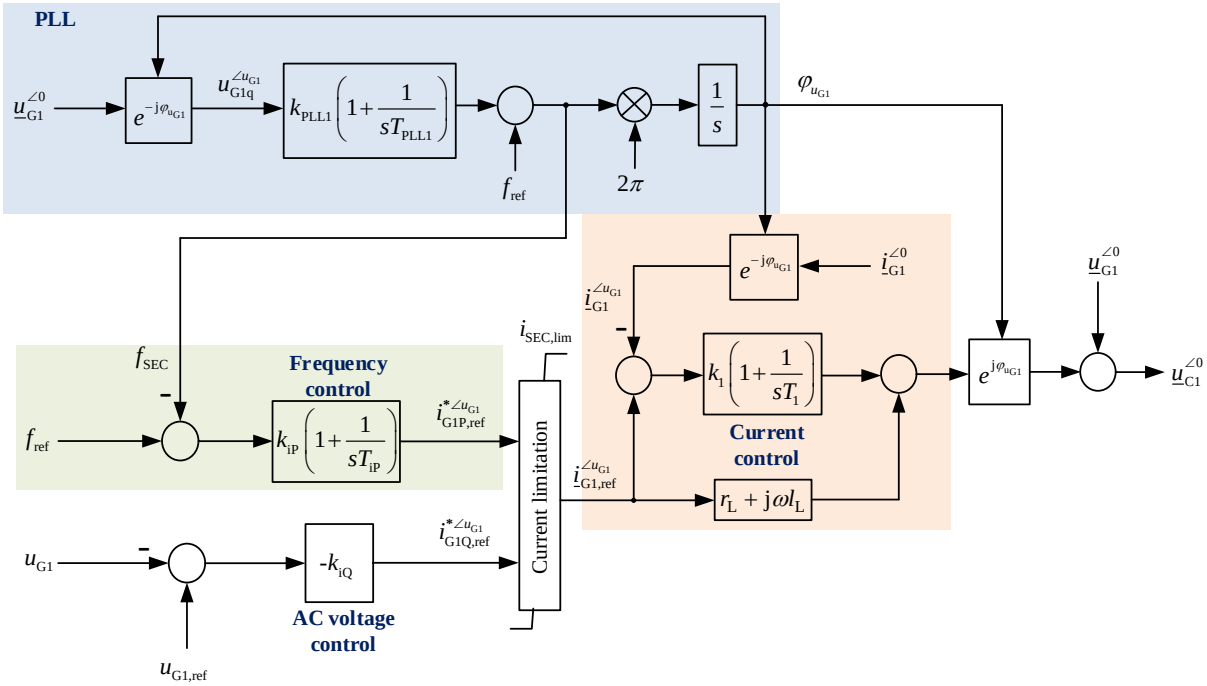

Figure 3-14: SEC control with inner current control and outer frequency and voltage controllers

Alternative SEC control with inner current control

In the following an alternative SEC control is derived from the VSC mathematical model. The idea here is to generate the transformation angle of the controller reference frame directly from the given reference frequency while utilizing the active current channel to compensate for phase deviations instead of the PLL. From equation (3.2) the dq- components in the positive sequence are given by:

$$u_{\mathrm{G1d}}^{\angle u_{\mathrm{G1}}} = u_{\mathrm{C1d}}^{\angle u_{\mathrm{G1}}} - r_{\mathrm{L}} i_{\mathrm{G1Q}}^{\angle u_{\mathrm{G1}}} - l_{\mathrm{L}} \frac{\mathrm{d}i_{\mathrm{G1Q}}^{\angle u_{\mathrm{G1}}}}{\mathrm{d}t} - \omega_0 l_{\mathrm{L}}\, i_{\mathrm{G1P}}^{\angle u_{\mathrm{G1}}} \tag{3.13}$$

$$u_{\mathrm{G1q}}^{\angle u_{\mathrm{G1}}} = u_{\mathrm{C1q}}^{\angle u_{\mathrm{G1}}} + r_{\mathrm{L}} i_{\mathrm{G1Q}}^{\angle u_{\mathrm{G1}}} + l_{\mathrm{L}} \frac{\mathrm{d}i_{\mathrm{G1Q}}^{\angle u_{\mathrm{G1}}}}{\mathrm{d}t} - \omega_0 l_{\mathrm{L}}\, i_{\mathrm{G1P}}^{\angle u_{\mathrm{G1}}} \tag{3.14}$$

In principle, both active and reactive current channels can be utilized to maintain the system alignment ($u_{\mathrm{G1q}}^{\angle u_{\mathrm{G1}}}$=0), but since the reactive channel is assigned to control the AC voltage magnitude, the active current channel is used here to ensure the measured phasor alignment to the given reference frame. This is achieved by compensating the phase angle deviation and thus replacing the PLL using the following PI-controller:

$$i_{\mathrm{G1P,ref}}^{\angle u_{\mathrm{G1}}} = -k_{\mathrm{uq}}\left(1+\frac{1}{sT_{\mathrm{uq}}}\right)\left(u_{\mathrm{G1q,ref}}^{\angle u_{\mathrm{G1}}} - u_{\mathrm{G1q}}^{\angle u_{\mathrm{G1}}}\right) \tag{3.15}$$

The proposed SEC control structure is shown in Figure 3-15, where $u_{\mathrm{G1q,ref}}^{\angle u_{\mathrm{G1}}}$ =0. If variable frequency operation is required from the SEC and stiff changes are given in the reference frequency, a simple low pass filter can be added as an open loop control term to smooth the frequency response to a step change.

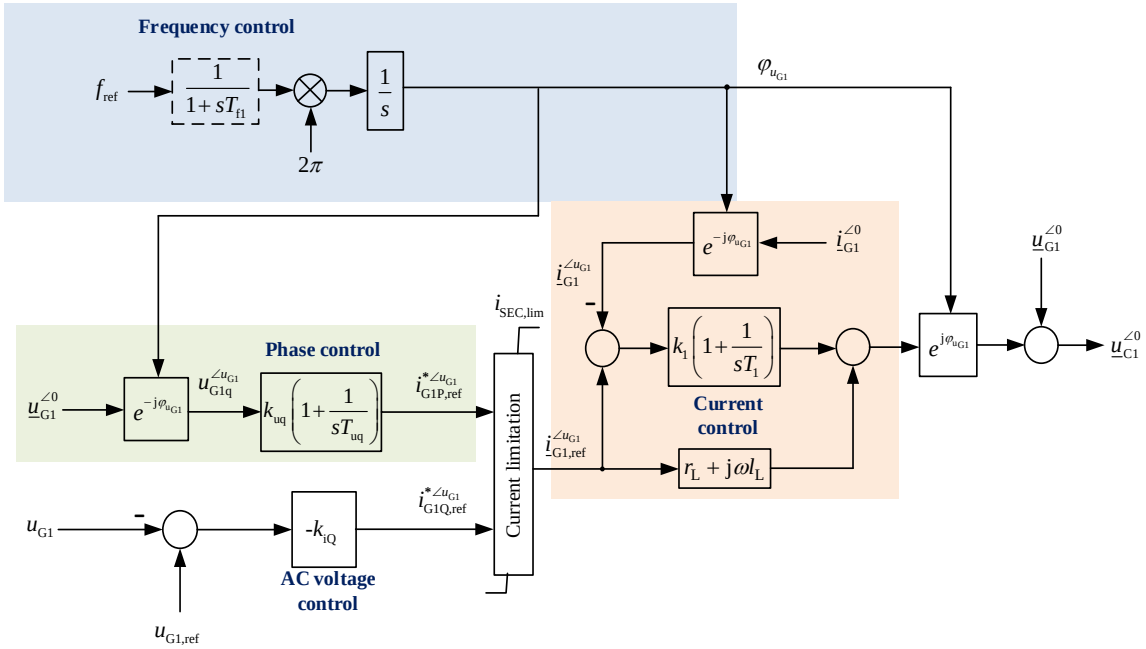

Figure 3-15: SEC control with inner current control and outer phase and voltage controllers

Figure 3-16 shows the step response of the offshore SEC frequency at 0.2 s and 0.5 s for the proposed SEC control. An EMT-type simulation model of an aggregated offshore WF and VSC-HVDC is used here. A step of 2 Hz in the offshore frequency during nearly nominal operating point can be achieved within 100 ms without significant transient over-currents. The level and duration of the transient period depends strongly on the dynamic response of the WTs controllers, which respond relatively fast as shown in the same figure (around 100-150 ms). In case the HVDC-SEC is required to replicates the onshore grid frequency, the rate of change of frequency (RoCoF) will be slower in reality than a stiff step response allowing therefore a smooth offshore frequency variation with negligible transients in offshore currents and voltages.

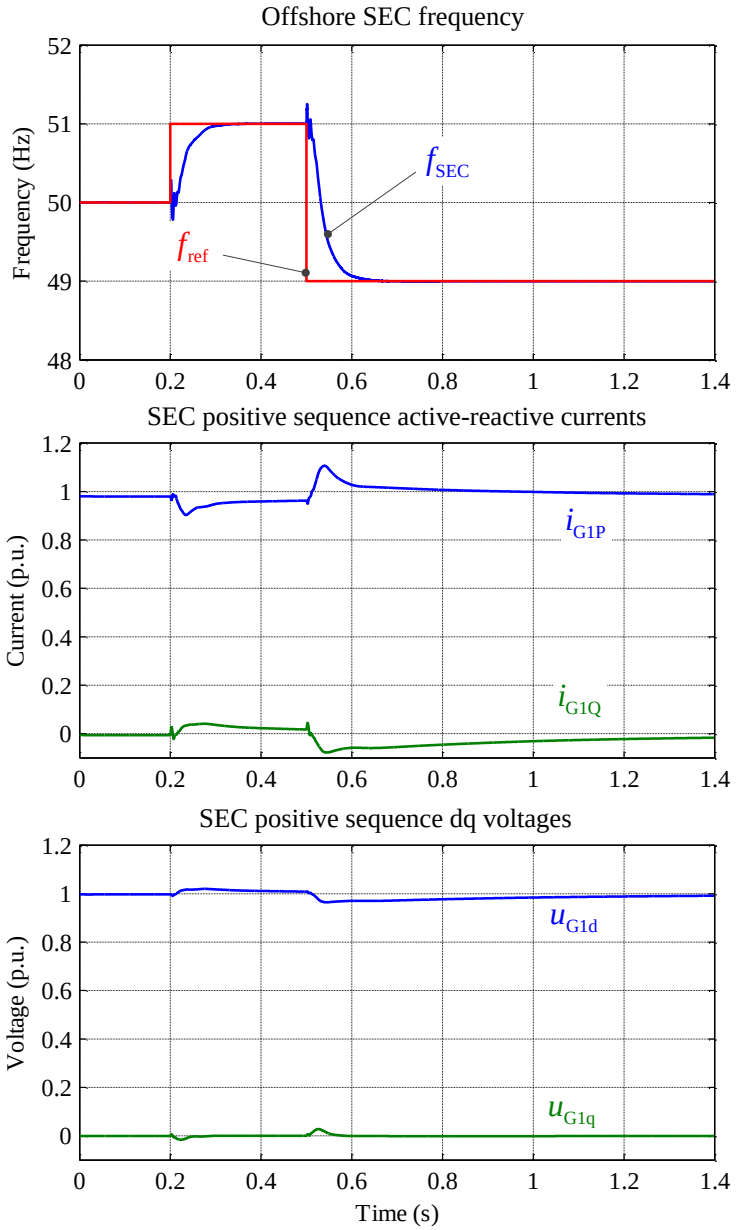

Figure 3-16: Offshore frequency step response by SEC control with inner current control and outer phase and voltage controllers

3.8 Negative sequence control for VSC-HVDC

The introduced positive sequence controller is sufficient for symmetrical grid conditions (including symmetrical faults). However, for unsymmetrical conditions, the existing negative sequence components must be taken into account in the VSC control design to allow the controllability of both positive and negative sequence current components and ensure an effective current and voltage limitation by the VSC controller. To realize this, the equivalent VSC voltage equation in the negative sequence must be determined. Analog to the positive sequence voltage equation, the negative sequence voltage equation is expressed as:

$$\underline{u}_{\mathrm{G2}}^{\angle -\omega_0} = -r_{\mathrm{L}}\,\underline{i}_{\mathrm{G2}}^{\angle -\omega_0} - l_{\mathrm{L}}\frac{\mathrm{d}\underline{i}_{\mathrm{G2}}^{\angle -\omega_0}}{\mathrm{d}t} - \mathrm{j}\omega_0 l_{\mathrm{L}}\,\underline{i}_{\mathrm{G2}}^{\angle -\omega_0} + \underline{u}_{\mathrm{C2}}^{\angle -\omega_0} \tag{3.16}$$

The negative sequence current controller is implemented in a similar manner to the positive sequence as shown in Figure 3-17, where $i_{\mathrm{G2P}}^{\angle u_{\mathrm{G1}}}$ and $i_{\mathrm{G2Q}}^{\angle u_{\mathrm{G1}}}$ are the negative sequence active and reactive current components respectively.

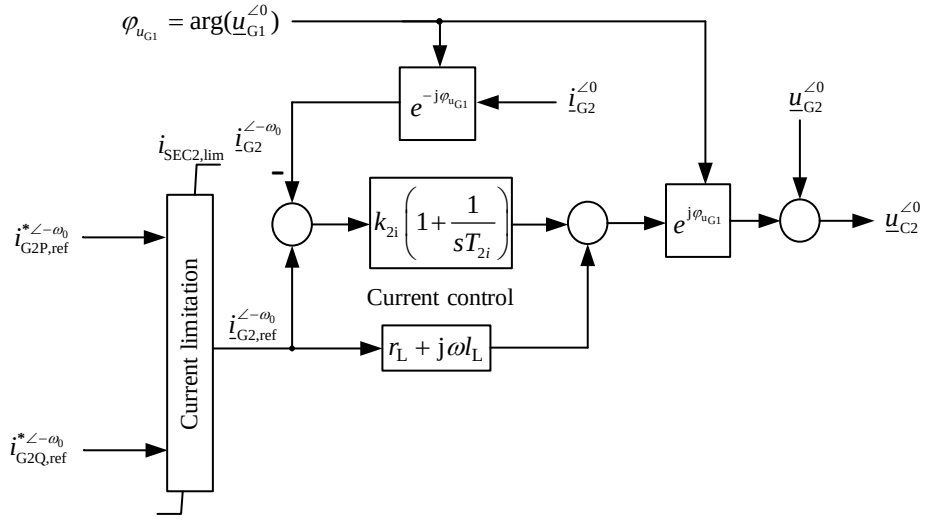

Figure 3-17: Negative sequence current control

The converter has to inject as a result both positive and negative sequence reference voltages according to the following equation:

$$\underline{u}_{\mathrm{C}}^{\angle 0} = \underline{u}_{\mathrm{C1}}^{\angle 0} + \underline{u}_{\mathrm{C2}}^{*\angle 0} \tag{3.17}$$

If the control objective is to suppress the negative sequence current to provide a symmetrical short-circuit current during unbalanced faults; the reference for both negative sequence active and reactive current components can be simply set to zero as following:

$$i_{\mathrm{G2P,ref}}^{*\angle -\omega_0} = 0 \tag{3.18}$$

$$i_{\mathrm{G2Q,ref}}^{*\angle -\omega_0} = 0 \tag{3.19}$$

In general, if no negative sequence current injection is foreseen, it is sufficient to forward directly the measured negative sequence grid voltage as the controller output without a current controller as following:

$$\underline{u}_{\mathrm{C2}}^{\angle 0} = \underline{u}_{\mathrm{G2}}^{\angle 0} \tag{3.20}$$

In [22] different control objectives for the negative sequence were proposed for LSC of the DFIG based WT. These objectives can be also applied to the REC of the VSC-HVDC. During unbalanced conditions, the SEC active power passing through the DC-link to the REC

contains in general components pulsating at twice the grid frequency. As a result the DC voltage can be pulsating with the same frequency. A dedicated negative sequence control for suppressing these pulsating components in the DC voltage has been introduced with simulation results in details in [4][23] and is not considered for investigation in this work.

Another negative sequence control objective would be to inject a defined amount of inductive negative sequence current proportional to the negative sequence grid voltage $\underline{u}_{G2}$ to reduce the voltage asymmetry during unbalanced conditions. To assure the correct alignment of the negative sequence active and reactive current components, the transformation angle of the negative sequence voltage $\underline{u}_{G2}$ must be detected and applied for this control objective instead of simply using the transformation angle of the positive sequence voltage [34].

The protection concept in the offshore grid must be coordinated closely with the HVDC-SEC control concept. During unsymmetrical faults at medium voltage level the HVDC-SEC injects both positive and negative sequence currents if the SEC operates only with a simple voltage control. If a separate positive/negative sequence current controllers are implemented the SEC can either suppress negative sequence currents at the HV-side or inject defined negative sequence currents. By controlling the negative sequence voltage to zero during normal operation, the voltage symmetry can be enhanced. However, during short-term unsymmetrical faults (150 ms) this control target seems to be ineffective.

For a FSCG based offshore WF, the short-circuit current is solely defined by the controllers of both HVDC-SEC and WTs converters. In case of line-to-line fault, the short-circuit current will be limited to the load level or nearly to zero. In such a scenario, the fault cannot be detected by conventional protection devices. In [33] a dedicated inductive negative sequence current injection proportional to the negative sequence voltage is proposed to overcome this problem. In this thesis, only the negative sequence current suppression scenario during unbalanced faults is considered as it is assumed that state-of-art protection devices in the offshore grid are capable of detecting faults despite low short-circuit currents.

3.9 VSC current limitation

Current limitation capability is an important aspect in VSC technology. The IGBT valves are designed for a certain nominal current value and can only withstand a limited overloading before being blocked to protect the power electronic components. The maximum allowed current value depends on several factors as thermal characteristics of the IGBTs, the different operating points and periods of dynamic overloading. These aspects are discussed in details in [23] and [24]. In general IGBTs are sensitive valves which must be protected against over-

currents by well-designed current controllers.

In this thesis, the current limitation of the current complex phasor is considered for the VSC in steady-state and dynamic conditions without considering detailed overloading characteristics. A switchable current injection priority can be defined according to the grid connection requirements during steady-state and faults conditions. Figure 3-18 illustrates current limitations options for the VSC. If no priority is defined between the active current i_P and the reactive current i_Q, the magnitude of the complex current phasor will be limited without changing the power factor. Typically during normal operation the active current has a priority over the reactive current; in this case the reactive current order will be limited to allow maximum possible injection of the active current. During fault events, the current priority can be switched to allow maximum possible reactive power support through reactive current injection.

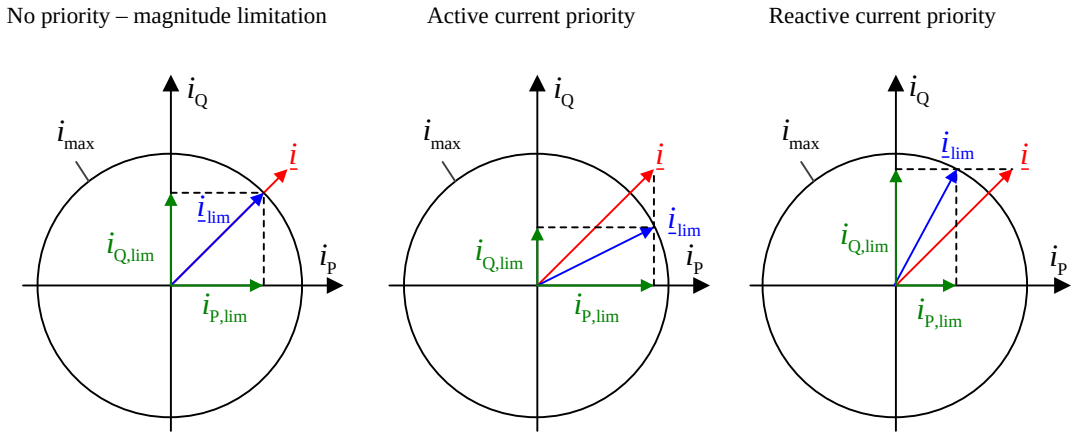

Figure 3-18: Current limitation options for the VSC

If a dedicated negative sequence control is applied, where a defined negative sequence reference current is generated, the negative sequence current must be considered in the total current limitation as illustrated in Figure 3-19. The current positive and negative sequence components are given as:

$$\underline{i}_G = \underline{i}_{G1} + \underline{i}_{G2}^* \tag{3.21}$$

The positive sequence current is usually given the highest priority and the limitation therefore can be defined by the flowing equations:

$$i_{G1,ref,max} = i_{G,max} \tag{3.22}$$

$$i_{G2,ref,max} = \sqrt{i_{G,max}^2 - i_{G1,ref}^2} \tag{3.23}$$

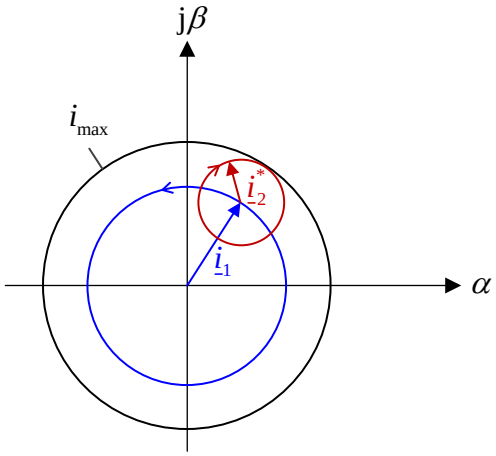

Figure 3-19: Current symmetrical components limitation with negative sequence control

3.10 VSC voltage limitation

The converter AC voltage is technically limited by the DC voltage level in accordance with the power circuit configuration. In sine wave modulation, the modulation index m describes the normalized value of the modulated AC voltage based on the half value of the DC voltage as following:

$$m = \frac{\hat{u}_{C,max}}{\frac{u_{DC}}{2}} \tag{3.24}$$

Thus the maximum modulation index in the standard case is limited to 1. However, in modern vector control approach, the modulation index can be increased by means of inserting a third harmonic "common mode" voltage component to the reference generated signal [23]. This results in a maximum modulation of:

$$m_{max} = \frac{2}{\sqrt{3}} = 1.155 \tag{3.25}$$

Over-modulation in general increases the harmonic generation and can overload the AC filters, one of the reasons for over-modulation is an over-voltage condition. Thus to avoid over-modulation, the modulation index must be properly limited by the controller. During unbalanced conditions, voltage limiting in the VSC control should consider the positive and negative sequence components of the reference voltage. Voltage limitation priorities were defined in [4][23] which harmonize with the current limitation priorities. In chapter 4, the priority is assigned for the positive sequence voltage according to the following equations:

$$u_{C1,max} = u_{C,max} \tag{3.26}$$

$$u_{C2,max} = u_{C,max} - u_{C1} \tag{3.27}$$

4 Dynamic studies for VSC-HVDC connected offshore WFs

Grid connection requirements were introduced recently in several European countries [35] for the grid integration of offshore WFs. In this chapter, the main related connection requirements according to the German grid code are briefly discussed. Dynamic simulations are performed afterwards to verify and assess the control strategies presented in chapter 3.

4.1.1 Grid connection requirements in Germany

Low voltage ride through (LVRT) requirements according to the German grid code (TenneT) are illustrated in Figure 4-1. The minimum continuous voltage level is defined as 0.9 p.u.. Three-phase short-circuit or fault -related symmetrical voltage dips must not lead to instability above the Limit Line 1 or to disconnection of the generating plant from the grid. The pair of values (voltage, time) is required as well for unsymmetrical faults with reference to the positive sequence system [25].

Within the shaded area and above the Limit Line 2 shown in Figure 4-1, all generating plants should stay connected to the grid during the fault. If, due to the grid connection concept (plant concept including generators), a generating plant cannot fulfill this requirement. The reactive power in-feed and resynchronization must take place so that the generating plant meets, in a suitable way, the respective requirements of the grid at the grid connection point [25].

In the other area the disconnection of the generation units is allowed but not a must. Depending on the WT control and manufacturer settings, the decision can be made to whether to continue or interrupt the operation.

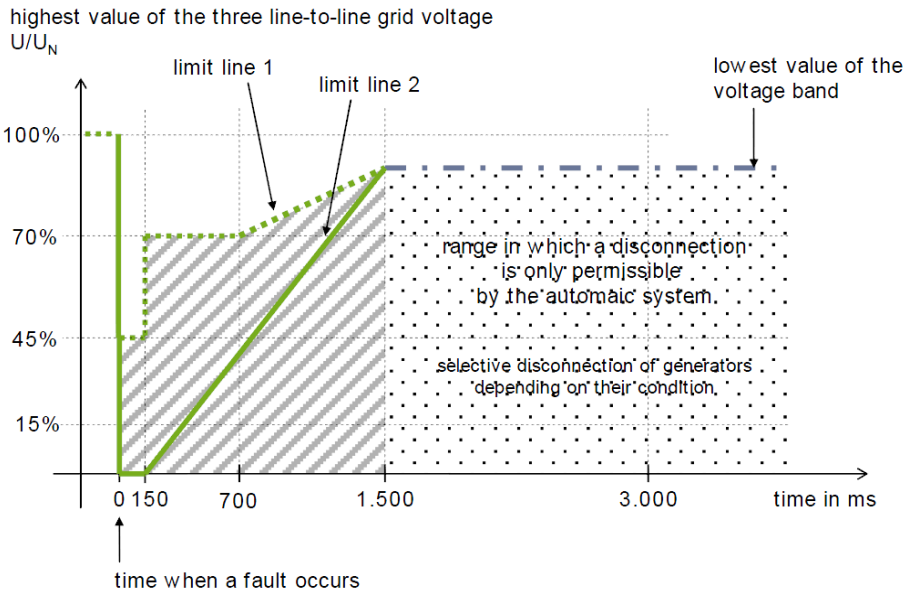

Figure 4-1: LVRT requirement for the offshore grid connection [25]

- *Fast voltage control requirement:*

The onshore REC of the VSC-HVDC system must respond to a sudden voltage collapse/increase with the corresponding fast reactive current output in accordance with Figure 4-2 which is based on the requirements in [30]. This should be implemented as a fast voltage control locally at the converter level. The Δv versus Δi_{Q1} typically corresponds to the values at the connection terminal (on the high voltage side).

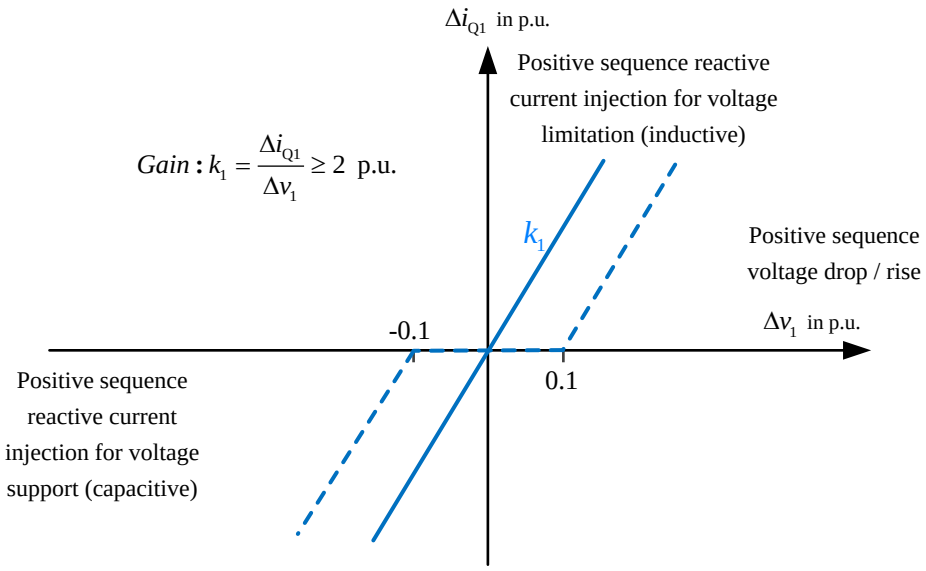

Figure 4-2: LVRT requirement for the offshore grid connection

Regarding negative sequence treatment during unbalanced faults, a draft standard [32] in Germany already suggests a reactive negative sequence current contribution during negative

sequence grid voltages. In [34] the negative sequence current contribution was investigated in details.

4.1.2 Test network

As discussed in section 3.3, the average model based on a 3-phase controlled voltage source is used to model the VSC-HVDC in the simulation studies in this chapter. The VSC-HVDC is interconnecting two offshore WFs of DFIG-based (type 3) WTs. Each offshore WF is aggregated by two WT units, where each WT unit represents an array of WTs connected either at the secondary or tertiary winding side of the MV-HV transformer as illustrated in Figure 4-3. The parameters for the sea AC cables are listed in appendix A.6. The following assumptions are considered in the simulation studies performed in this chapter:

- An offshore-side fault represents permanent cable damage in one or more phases.
- Protection devices in the offshore grid are not modeled. The fault clearance in the offshore grid is simply simulated by opening the nearby circuit breaker and isolating thereby the faulty part of the grid.
- The offshore WTs in the 'faulty' isolated part are supposed to be able to trip safely after entering the islanded mode.

In the EMT-type simulation models developed in this work, the dead-time of the measurements that exists in real systems is neglected. A simple second order low-pass filter is considered to represent the measurements delay. The control strategies presented in chapter 3 will be verified and evaluated through the simulation studies conducted in the following sections. The symbols of the measured quantities used in this chapter are listed with their description in appendix A.3.

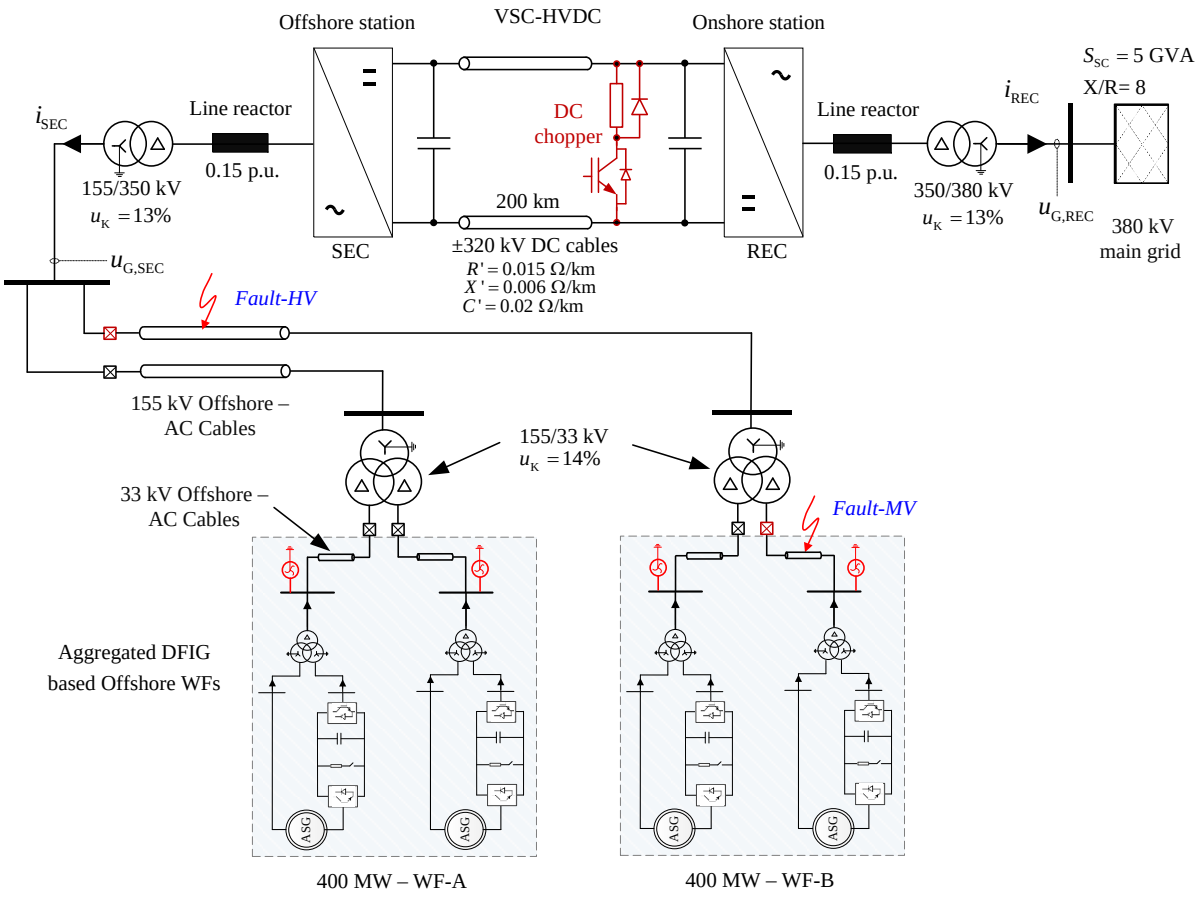

Figure 4-3: VSC-HVDC with offshore WF test network

4.2 Onshore-side grid faults

The onshore-side HVDC-REC is the connection point of the offshore WF to the onshore (main) grid and should be able to provide FRT capability during grid faults in a similar manner to a generation unit. Since the offshore SEC does not directly control the active power, a fast active current reduction by the SEC will cause strong interactions with the power controllers of the WTs. This leads in a worst case scenario to instability and WT tripping in the offshore grid. Possible strategies to allow a successful fault ride through in this case are discussed in details in [4]. The most robust strategy that is currently considered in practice is the full-rated HVDC chopper.

Symmetrical three phase and double line to ground (DLG) solid faults at the PCC with 200 ms duration are illustrated in Figure 4-4. The full-rated HVDC chopper is switching on and off by a simple to point hysteresis characteristic depending on the DC voltage level. The SEC power is nearly unchanged during the fault; thus the offshore WF grid is totally decoupled from the onshore fault. During unsymmetrical faults, the negative sequence current is suppressed, which means the HVDC converter injects only symmetrical currents during

unsymmetrical faults. The positive sequence reactive current injection is given the priority during the fault. The fast current controllers in the HVDC-REC offer a robust current limitation during the both faults, the maximum apparent current is set to 1.1 p.u..

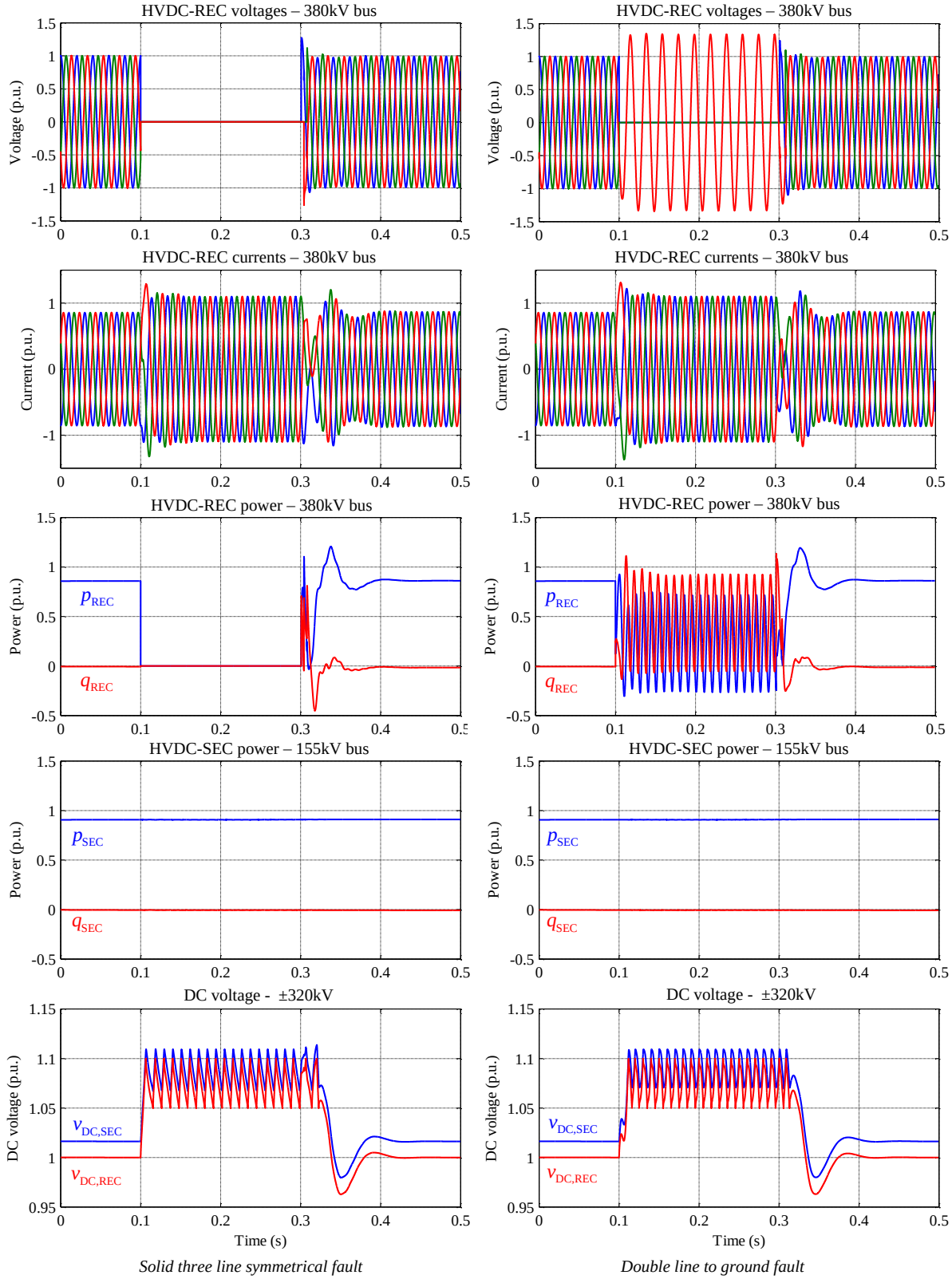

Figure 4-4: Simulation results for three-phase fault and double line to ground fault at the onshore HVDC-REC grid connection point – 380 kV bus

4.3 Offshore-side grid faults

Submarine cable faults have a different nature from overhead lines faults. Unlike transient lightening faults in overhead lines, an AC submarine cable fault is typically caused by a persistent mechanical cable defect. Thus the fault location must be isolated as fast as possible to avoid tripping the whole offshore WF grid. The number of offshore WTs that can ride-through the fault depends on fault location, selectivity and fast detection of the protection devices in the offshore grid. The worst-case fault scenario would be a solid fault that occurs directly at the main HVDC-SEC collector. The fault isolation by opening nearby circuit breakers will create an islanded operation for the offshore WFs. The offshore WFs must initiate therefore a tripping sequence since no alternative power transmission path is available. In this particular fault scenario a FRT in the offshore grid is impossible. Since the detailed de-energizing (tripping) and reenergizing sequences in the offshore grid are out of scope of this thesis, this fault scenario is not considered in the simulation studies.

If the offshore grid fault occurred in one of the two parallel transmission HVAC (155 kV) cables connecting both offshore WFs as illustrated in the test network (Figure 4-3), a FRT operation could be possible for one offshore WF if the fault clearance (isolation) is successful.

4.3.1 Short-circuit level of the offshore WF grid

The offshore WF grid can be considered as an islanded grid with solely asynchronous generation units. Since no considerable loads exist in the offshore grid and the voltage magnitude and frequency is established by the HVDC-SEC, no considerable inertial responses exist to affect the frequency level. Furthermore, the current controllers at the offshore WF converters adapt fast to any step change in the offshore frequency setpoint. Therefore, any frequency stability and control requirements in grid codes are only related to the onshore grid frequency. Typically the offshore WF grid features a high impedance path between the HVDC-SEC and the WT units due to the impedances of the converter reactor and transformer, HV-MV offshore grid transformer and the MV-LV WT transformer (see Figure 4-3). As a result, the short-circuit level (SCL) in the offshore WF is relatively low. Figure 4-5 demonstrates the SCL for two cases: three-phase solid fault at the HV level and three-phase solid fault at the MV level of the offshore grid. In reality, the IGBTs of the HVDC-SEC cannot withstand such over-currents and will be blocked.

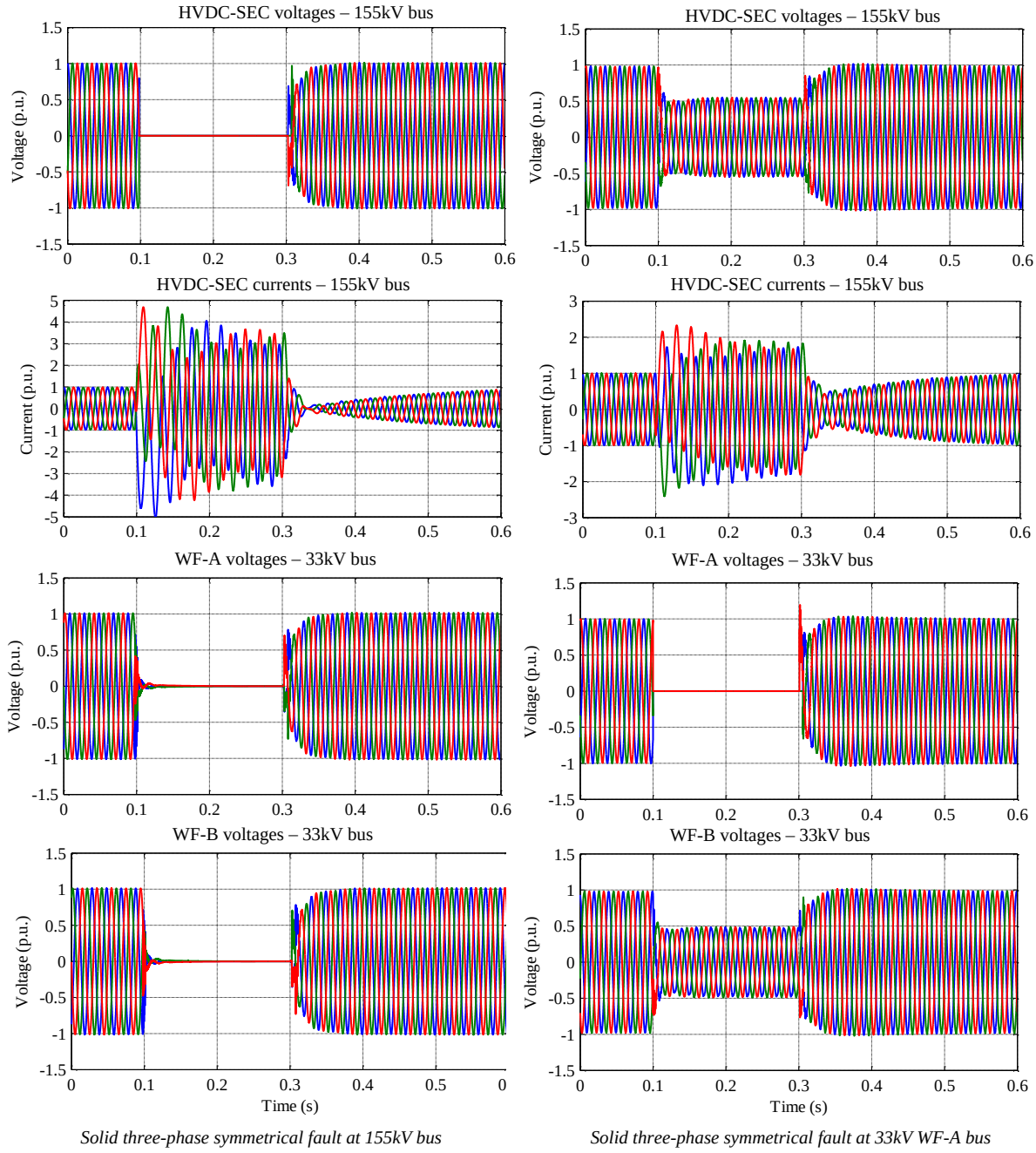

Figure 4-5: Simulation results for three-phase solid fault at 155 kV bus and three-phase solid fault at 33 kV bus of WF-A without IGBTs blocking of HVDC-SEC

4.3.2 HVDC-SEC indirect current limitation during offshore grid faults

The performance of the SEC control strategy with indirect current limitation presented in section 3.7.2 is evaluated in this subsection. A three-phase fault is simulated at the 155 kV submarine AC cable connecting offshore WF-B as shown in Figure 4-3.

The simulation results in Figure 4-6 shows on the right hand side a simulation case with no current limitation by the HVSC-SEC, in reality the IGBT valves of the HVDC-SEC cannot withstand such over-currents and will be blocked. Hence this case is only visualized to show

the voltage dip level and the HVDC short-circuit contribution in case of no current limitation. The performance of the indirect current limitation strategy is shown on the left-hand side of Figure 4-6. As the cable fault is detected, the reference voltage is dropped as function of the fault depth upon a defined over-current threshold (here 1.5 p.u.). Considering the measurement filter delay, the measured impedance drop ($\underline{u}_G / \underline{i}_G$) at the HVDC-SEC terminals can give a faster indicator than the current rise due to the simultaneous voltage drop. A minimum threshold for the measured impedance can be defined (for example 0.5 p.u.) for decreasing the reference voltage.

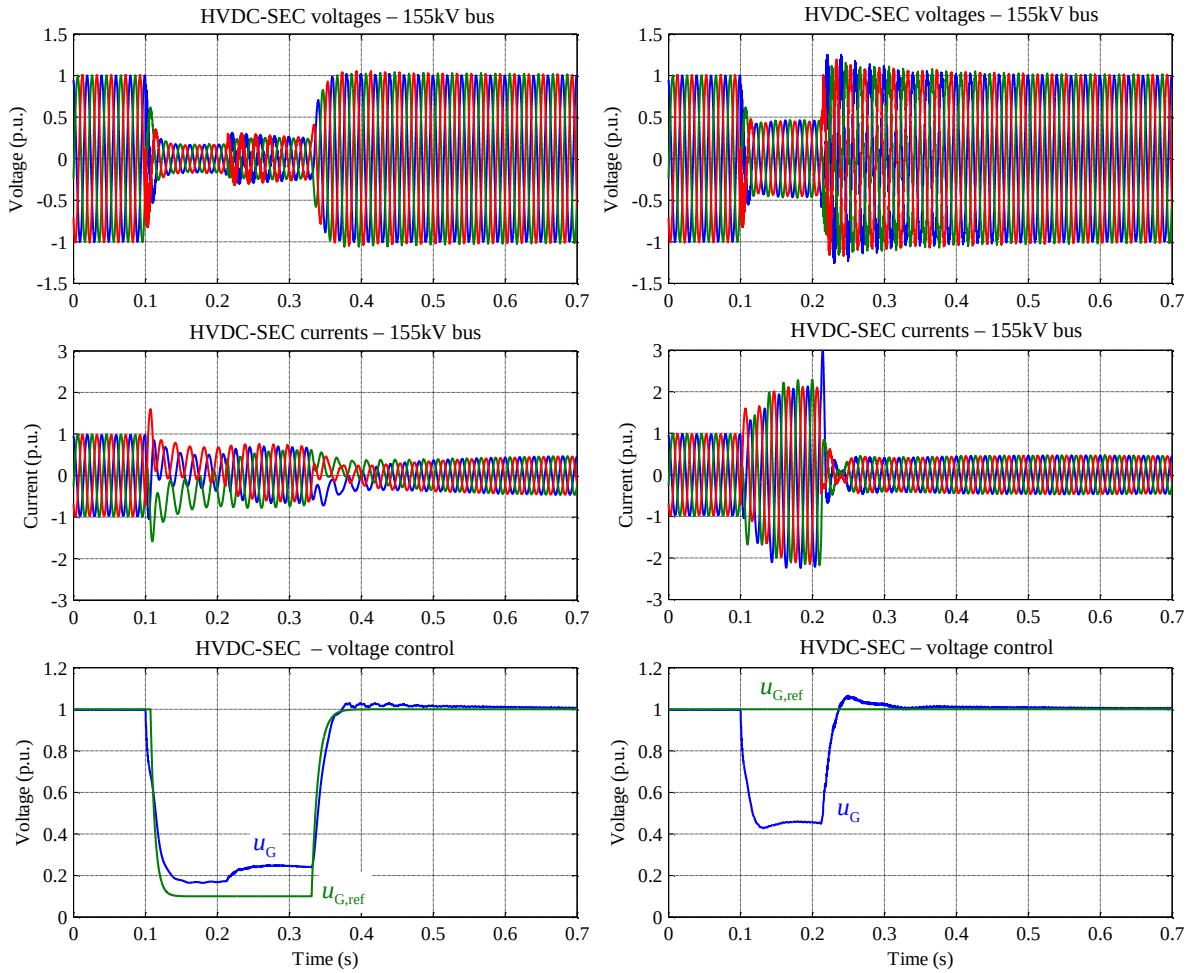

Figure 4-6: Simulation results for three-phase fault at 155 kV cable (WF-B) with indirect current limitation

If the fault is successfully detected and isolated within 100 ms by the protection relays, WF-B will be islanded around the time 0.2 s and must be tripped safely afterwards. The detection of the fault clearance by the HVDC-SEC without any coordination with the protection system in the offshore grid can be challenging, since the only indicator would be the slight increase in the measured phase voltages at nearly 0.2 s which cannot guarantee always that the fault is

cleared. An exact estimation of the possible fault clearing time for different fault types and locations is as well hard in practice. Therefore, the HVDC-SEC can try 'blindly' to ramp up the voltage reference to the nominal value while observing carefully the measured currents and voltages. If the fault is still not isolated, the voltage reference will be dropped again and the control system will initiate another trial after a certain delay, depending on the fault type another current peak might lead to blocking the IGBT valves of the SEC. In the simulation results in Figure 4-6, the fault is successfully cleared after nearly 100 ms. The HVDC-SEC ramps up the voltage reference after a predefined delay of 200 ms.

For very low impedance faults at the HV level (155 kV) the high current peak that cannot be limited in this control strategy leads to blocking the IGBTs of the HVDC-SEC. Figure 4-7 illustrates the simulation results for a stronger fault (very low fault impedance in comparison to the case in Figure 4-6) at the same location in the offshore grid and is successfully isolated after 200 ms. The indirect current limitation cannot act fast enough to limit the current peak; hence the IGBTs at the HVDC-SEC will be blocked when exceeding an upper threshold (set in all simulations to 1.8 p.u.). Consequently, the SEC voltages and currents drop nearly to zero during the blocking period. In this scenario the fault clearance takes around 200 ms due to the high DC components in the short-circuit current of the DFIG based WF. If the HVDC-SEC de-blocks the IGBTs after only 100 ms and tries ramp up the reference voltage, a second over-current event takes place as shown in the same figure and the SEC will be blocked again. Depending on the IGBTs sensitivity of the SEC and the protection philosophy of the offshore WFs, a second de-blocking attempt could be initiated after a certain delay before tripping all components in the offshore grid. In this scenario, the second de-blocking attempt is successful since the fault is isolated and the offshore voltage is ramped up to the nominal value with the offshore WF-A in operation.

In this presented scenario a FRT can be technically challenging and is only possible for certain fault locations and requires fast fault isolation.

The main drawbacks of the indirect current limitation method are:

- The first current peak before the limitation action takes place cannot be avoided. Thus the strategy is limited to certain voltage dip level depending on fault type and R/X ratio.
- Detecting the fault clearance in order to ramp up the reference voltage is a challenging task.

Depending on the offshore grid topology, if the overall protection philosophy does not consider a FRT possibility for strong faults at the offshore HVAC cables and the protection system for blocking the IGBT valves of the HVDC-SEC is reliable, the SEC control strategy with indirect current limitation could be sufficient.

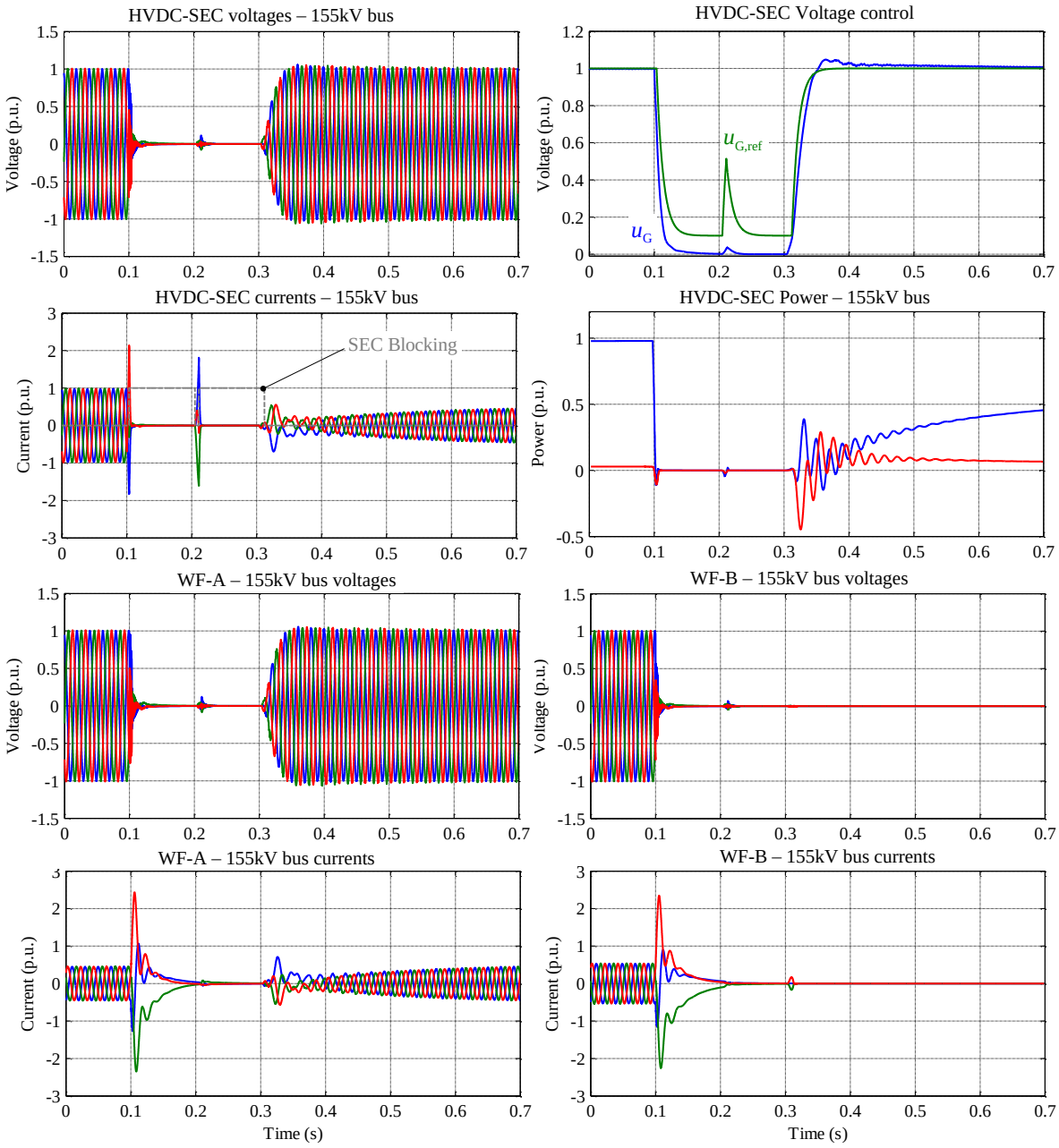

Figure 4-7: Simulation results for three-phase fault at 155 kV cable (WF-B) with indirect current limitation and blocking HVDC-SEC

4.3.3 Offshore grid faults with current-controlled HVDC-SEC

The offshore HVDC-SEC control in this study case is based on the layout in the proposed control in section 3.7.3 (Figure 3-15). Negative sequence current suppression strategy is applied in the different fault scenarios presented in this section. During normal operation, the positive sequence active current i_{G1P} has the priority over the positive sequence reactive current i_{G1Q}. Only during the fault period, the priority is switched to the reactive current. In the following fault scenarios, symmetrical and unsymmetrical faults will be applied on the 155

kV AC cable feeding the HVDC from WF-B as illustrated in Figure 4-3, within 100 ms the fault is cleared by isolating the faulty part of the offshore grid (in this case WF-B) to allow WF-A to ride through the fault and continue operating without interruption. For easier comparison, it is supposed that both offshore WFs have identical pre-fault power flow values with constant wind speed. Therefore, the post-fault steady-state active power at the HVDC-SEC drops by 50% due to the loss of WF-B.

Figure 4-8 shows the simulation results for a solid three-phase fault scenario. During the fault period, the offshore HVDC-SEC limits its current contribution to a defined limit (here 1.1 p.u.) and gives the priority to positive sequence reactive current injection by reducing the active current reference value. Both offshore WFs will experience a heavy fault condition causing the protection systems in the DFIG based WTs to block the MSCs to protect its IGBT valves. As the fault is cleared for WF-A, the WTs will de-block the IGBTs of the MSC and continue feeding in the generated wind power. WF-B will enter an islanded mode where the WTs are tripped after nearly 50 ms from the fault clearance.

One distinctive feature of offshore WF with DFIG based WTs is the high DC components in the short-circuit currents which can delay the activation of the protection relay for several periods until the zero crossing occurs in all phases. For FSCG based WTs the short-circuit currents are defined and limited by the LSC and no DC components exist in such case.

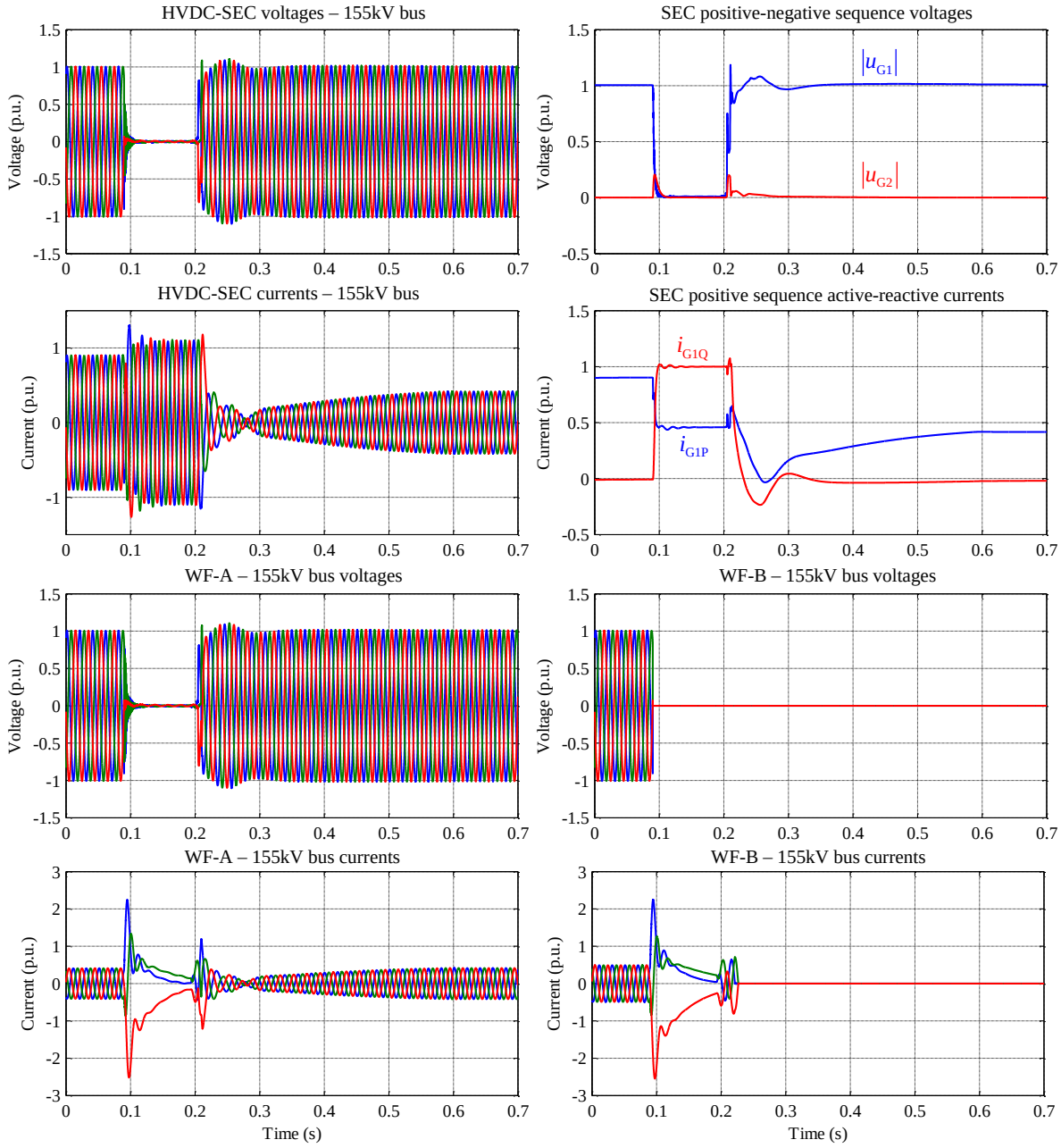

Figure 4-8: Simulation results for three-phase fault at 155 kV bus with current controlled HVDC-SEC

The simulation results of a Line-to-Line fault at the same fault location are shown in Figure 4-9. The short circuit current contribution of the HVDC-SEC is nearly identical to the case for symmetrical three-phase fault. This is due to the negative sequence current suppression in the SEC control. Thus only positive sequence current is injected during the fault with a reactive current priority. The DFIG based WTs provide during the unsymmetrical fault a natural negative sequence current contribution from the stator side as shown in the bottom of the same figure. No negative sequence control is implemented here for the DFIG based WTs.

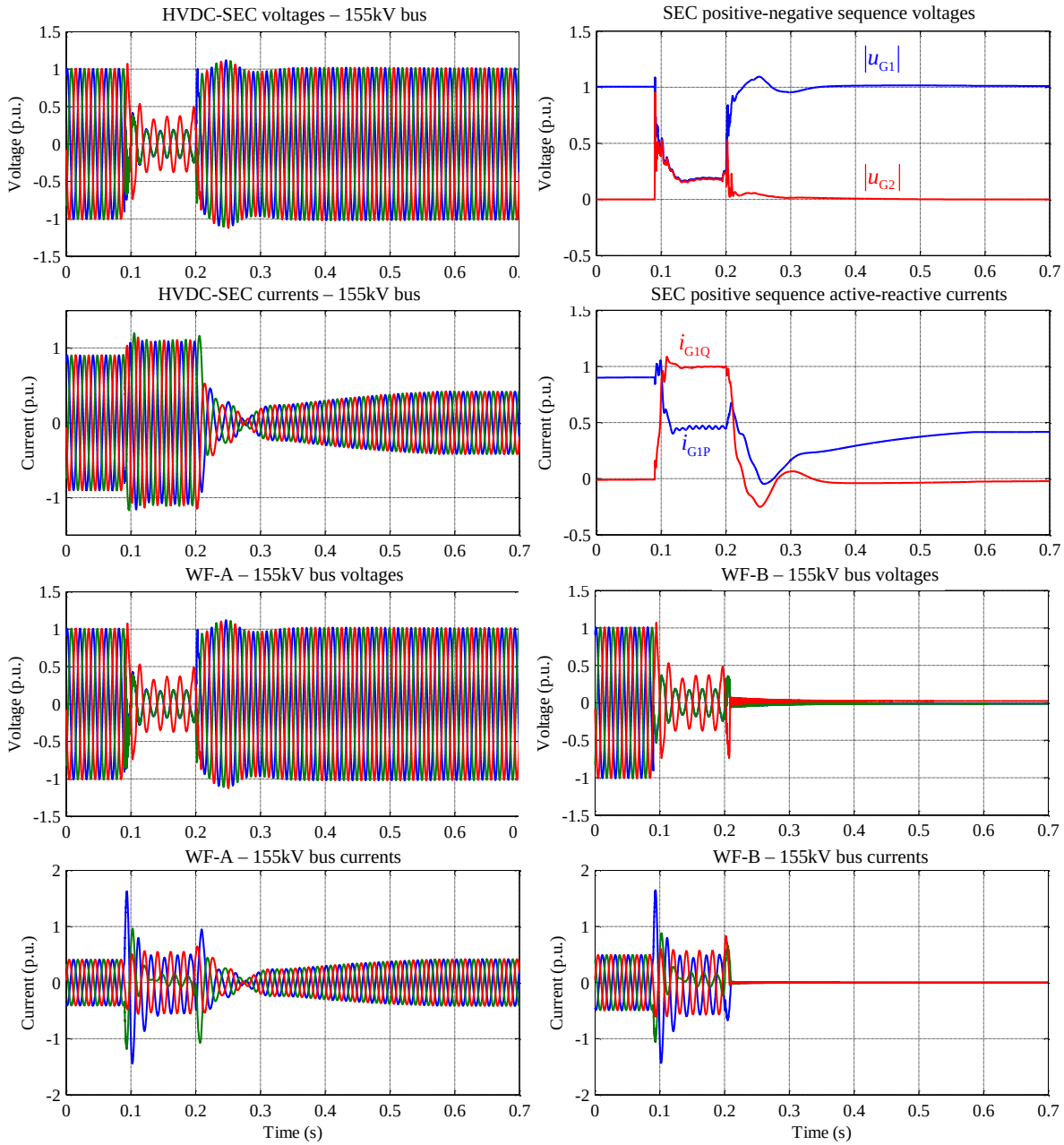

Figure 4-9: Simulation results for Line-to-Line fault at 155 kV bus with current controlled HVDC-SEC

The simulation results for a SLG fault at the same fault location are presented in Figure 4-10. Similar to the case of line-to-line fault, the HVSC-SEC injects only a positive sequence current with reactive current priority during the fault.

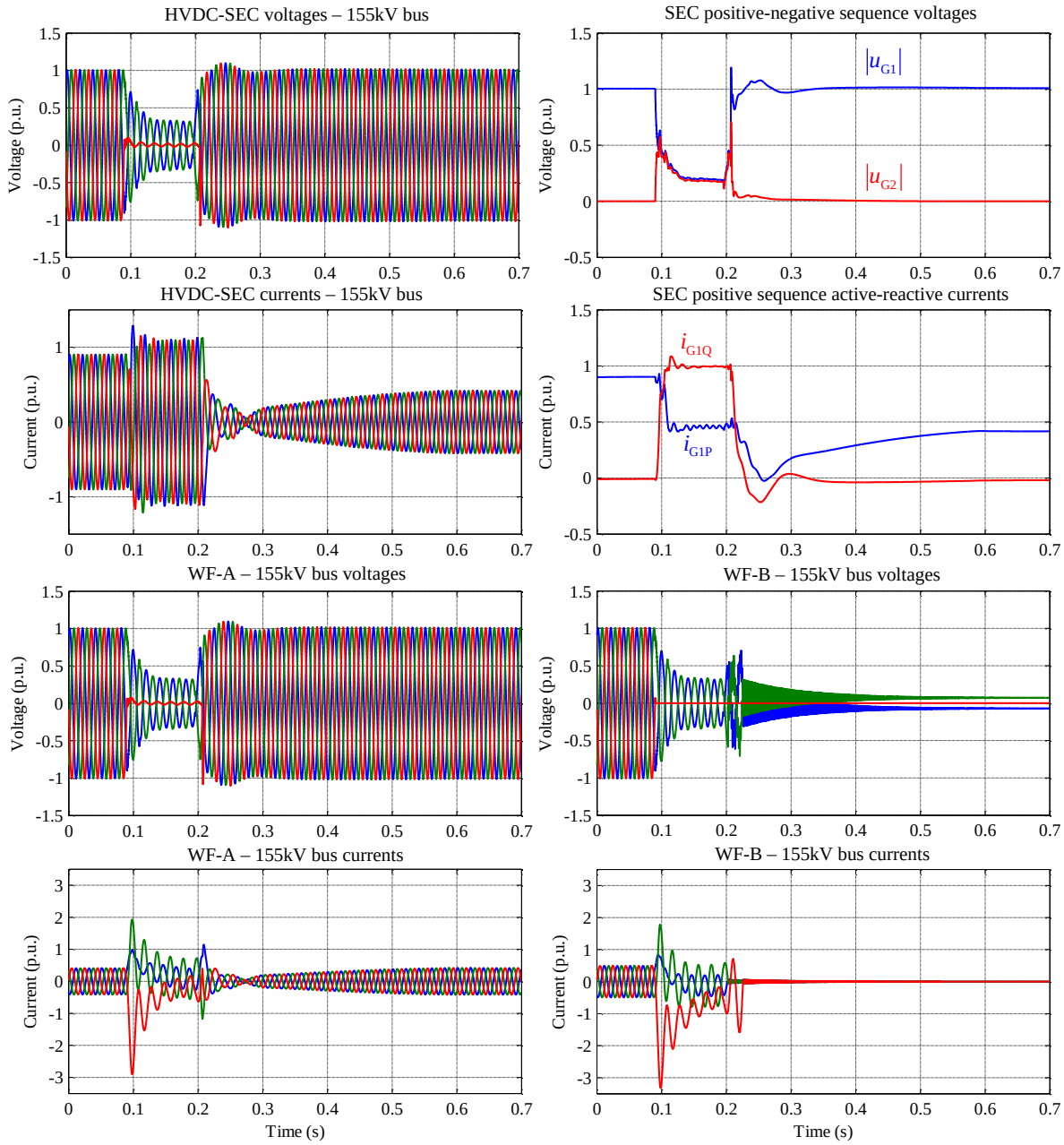

Figure 4-10: Simulation results for SLG fault at 155 kV bus with current controlled HVDC-SEC

4.4 Summary

The SEC with the presented indirect current limitation strategy is unable of limiting effectively the short-circuit current peak during nearly faults with deep voltage sag which leads to blocking the IGBT valves of the SEC. The de-blocking procedure is only successful when initiated after fault clearance. With Current control strategy and for a well-designed controller, the short-circuit currents are always limited independent from the fault strength. A FRT without blocking the SEC in this case is possible if the fault was successfully cleared.

Current-controlled converters can excite resonances in the range up to 500 Hz [36][37], both the current controller and the PLL of the SEC should be therefore carefully parameterized to avoid any undesired control interactions with the WT current-controlled converters that would lead to poor damping or in worst-case scenario to un-damped behavior. Thus a considerable advantage of the indirect current limitation method over using current controllers is reducing the possibility of controller interactions between the HVDC-SEC and the offshore WTs converters. However, if the designed SEC current controllers provide a stable behavior and do not trigger any undesired control interactions based on simulation tests with accurate models of both the HVDC system and the offshore WF, the afore-mentioned advantage of employing the indirect current limitation method would be no longer substantial. In principle, the outcome of evaluation studies on possible control interactions cannot be generalized to all offshore WFs projects, since even for similar WT types no standards exist for the WT converter controllers and the related short-circuit behavior of WTs.

5 Frequency support by VSC-HVDC connected offshore WTs

Modern multi-mega WT systems as previously discussed are mostly available nowadays in two types: DFIG (type 3) and FSCG (type 4). In the FSCG configuration the stator circuit is connected to the grid through the frequency converters which decouples totally the generator from the grid frequency, while the rotor frequency of the DFIG is almost decoupled from the grid frequency by means of frequency converters in the rotor circuit. This means that modern wind generation systems do not naturally possess the inertial response for frequency disturbance events as the case for synchronous generators of conventional power plants. Moreover, the VSC-HVDC transmission system introduces additional decoupling of the onshore and offshore side AC networks. This chapter explores and evaluates the existing strategies that can enable the offshore WFs to participate in the grid frequency control with focus on the primary frequency response. Improvements to those control strategies are proposed through combined control strategies. A new control strategy is proposed here and its performance is compared with other existing strategies.

The most common type of disturbance in an interconnected grid is associated with a loss of generation unit, which causes a temporary decline in frequency, before it starts to recover by means of primary and secondary frequency control. In this chapter an overview on the frequency support strategies by WTs during under-frequency events will be given.

Overfrequency events caused by a sudden loss of load or energy excess in a grid is discussed in chapter 6.

5.1 Frequency response characteristics

To ensure stable and reliable power transmission the frequency must be maintained within certain boundaries, this can be achieved by fast response to generation-load imbalances in the grid. The controllability, characteristics and response time of both generation units and loads are key aspects for defining the frequency control strategy of the whole grid. In general the frequency control can be classified into three main levels [41]:

- Primary frequency response/control: it is initially shaped by the inertial response in the first few seconds followed by the system governor response which can last for 30-60 s. Load response by typical rotating motors participates in shaping this frequency response (load-frequency dependency). The primary control is characterized by being proportional and predominantly local with fast time reaction.

- Secondary frequency control: represents centralized and quasi-static actions on a slower time scale (minutes) which provide balancing services to restore the frequency to its nominal value. Most common terms associated with this response are "Load-Frequency control" and "Automatic Generation control" and is related to manual or automatic dispatch from a centralized control system. The secondary control represents an integral control action to eliminate the frequency offset.
- Tertiary frequency control: after restoring the frequency level to its pre-disturbance scheduled value, the tertiary control replaces the secondary to reestablish the planned reserves in different areas of the grid. An important aspect is that tertiary control actions have a net zero effect regarding frequency level. As a result, the grid reserves are reconfigured again to be ready to response to new disturbances. The time range of this control phase is from couple of minutes and last for several hours.

In this thesis the focus will be only on the primary frequency response and the control strategies that can enable the offshore WFs to participate in the primary frequency control. A similar but mirrored frequency response can occur in a grid caused by a sudden loss of a load. Figure 5-1 shows a typical frequency response with the focus on the primary and secondary control periods.

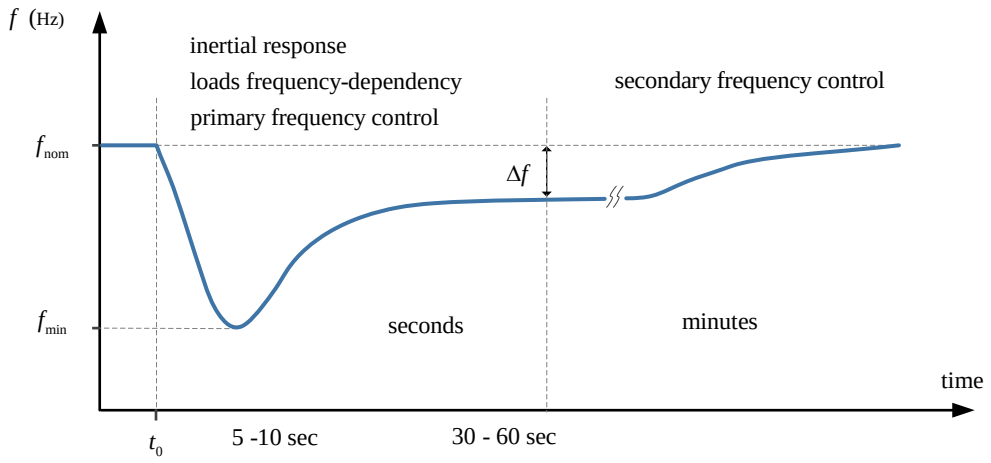

Figure 5-1: Frequency response following a sudden loss of generation in the grid

Over and underfrequency events occur due to sudden generation-load power imbalance in the electrical power system. The power imbalance ΔP_{imb} can be simply expressed as:

$$\Delta P_{\text{imb}} = \sum P_{\text{gen}} - \sum P_{\text{T,losses}} - \sum P_{\text{Load}} \tag{5.1}$$

Where $\sum P_{\text{Load}}$ the sum of all loads and $\sum P_{\text{T,Losses}}$ is the sum of all transmission losses in the considered network. Equation (5.1) neglects frequency and voltage dependencies of the loads. In steady-state and according to the swing equation, the RoCoF can be defined as:

$$\frac{\mathrm{d}\omega_{\mathrm{S}}}{\mathrm{d}t} = 2\pi \frac{\mathrm{d}f_{\mathrm{S}}}{\mathrm{d}t} = \frac{\Delta P_{\mathrm{imb}}}{2H_{\Sigma}} \tag{5.2}$$

Here f_{S} represent the network frequency, while H_{Σ} is the total inertia time constant in the network defined in seconds. The variation in the transmission losses during the first seconds of the power imbalance can be considered unchanged; hence the power imbalance represents solely a variation in load or generation power [43]. Equation (5.2) shows that the RoCoF is inverse proportional to the inertia time constant. As the share of inertia-less generation units increase in a network, the RoCoF will increase according to the given relationship. The transient response of a power system to a power imbalance caused by a loss of generator starts initially with rotor swings in all other the generators [44]. The next stage will be a frequency drop caused by the slowdown of the generators due to the power imbalance. During this stage each generator responses to the power imbalance according to its inertia time constant. The primary frequency control stage takes place afterwards which mainly depends on the overall spinning reserve and the generators governor in the power system. The load reaction to the frequency drop also contributes to the dynamics in this stage.

5.2 Frequency control modeling aspects

RMS-type simulation models are used for all frequency studies in this thesis since the focus in such studies is on the electromechanical coupling interactions in the electrical grid. Furthermore the simulation effort is highly reduced when considering simulation time of 60-140 s. The simulation models where developed in the simulation environment DIgSILENT PowerFactory with a simulation time step of 1-5 ms.

5.2.1 Enabling frequency control by offshore WF via HVDC connection

In principle, frequency control methods by offshore WFs target only the main onshore grid frequency. The offshore WF frequency is not an indicator of disturbances in the main grid due to the frequency decoupling by the VSC-HVDC system. Thus the grid frequency deviation must be made available for each offshore WT to be able to contribute to the primary frequency control. This can be done either by sending the grid frequency measurement through a communication link from the onshore station or by replicating the grid frequency on the offshore side through the artificially coupling of the AC frequencies at by a modulating the DC voltage as a function of the onshore frequency [4][45][46]. In this strategy, the onshore HVDC-REC varies the DC voltage as a function of the frequency deviation according to a defined linear characteristic with a certain dead band. The variation in the DC voltage is

then detected by the offshore HVDC-SEC and translated into a deviation in the reference frequency at the offshore side. If both under- and Overfrequency conditions are replicated at the offshore grid, the resulting DC voltage deviation should be kept under the activation threshold of the DC protection chopper. This issue can be critical near full-load operation of the HVDC where the steady-state DC voltage is at its highest level compared to no-load operation.

In case of reliable communication signal, the measured onshore frequency can be used as the reference frequency for the offshore grid. In principle, a communication delay of no more than a few tens of milliseconds does not have a big impact on the control performance regarding the frequency response.

5.2.2 Inertia emulation by VSC-HVDC

In the published ENTSO draft [55] it is stated that transmission system operator (TSO) has the right to require that the HVDC connection should provide inertia emulation capability in response to frequency changes. Thus the HVDC converters should be capable if required to control rapidly the active power flow to limit the RoCoF. So far no specific requirements are defined regarding the inertia emulation control concept and its performance parameters. For HVDC systems interconnecting two active AC grids, the inertia emulation is realized by detecting the frequency deviation in the HVDC converter controlling the active power flow. The HVDC converter is able in this case to adjust rapidly the active power and thus emulate the inertial response. In case of integrating offshore WFs via HVDC system, a direct active power control at the offshore HVDC SEC will cause undesired controllers' interactions with the offshore WF power controllers and likely leads to instabilities in operation. Therefore, a coordination control strategy with the offshore WF must be implemented to provide the desired inertia support for the onshore grid.

In [57] an inertia emulation strategy by the HVDC system is proposed by utilizing the stored energy in the DC capacitors installed at the HVDC link. Once a frequency deviation occurs, the DC voltage controller quickly responds by changing the DC voltage level to provide an active power response which emulates a certain inertia time constant. The DC capacitors should have an energy storage capacity sufficient to obtain an active power response that can last for a couple of seconds which can limit effectively the RoCoF. The DC capacitors installed typically at each converter station reduces the harmonics ripple on the DC voltage [17] and provide certain energy storage with sufficient DC time constant to allow controlling the power flow. In the normal design, the stored energy in the DC capacitors is equivalent to a

time constant of around 2 ms of full power transmission [17]. The relation between the capacitance C_{DC} and the DC time constant τ_{DC} are defined as:

$$C_{\mathrm{DC}} = \frac{2E_{\mathrm{C}}}{V_{\mathrm{DC,nom}}^2} = \frac{2P_{\mathrm{DC,nom}}\tau_{\mathrm{DC}}}{V_{\mathrm{DC,nom}}^2} \tag{5.3}$$

$$\tau_{\mathrm{DC}} = \frac{V_{\mathrm{DC,nom}}^2 C_{\mathrm{DC}}}{2P_{\mathrm{DC,nom}}} \tag{5.4}$$

with the capacitor energy E_{C}.

The required power balance is obtained through maintaining the DC voltage level at the onshore REC while variable wind power is transmitted by the offshore SEC station. Thus under normal design considerations with $\tau_{\mathrm{DC}} = 2\ \mathrm{ms}$, the energy stored in the DC capacitors cannot provide sufficient power response to emulate an inertia response. In [57] however, the HVDC capacitance was chosen to provide a time constant of nearly $\tau_{\mathrm{DC}} = 500\ \mathrm{ms}$ in order for the HVDC to be able to provide a considerable synthetic inertia response. Even with such a high DC capacitance, a significant frequency support cannot be achieved. This means much higher investment costs for significantly larger capacitors are required. As long as energy storage in the DC link brings no significant economic advantages nor strictly required through grid requirements, this HVDC emulation strategy do not seems to offer an attractive solution. In the following sections, strategies for enabling inertial response and frequency support by the offshore WFs are discussed. The frequency deviation at the onshore grid is supposed to be replicated at the offshore grid by the HVDC SEC as proposed in the design of the SEC control in section 3.7.

5.2.3 Test grid

A two-area, weakly coupled test grid is used in this frequency study as given in Figure 5-2. The hydro power plant is assumed to have a primary power reserve of 15% (nearly 200 MW). The thermal plants only respond to frequency changes in accordance with their inherent grid coupling property and therefore do not participate in the primary frequency control. The inertia time constant *H* is set for all Synchronous generators to 10 s.

The loads L1 and L2 each have a value of (1000 + j100) MVA, while L3 is a larger load of approximately (1900 + j150) MVA. The frequency dependency of the loads has been considered in the load models. The smaller load L21 (Figure 5-2) with a value of (160 + j50) MVA is used to test the frequency response of the grid. For under-frequency studies the load L21 will be switched on at one instant to the grid, this results in a frequency drop to nearly 49

Hz (in a 50 Hz-system) without any controlled influence by the offshore WFs with VSC-HVDC connection.

The minimum underfrequency level before activating load shedding protection relays is supposed to be 49 Hz. Since the focus of this work is on the control strategies that enable the offshore WFs to participate in the primary frequency control, no load shedding scenarios are considered for investigations.

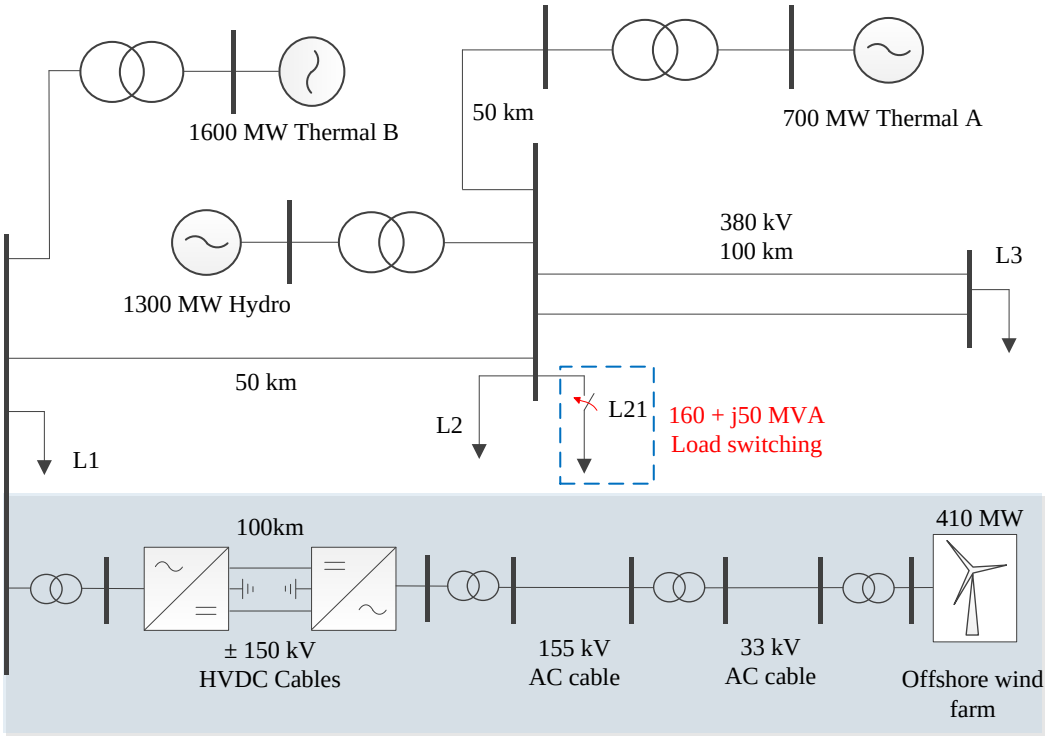

Figure 5-2: Test grid for frequency stability studies

The total generated power of conventional plants adds up to 3.6 GW, in addition to the offshore wind power of approximately 400 MW. Table 5-1 shows the share of each generation unit in the test power system of Figure 5-2. The wind power share of generation is about 10% in this case. In the simulation studies the wind share will be varied to analyze the effect on the frequency response. In appendix A.4, the power generation in the test power system is presented for the cases with 20%, 50% and 70% wind power share. The offshore WF is supposed to be consisting of DFIG based WTs and is aggregated by one equivalent unit. Variations of the wind speed during the primary frequency response period will be neglected in the simulation studies in this thesis.

Table 5-1: Active power distribution for the scenario with 10% wind power

Power plant	Active power output	share of total generation	Reserve power
Thermal plant A	800 MW	20 %	0 MW
Thermal plant B	1600 MW	40 %	0 MW
Hydro plant	1200 MW	30 %	200 MW
Offshore WF	400 MW	10 %	0 MW
Total	4000 MW		200 MW

The governor of the hydro power plant is modeled according to [47], the hydro governor model is shown in Figure 5-3.

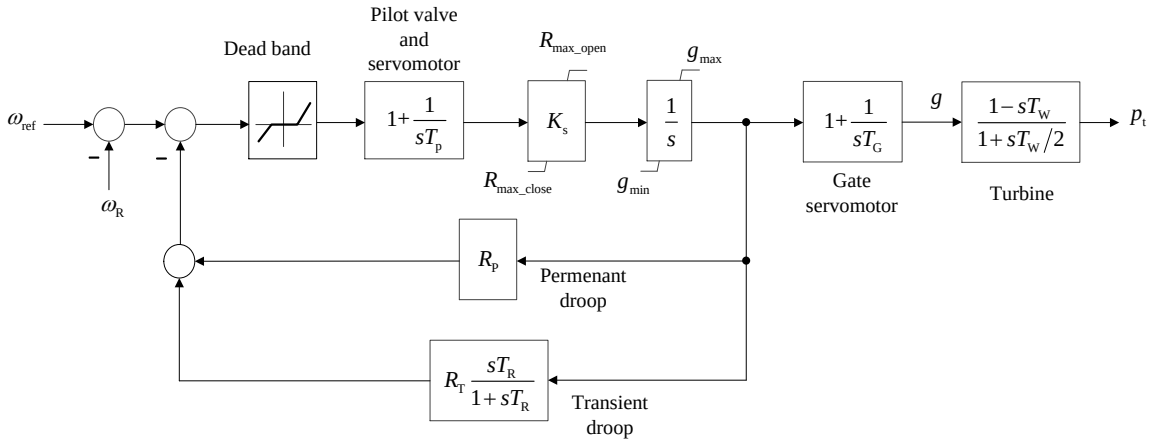

Figure 5-3: Hydro turbine governor model [47]

The primary frequency response at the hydro plant is shown in Figure 5-4.

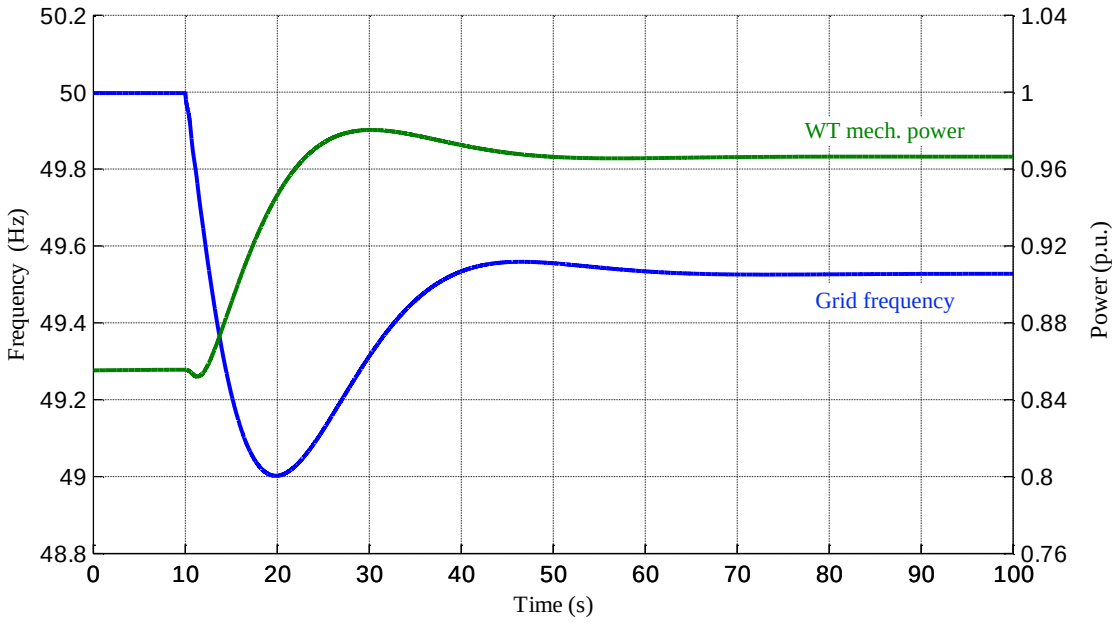

Figure 5-4: Typical primary frequency response of a hydro turbine governor

5.2.4 Influence of wind power share on the primary frequency response

The wind power in a grid is variable by its nature and during low wind speeds the required energy demand is covered by the rest of the synchronous generators in the grid. It is assumed however in all following frequency studies that the wind speed is constant during the primary frequency response period.

One aspect of studying the impact of integration of large wind power into a grid is to analyze the primary frequency response for different wind share levels. In other words, the synchronous generation units will be replaced by non-synchronous generation units which are the HVDC connected offshore WTs in this case. For this purpose, the thermal plants in the test grid (Figure 5-2) are replaced gradually by wind power. The 10% wind share case is considered as the reference case (Table 5-1). In appendix A.4 the grid generation data for each generation unit are presented for 20%, 50 % and 70% wind share cases. The hydro plant generated power share with its defined reserve is kept unchanged for the different cases. The hydro governor parameters are also kept constant for all cases.

As observed in Figure 5-5, with the increase of wind power share the RoCoF increases due to the drop of the total network inertia. The weaker inertial response leads to a stronger frequency drop as the wind share increases. The frequency response for the case with 70% wind share shows a small oscillation behavior.

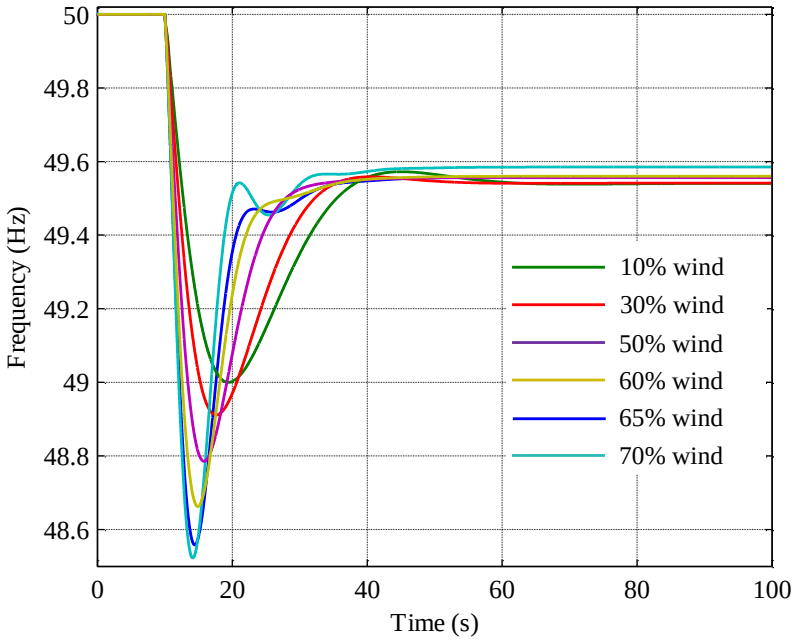

Figure 5-5: Primary frequency response for different wind share levels and same load switching event

For a better understanding of the wind share effect on the primary frequency response of the test grid, the power in MW of the additionally connected load is reduced as the wind share

increases to obtain the same minimum frequency level for different wind shares as shown in Figure 5-6. The hydro governor parameters are kept unchanged for all cases. As wind share increases and total inertia of the grid drops, the RoCoF increases and the minimum frequency level of 50 Hz is reached faster as seen for the case of 70% wind power share. Interestingly, the hydro governor action has a stronger impact on the frequency as the inertia level decreases in the grid. This effect takes place due to the increased frequency sensitivity to changes in the active power. For the 70% wind power share case, only the hydro plant is electromechanically coupled to the grid and its governor needs less reserve power to increase the settling frequency level in comparison with the other cases with lower wind power share. The impact of the governor proportional gain on the hydro turbine power can be clearly observed in Figure 5-6.

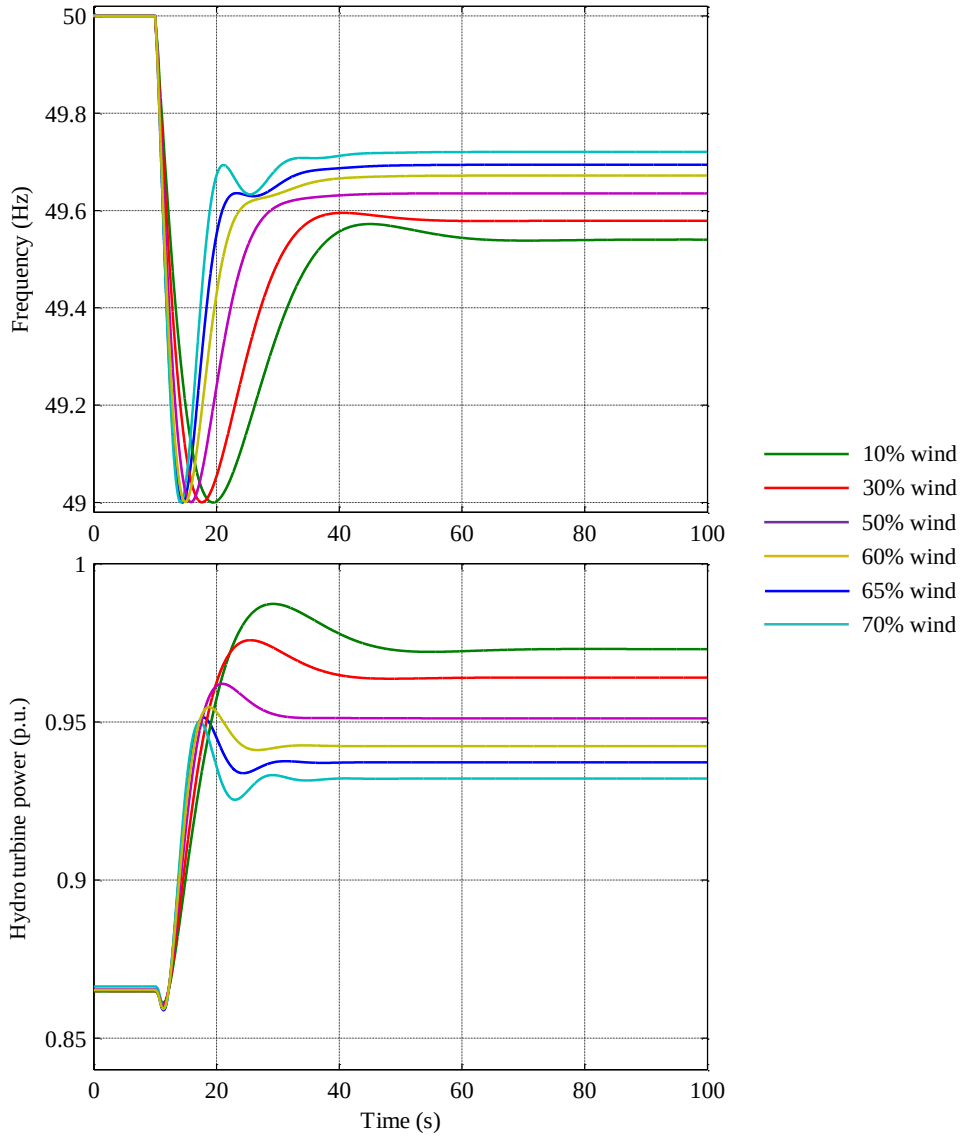

Figure 5-6: Primary frequency response for different wind share levels and same minimum frequency level

5.3 Frequency control by WTs during under-frequency events

Generally, the concepts for the frequency control by WTs can be divided into two categories:

- Frequency control with a defined power reserve (with de-loading).
- Frequency control without power reserve (without de-loading).

The first concept proposes de-loading the wind generator to create a specific power reserve to be always available during normal operation, while the latter concept targets only the release of the naturally stored kinetic energy in the WT rotor. In the following sections, the WT speed and pitch control with the power conversion model introduced in sections 2.2.3 and 2.2.4 will be extended to enable the WT to provide primary frequency support.

5.3.1 Frequency support by de-loaded power operation

This is a well-known concept which is based on maintaining continuously a considerable reserve capacity of active power during the WT operation to be used for frequency support. The idea is to drive the WT at a lower active power output than the possible value given for the actual wind speed, in other words the WT will have to operate in a de-loaded power mode. Methods for de-loading the WT are presented in the following.

5.3.1.1 Frequency support by Over-Speeding operation

This strategy suggests controlling the wind generator to run always at higher rotor speeds than the designated one for the same wind speed, thus leading to a reduced power output at each operating point [42]. As a result a defined amount of kinetic energy is stored in the rotor during the normal operation time. At the event of frequency drop, this extra kinetic energy is released through a modification in the active power reference of the WT control. This method has serious drawbacks such as the use of the wind speed as an input variable and the mechanical stresses that results from increasing the rotor speed above the nominal values for a long period. Additionally, operating with high slip values has a negative effect on the MSC and LSC in for the DFIG base WTs.

5.3.1.2 Frequency support by pitch control (FSPC)

In this control strategy no over-speeding is used for active power de-loading. The de-loading is alternatively achieved by introducing a pitch angle deviation $\Delta\beta_o$ in the pitch control which corresponds to the desired reserve capacity Δp. In this manner, the pitch actuator will always keep a defined pitch angle value at an operating point. Thus at any instant it is possible through pitching the rotor blades to release a defined amount of energy into the grid for

frequency support. This strategy is clearly superior to the over-speeding strategy because the WT is de-loaded without having serious adverse effect on the mechanical and electrical components. Figure 5-7 shows (in blue) a possible scheme to realize the FSPC, the pitch control modification with the extra steady state offset $\Delta\beta_o$ requires extensive knowledge of the behavior of the WT mechanical system, since this offset has to be calculated and changed for nearly every new operating point and the reference rotor speed ω_{R_ref0} of the pitch control must be adjusted accordingly. The control action is realized by the angle deviation $\Delta\beta_{FS}$ determined by frequency deviation and proportional gain K_{FS}. The communication and measurement filter time delays are considered in the measured frequency signal. A washout filter can be used if acting only on transients is required.

The obvious drawback of this method is that it limits the generation ability of the WTs by operating continuously in a de-loaded power mode. Therefore the total energy production is reduced for the long term. In this study a de-loading of around 7% is assumed to be reserved for the frequency support.

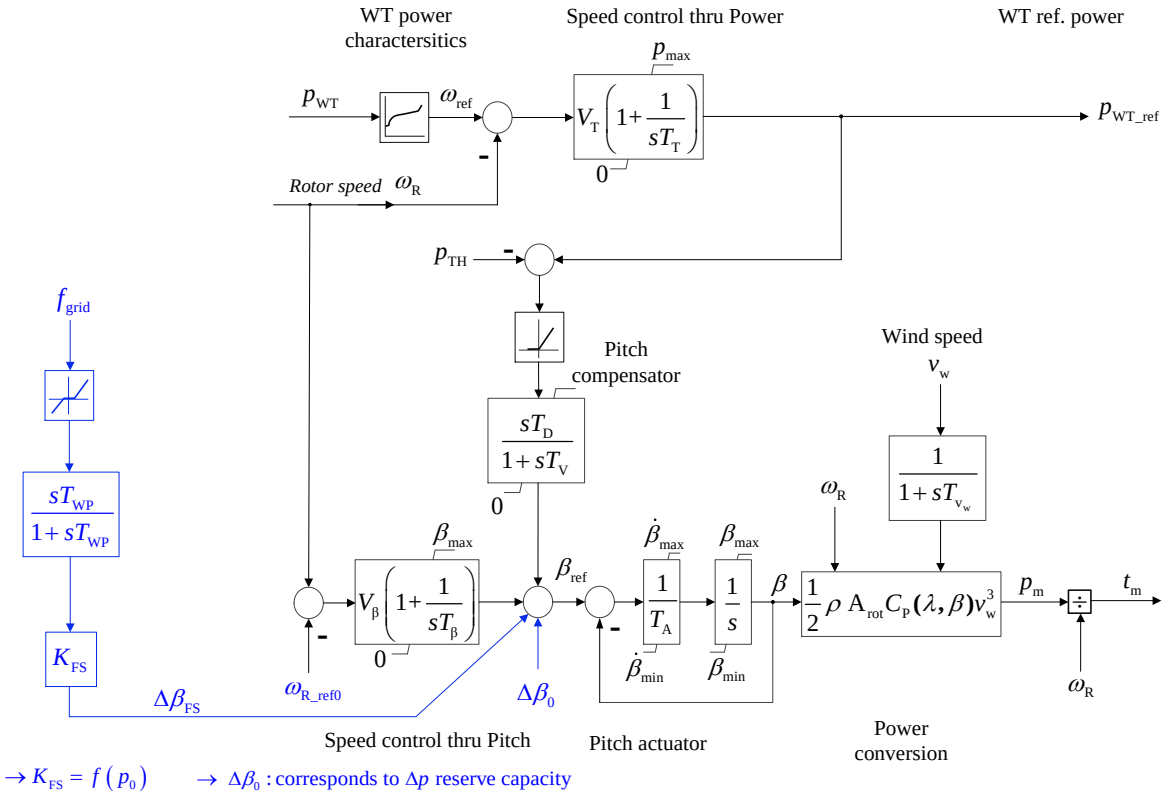

Figure 5-7: WT Power control and conversion with added FSPC

I. Partial-load operation - under nominal wind speed

When the wind speed level is under nominal speed value (here 1.2 p.u.), the pitch control is normally inactive and the pitch angle β will be zero. Figure 5-8 shows the performance of

the FSPC strategy for an operating point under nominal wind speed (wind share is 10% of total generation in the grid). A high time constant (1000 s) is set for the washout filter to show solely the proportional response of the control. The power de-loading level is about 7% as shown in the same figure which corresponds to $\Delta\beta_o = 2.5°$ (for $\beta_{\text{ref}} = 0$). The FSPC strategy is able to support the inertial response and also participate in raising the frequency until the secondary control takes place. A further de-loading of the WT will obviously limit the frequency drop much further as long as the pitch actuators are fast enough to release the reserved power before the frequency hit its minimum. From an economic point of view as a WF operator, the de-loading percentage should be as less as possible in order not to affect significantly the energy production level. On the other hand, the grid operator prefers that WFs participate effectively in the primary power reserve especially when the wind power share is high in the grid. A trade-off must be taken into account considering these two aspects.

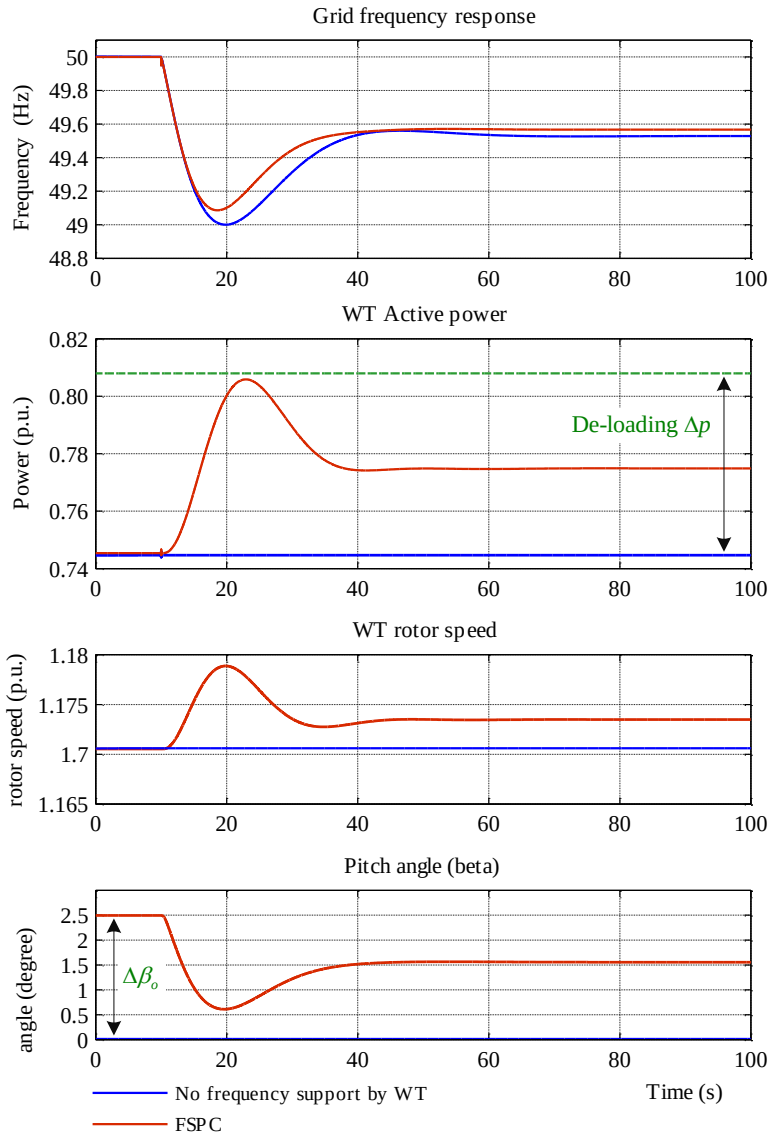

Figure 5-8: Primary frequency response with FSPC for operation under nominal wind speed

II. Full-load operation – above nominal wind speed

The same de-loading concept can be in principle applied during high wind speed. However, during high wind speed conditions, the pitch controller limits actively the mechanical power through controlling the rotor speed according to the given reference value. Considering that the WT can be slightly overloaded (up to 1.05 p.u.) for a couple of seconds within defined rotor speed limits (up to 1.3 p.u.) without having adverse effects on the WT operation, FSPC scheme can be extended to allow considerable frequency support without De-loading during high wind speeds. As the wind speed exceeds the nominal value, the pitch control will increase the pitch angle β accordingly. In this case the WT control can reduce gradually the de-loading offset $\Delta\beta_o$ until it reaches zero after a certain high wind speed. Figure 5-9 shows the improved FSPC by adding the offset signal $\Delta\omega_{FS}$ (in red) to the input of the pitch controller, which forces the pitch controller to decrease the reference pitch angle and therefore increase the mechanical power during the frequency drop.. In general, the added offset $\Delta\omega_{FS}$ has a weaker effect, if any, on the FSPC response during low wind speeds (under nominal value).

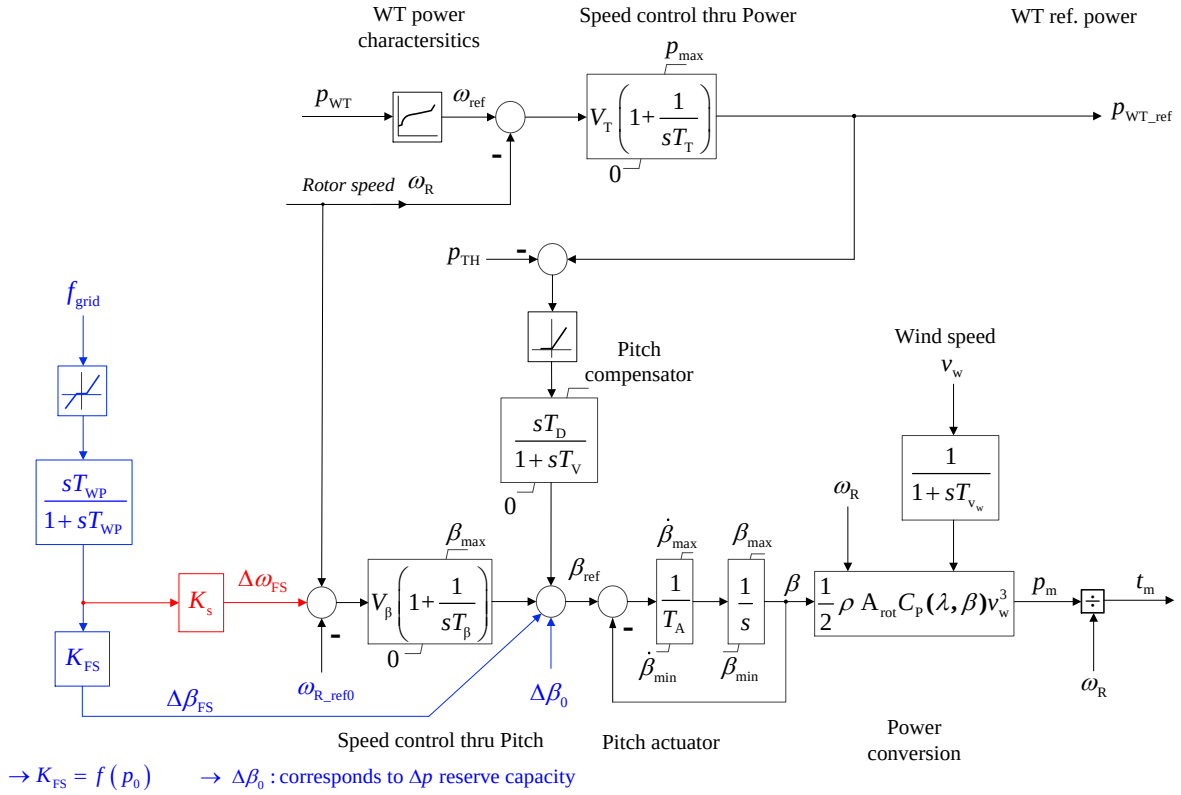

Figure 5-9: WT Power control and conversion with improved FSPC

Figure 5-10 provides a comparison between the performance of the de-loading method (dashed green line) and the improved FSPC (in red). A 7 % de-loading at this operating point

is realized with an offset $\Delta\beta_o = 1.5°$ (for $\beta_{\text{ref}} = 6°$). A high time constant (1000 s) is set for the washout filter to allow clear comparison of the settling values in both cases.

The steady-state value of the pitch angle is 6° by nominal rotor speed (1.2 p.u.) and nominal active power (1 p.u.), the improved FSPC decreases temporarily the pitch angle to allow the frequency support by overloading the WT for a short term. However, the stead-state power/speed overloading might not be permissible by the WT manufacturer for a long period; this means the WT will have to restore the original pitch angle ending thereby the frequency support action. It is clear from Figure 5-10 that primary frequency response using FSPC with de-loading is superior to the case without de-loading; nevertheless, avoiding de-loading during high wind speed seems to be a good compromise to rise up the total energy generation yield for the long term while keeping a relatively acceptable level of frequency support for different operating points.

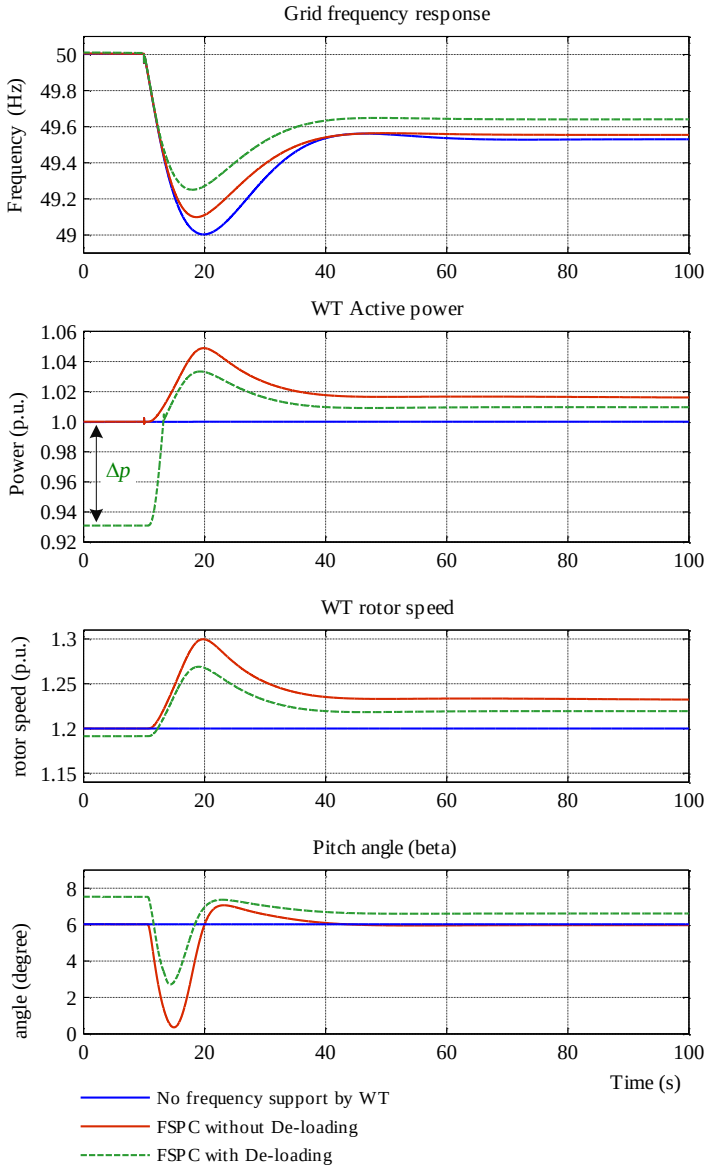

Figure 5-10: Primary frequency response with FSPC - above nominal wind speed operation

- ***Frequency Support Duration***

The frequency support by the WF can be assigned only for the primary frequency response period (typically up to 60 s) or could be extended for a couple of minutes. After the support period the WT should reduce its output power again to build the assigned power reserve. As discussed before, in case of FSPC without de-loading during high wind speeds a fast restoring of the pitch angle might be required to keep both power and speed within their steady-state limits. In the FSPC scheme, the support duration can be realized by adjusting the washout filter time constant, which determines the frequency support duration as shown in Figure 5-11. The frequency nadir is nearly the same with different settings of the washout filter time constant.

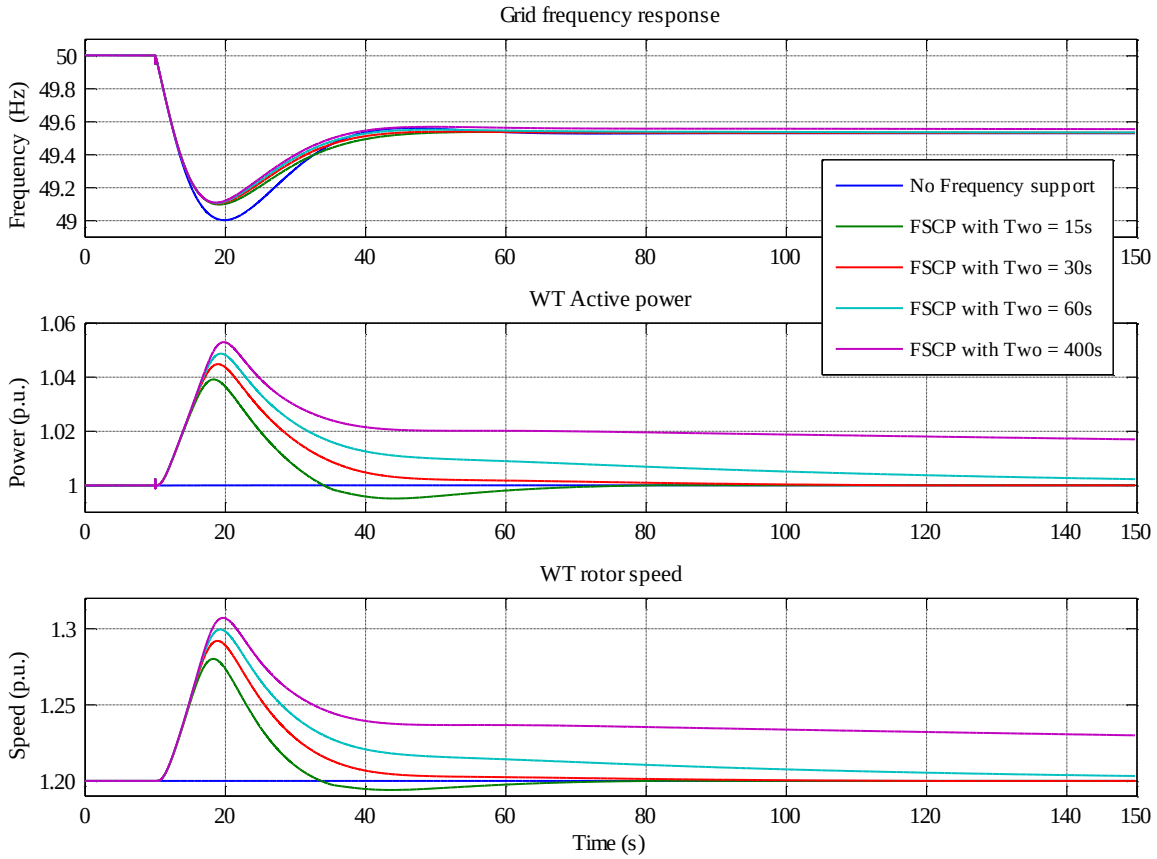

Figure 5-11: Primary frequency response with FSPC for different washout filter time constants

Alternative methods target releasing the kinetic energy stored in the rotating mass of the turbine rotor without the need for a de-loaded power operation as in FSPC. These methods will be addressed in more depth in the next sections accompanied with simulation results.

5.3.2 Frequency support by kinetic energy control (KEC)

Inertia control schemes are proposed for the WF in [48] , where the active power control at each WT is extended to respond to a drop in grid frequency by releasing the kinetic energy in

the rotating masses for a limited time and within the allowable range of the WT rotational speed. Compared to frequency support by pitch control, the main advantage of this strategy is that it does not entail foregoing any energy from the WT during normal operation. Additionally the KEC methods target the emulation of the inertial response in the synchronous generators of conventional power plants and thus should possess a faster response than the FSPC strategy which is limited by the pitching speed of the actuator.

Two KEC control strategies for utilizing the energy of the rotating masses are presented and analyzed in this thesis. The first (KEC I) represents a common, intuitive approach, while a second, less intuitive approach (KEC II) is introduced in [48] and will be evaluated in the following sections. The evaluation of KEC concepts will focus only on their impact at different WT operating points and their interaction with pitch controller at high wind speeds.

5.3.2.1 KEC I

KEC I is a well-known method for extracting the kinetic energy from the rotating masses of the WT which has been presented in several pervious works [48][49][50].

Figure 5-12 shows the proposed realization of the frequency support strategy KEC I in [48]. The washout filter is utilized to act only on transient frequency changes. The actual control action is realized by the lead-lag compensator and the proportional gain K_I, a dead band is applied to reduce the sensitivity of the controller. To ensure stable operation for all operating points, KEC I is limited to a specific rotor speed range.

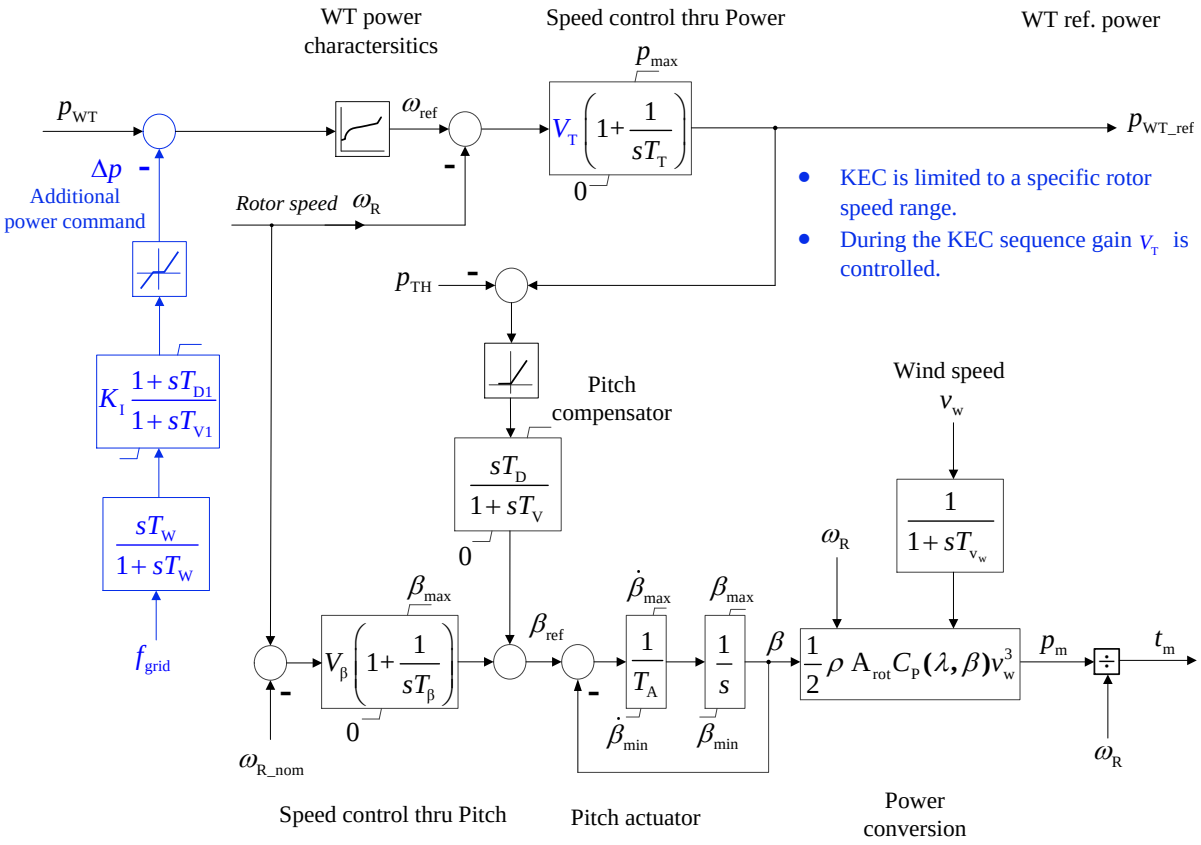

Figure 5-12: WT Power control and conversion with KEC I control structure [48]

Although there are some differences in the realization of the controller for KEC I, the behavior of the WT is more or less the same, which is described in two phases as following:

I. Support phase: WT controlled to deliver more power → rotor decelerates → Kinetic energy discharge.

II. Recovery phase: WT controlled to restore the rotor speed → reestablishing kinetic energy.

The recovery phase varies according to the operating point of the WT. At low wind speeds (under nominal values), the acceleration energy required to restore the pre-fault rotor speed is drawn from the grid as shown in Figure 5-13. At high wind speed, the recovery phase does not include any power drops under the pre-fault steady-state value. The reason is that the rotor speed drop is too slight with very short deceleration and acceleration periods. The pitch controller response to the additional KEC I signal through decreasing the pitch angle which increases as a result the mechanical WT power. Consequently, the kinetic energy is released in a shorter period and is followed by extra energy support from the temporary increase in the WT turbine power as shown in Figure 5-14.

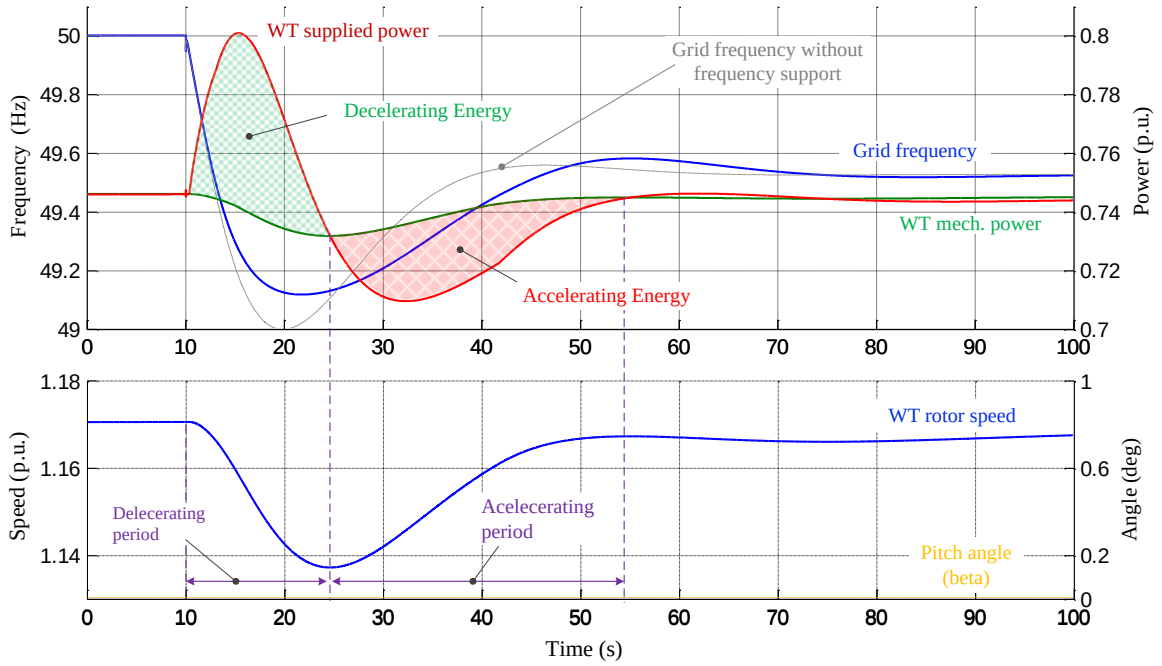

Figure 5-13: Frequency support by KEC I during low wind speed (under nominal value)

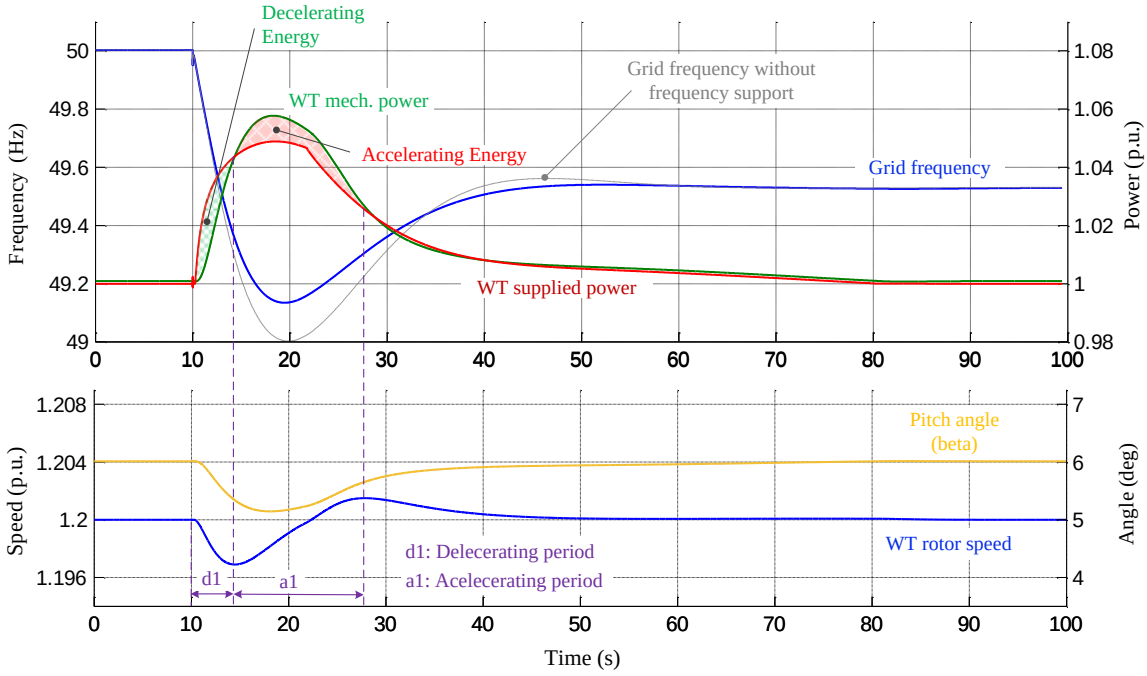

Figure 5-14: Frequency support by KEC I during high wind speed (above nominal value)

The modeling and tuning of any KEC strategy must consider the following issues:

- Maximum active power overloading during the support period.
- Maximum and minimum allowable rotor speed range.
- Interaction with the speed controller.
- Interaction with the pitch controller at operations above nominal wind speeds.
- Best response for the allowed range of operation

- Variability of the wind power generation and thus different grid frequency responses are expected.

The main concern in KEC I strategy is its interaction with the speed controller during the frequency support time. The comparatively large gain V_T of the speed controller can induce extra frequency oscillations with a badly tuned parameter at some operating points. In [48], it is proposed to limit the gain V_T or control it during the frequency support period, a ramp function is proposed to reset smoothly the gain value.

In [49] it is suggested to apply a permanent modification the proportional and integral parameters of the speed controller when the frequency support function is enabled. Such modifications as suggested weaken the dynamic response of the speed control during normal operations and are not considered as a satisfying solution.

The response of KEC I for different wind share was investigated in [7][51]. The simulation results showed that the recovery phase can be a critical problem for high wind share in the grid. Also it showed that by tuning the controller parameter for a certain wind share level the KEC I can negatively affect the frequency response in case of higher wind shares.

To study the effect of the WT operating point on the KEC I response independent from the wind share variability, the load flow and thus the wind share of power generation in MWs will be fixed for different WT operating points with the corresponding number of operating WTs. In Figure 5-15 the wind power share is fixed to 10% of the total power generation in the grid. The wind speed v_w is varied from 10.5 m/s to 14 m/s where the nominal wind speed is 12 m/s. The wind speed 10.5 m/s corresponds to a WT mechanical power of 0.72 p.u., which means that the investigated power range is: 0.72 to 1 p.u.. The KEC I parameters are tuned to give the best possible results at 10.5 m/s, the time constant for the washout filter is set to 60 s. For wind speeds above the nominal value (12 m/s) the pitch controller limits the WT rotor speed by a specific pitch angle.

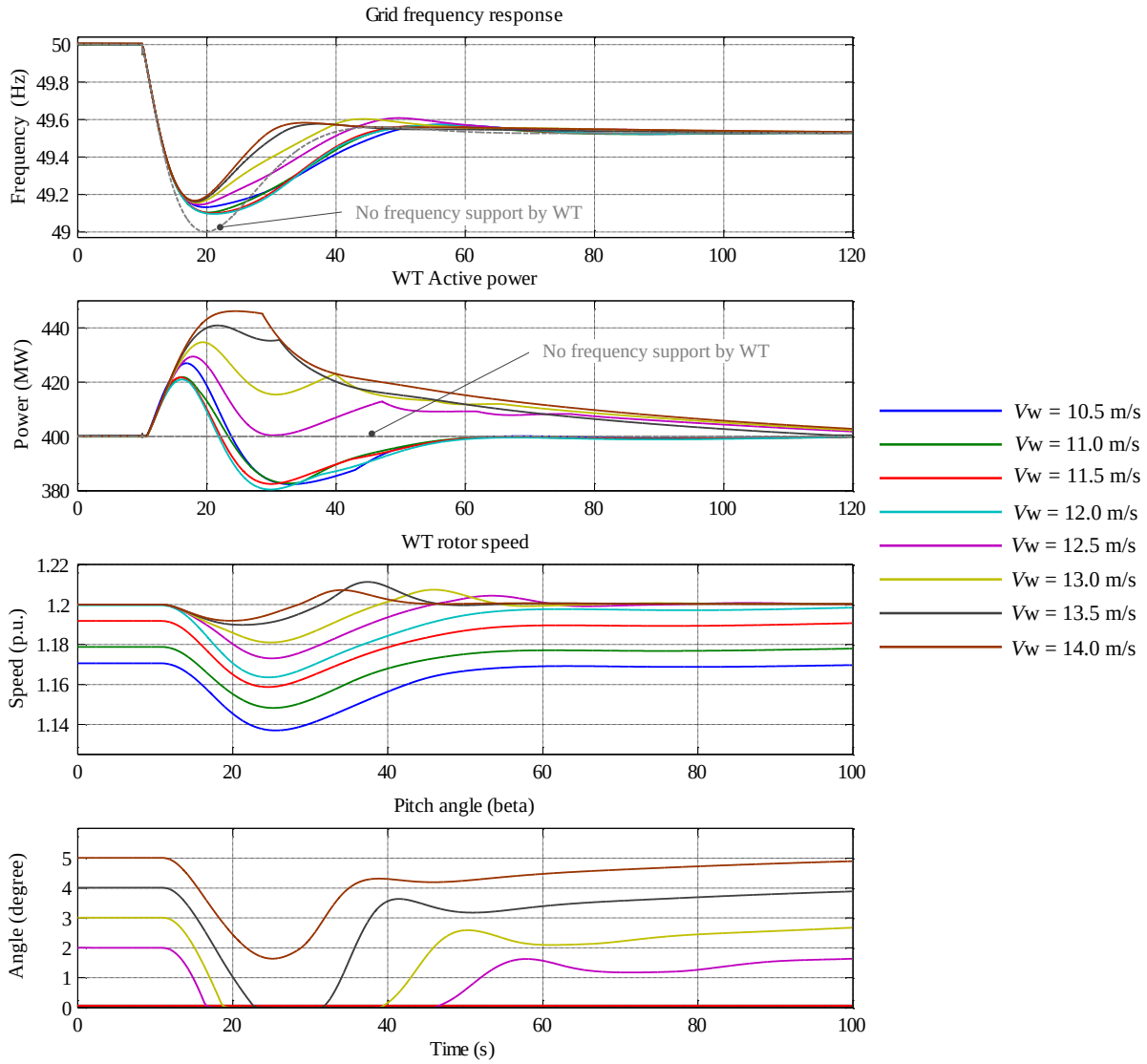

Figure 5-15: Frequency support by KEC I for same wind power share (MW) with different wind speeds

The simulation results Figure 5-15 show that the additional power order from KEC I which initially targets decelerating the WT rotor causes the pitch controller to reduce the pitch angle. As a result, the mechanical WT power will increase to boost the frequency support further and eliminate in the same time the recovery period that exists for the case of lower wind speeds. Despite the positive interaction of KEC I and pitch controller to boost the frequency support, the resulting power overloading takes relatively a long time to settle down for high wind speed situations. To limit the overloading time, a shorter wash out time constant can be chosen, however, this modification will have an adverse impact when the frequency event occurs at low speed conditions since the shorter window for KEC I action can induce extra frequency oscillations due to stronger interaction with the speed controller.

5.3.2.2 KEC II

The kinetic energy in this strategy is not extracted directly after the frequency disturbance event. Before doing this KEC II targets accelerating the WT rotor to gain more mechanical power for a short moment and then supporting the grid with kinetic energy once the short acceleration time is over [48]. KEC II can be divided into three major phases:

I. WT controller to deliver less power → rotor accelerates.
II. WT controlled to deliver more power → rotor decelerate and frequency is supported.
III. WT controlled to operate at optimal speed → rotor reaccelerates.

Figure 5-16 shows a possible layout of KEC II strategy. The main difference to KEC is the plus sign instead of minus. One important advantage of KEC II that it does not require any adjustment of the speed controller gain V_T as the case for KEC I.

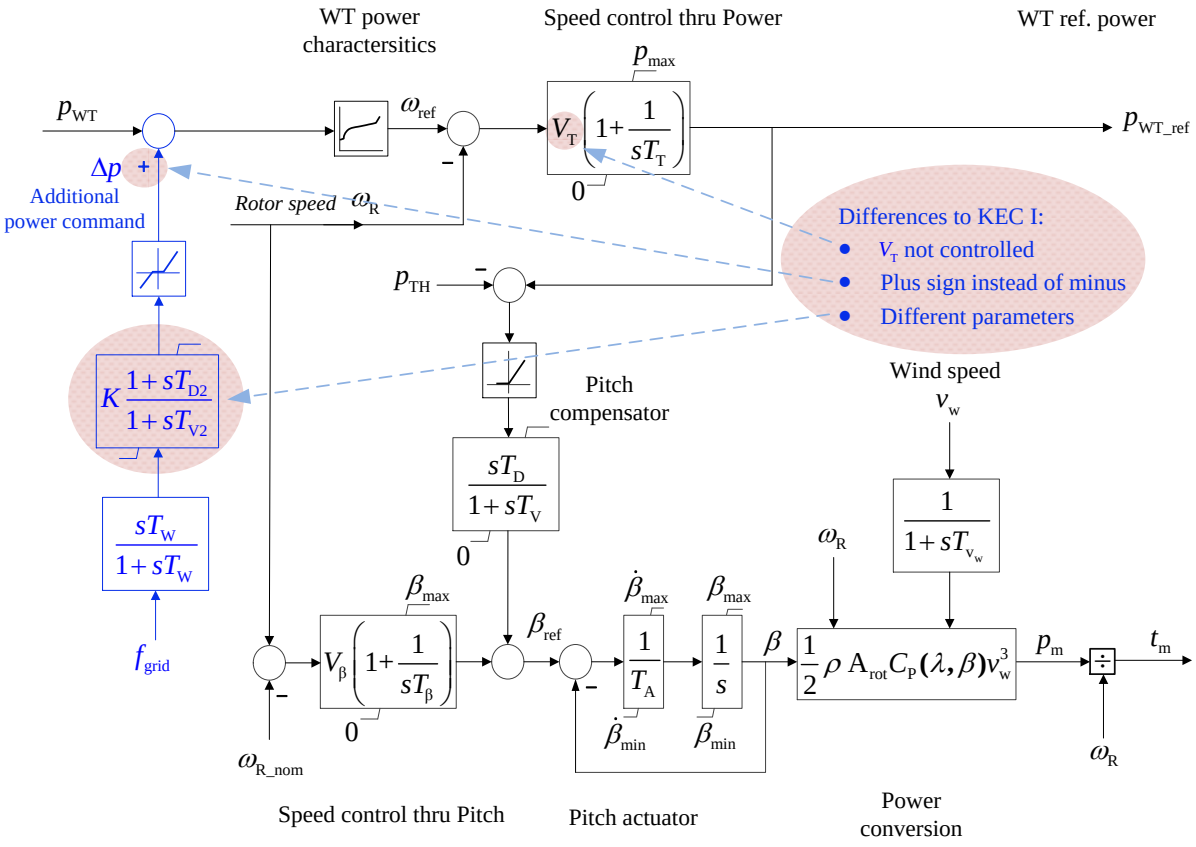

Figure 5-16: WT Power control and conversion with KEC II control structure [48]

The response of KEC II to the same disturbance during wind speeds lower than nominal value and with the same steady-state conditions as the case for KEC I is illustrated in Figure 5-17. At the beginning the frequency drops faster due to the required acceleration energy in the first phase. Once the rotor speed reaches its maximum the actual frequency support starts and continues until the rotor speed reduces to its minimum. After that a slight recovery period takes place to restore the rotor speed to its pre-fault level. Only a slight drop in the rotor speed

occurs in comparison with the case for KEC I.

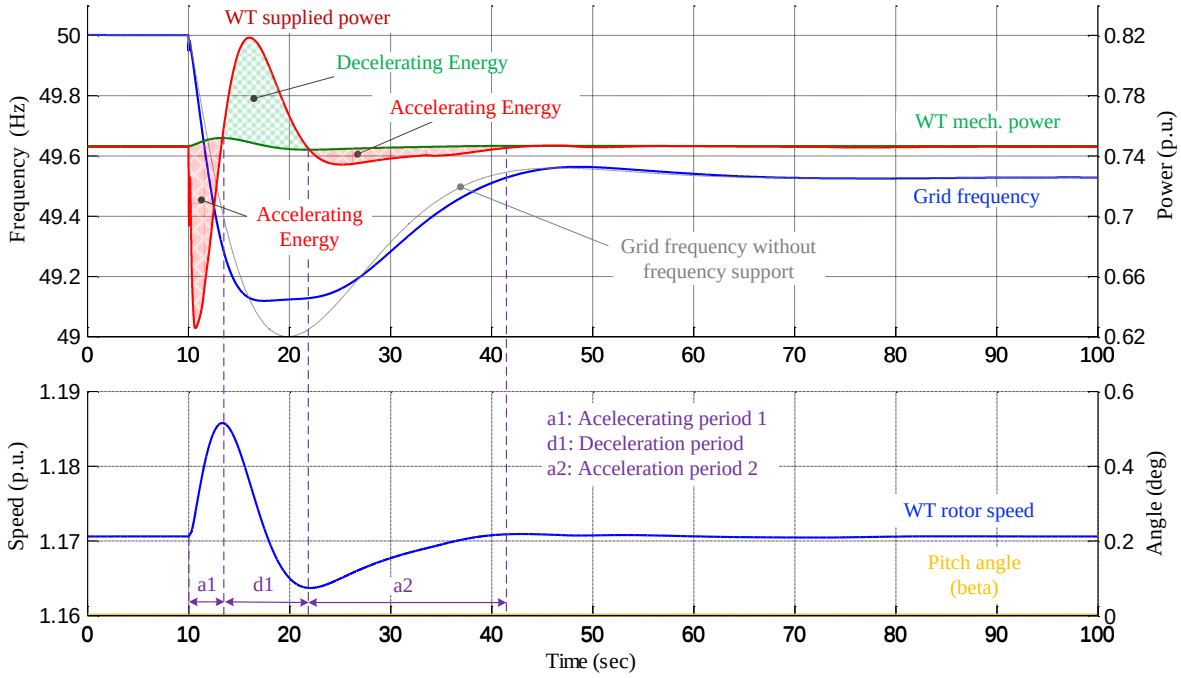

Figure 5-17: Frequency support by KEC II during low wind speed (under nominal value)

During high wind speed (above nominal) operation the pitch controller is active. Once the rotor speed exceeds the nominal value; the pitch control increases the pitch angle reducing thereby the WT mechanical power. If pitching action is relatively fast, the mechanical power will drop as the speed controller accelerates the WT rotor, thus, it will not only cancel the desired action by KEC II but rather worsen the frequency response as illustrated in Figure 5-18. A simple solution to overcome this drawback is to block the pitching action during the frequency support phase by KEC II when the WT is operating near the nominal rotor speed. However, the frequency support will be still much weaker compared to the low wind speed case even when trying to retune the parameters of the KEC II. This is due to the fact that KEC II accelerates the WT rotor over the nominal speed, where the WT enters the dynamic overload region of the power-speed characteristics (see section 2.2.3), where the additional power command generates only a limited change in the rotor reference speed.

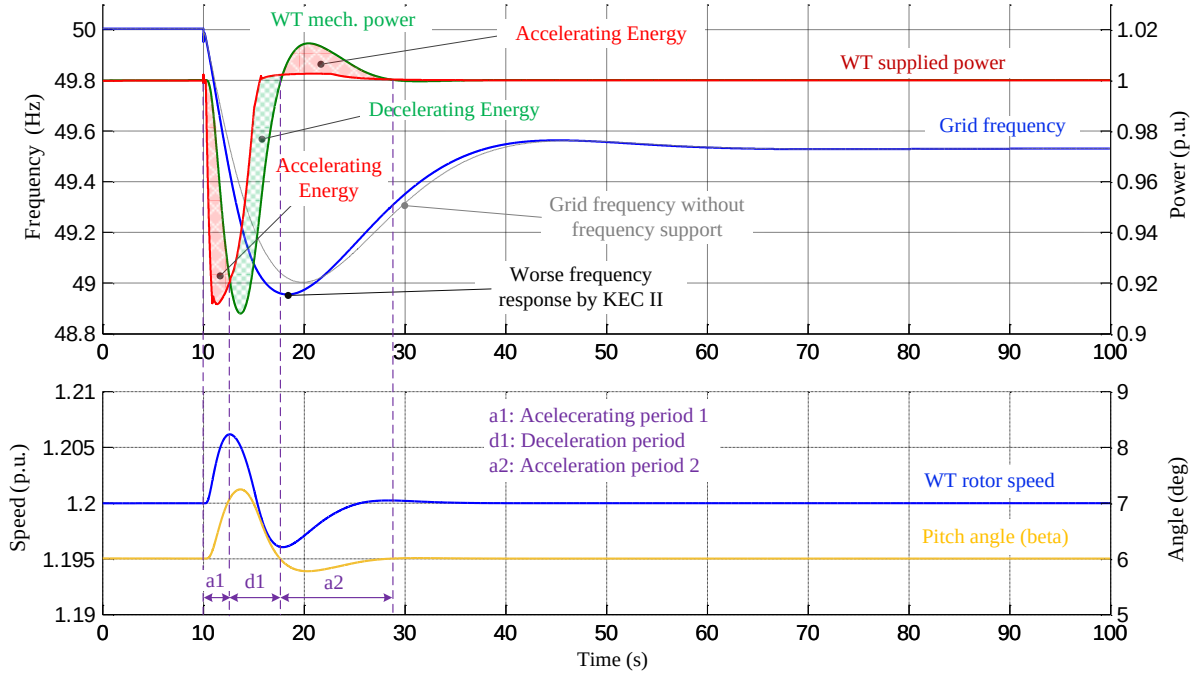

Figure 5-18: Frequency support by KEC II during high wind speed (above nominal value) with active pitching

A slight modification on the dynamic overload of the WT power-speed characteristics as shown in Figure 5-19 can significantly increase the efficiency of KEC II as shown in Figure 5-20 . The drawback of such a modification is that the margin between nominal and cut-off speed will be smaller.

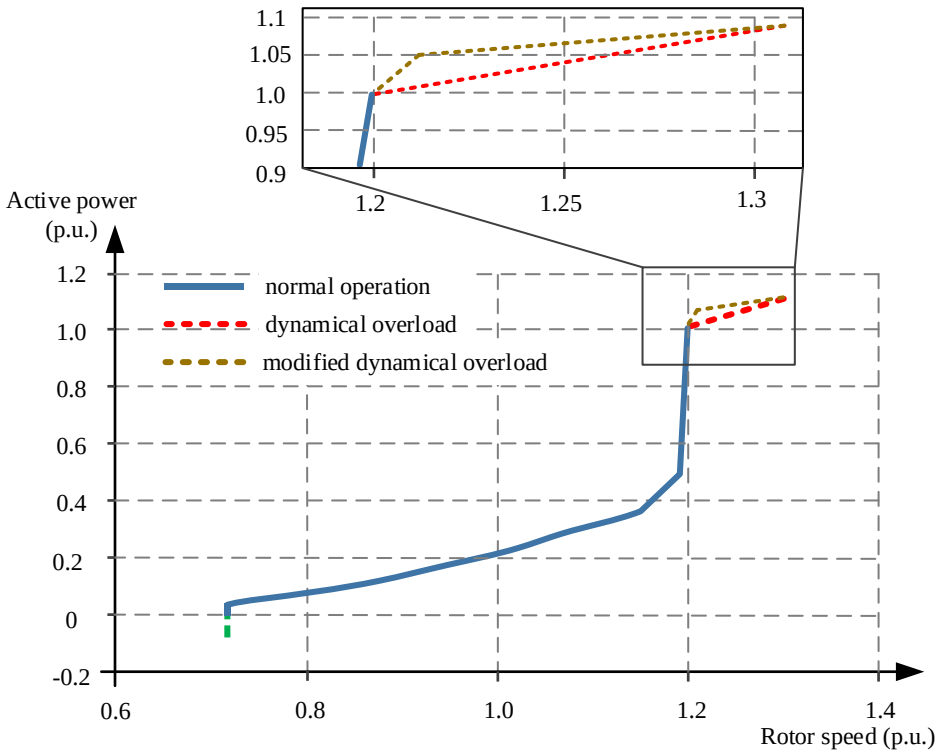

Figure 5-19: Modified dynamical overload of the WT power-speed characteristics

The comparison results in Figure 5-20 shows the positive impact of blocking the pitch control during the operation of KEC II. The de-blocking takes place after 40s from the frequency drop event. In general, the pitch control should have the priority to maintain the WT rotor speed in case a sudden rise in the wind speed.

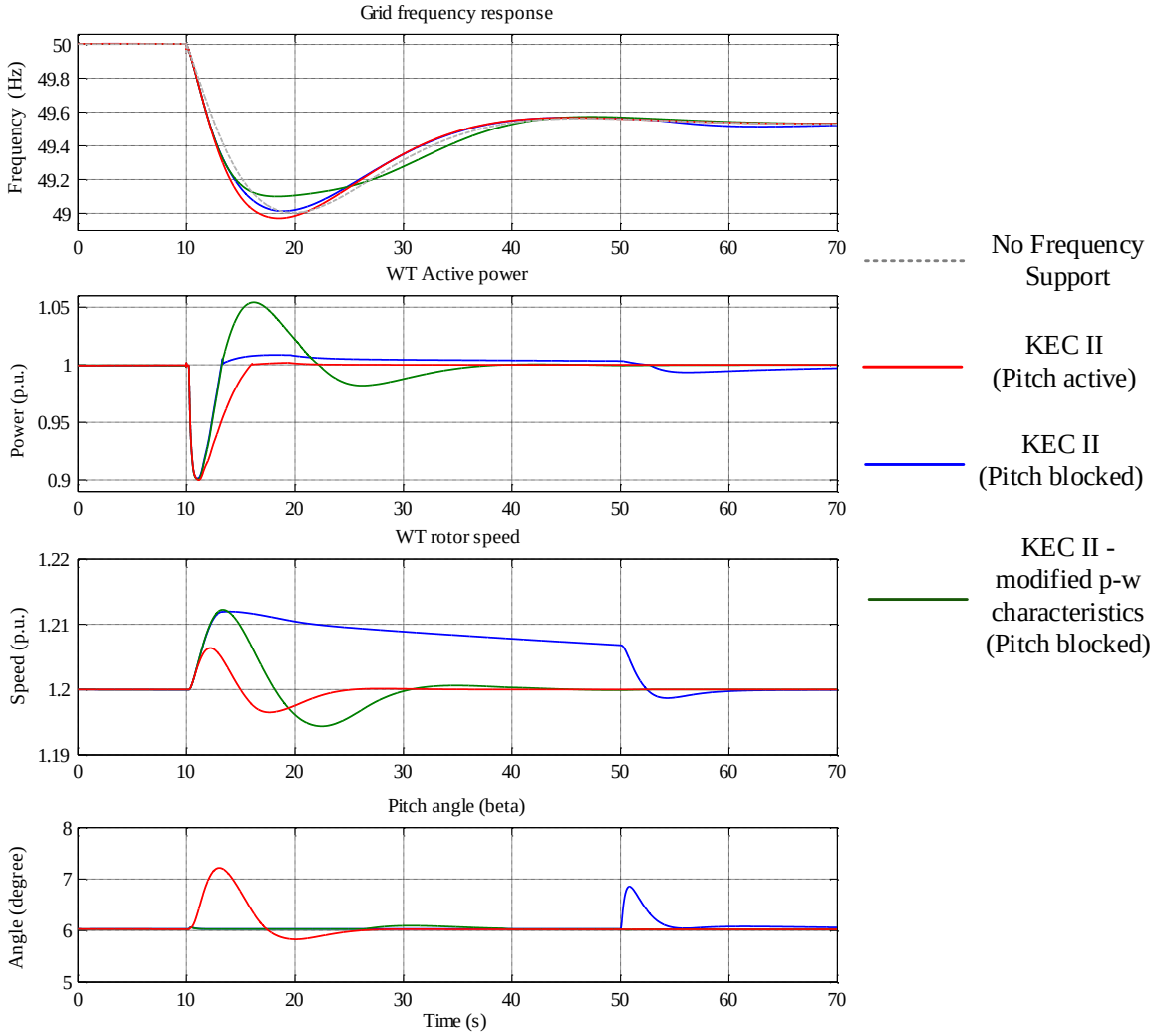

Figure 5-20: Frequency support by KEC II for different control settings

In Figure 5-21(analog to Figure 5-15) the wind power share is fixed to 10% of the total power generation in the grid. The wind speed v_w is varied from 10.5 m/s to 14 m/s with a nominal wind speed of 12 m/s to test the response of KEC II. A washout time constant of 60 s is applied. The pitch controller is blocked during the action of KEC II. In addition the proposed modification for the dynamic overload of the WT characteristics in Figure 5-19 is implemented. Since KEC II does not interact with speed controller, it provides under nominal speed operation clearly more uniform behavior in comparison to KEC I (Figure 5-15).

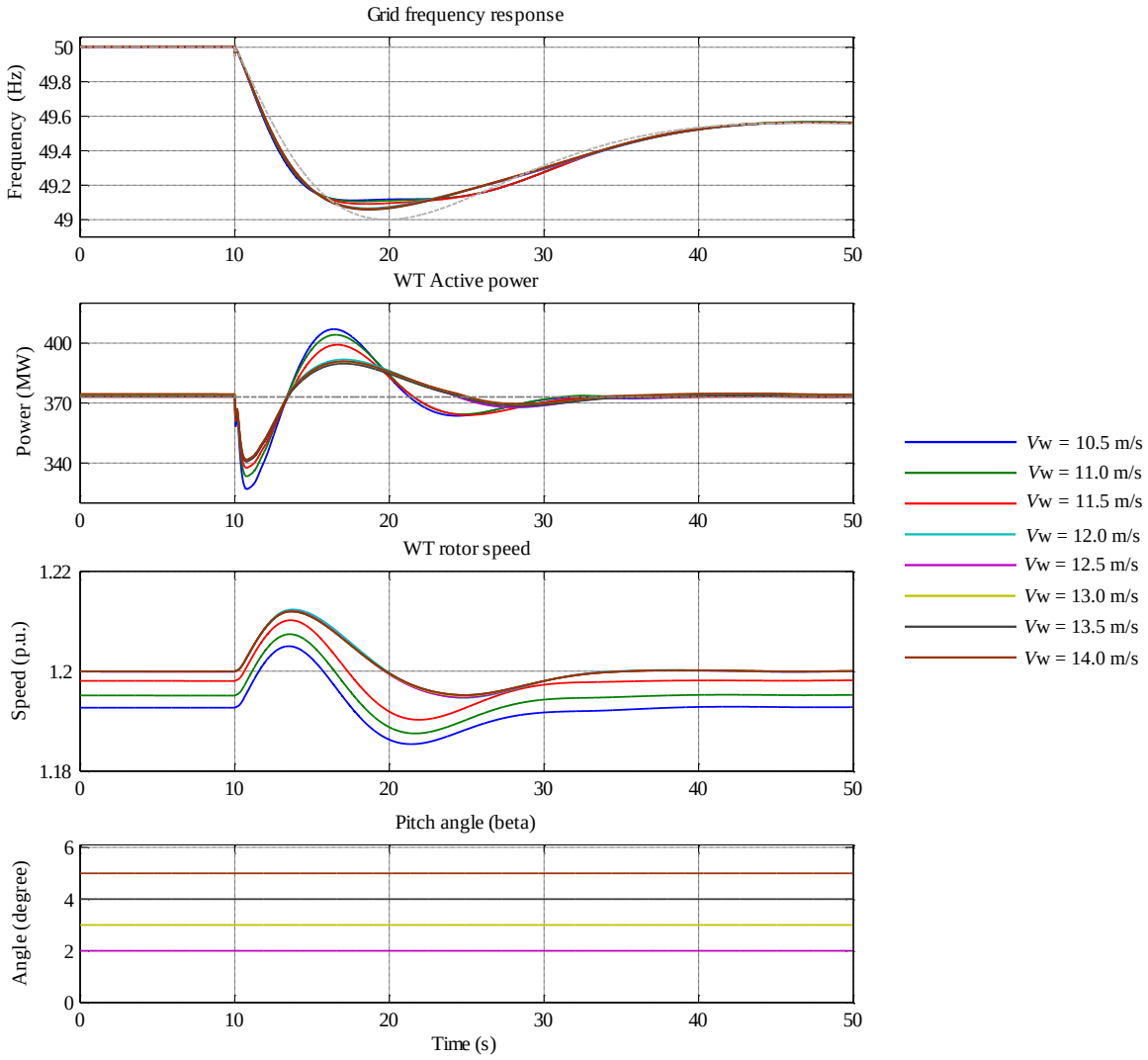

Figure 5-21: Frequency support by modified KEC II for same wind power share (MW) with different wind speeds

5.3.3 Frequency support by combined FSPC and KEC strategies

If a specific de-loading (power reserve) is required from the WTs in a grid along with a requirement for inertial response support, KEC strategies can offer a fast response followed by a smooth power reduction by pitch control. Simulation results in Figure 5-22 show that the combined strategies of KEC I and FSPC offer a further enhancement to the frequency response for both low wind (under nominal) speed and high wind (above nominal) speed cases. While in Figure 5-23, the combined strategies of KEC II and FSPC only have a positive effect during low wind speeds (lower than nominal speed).

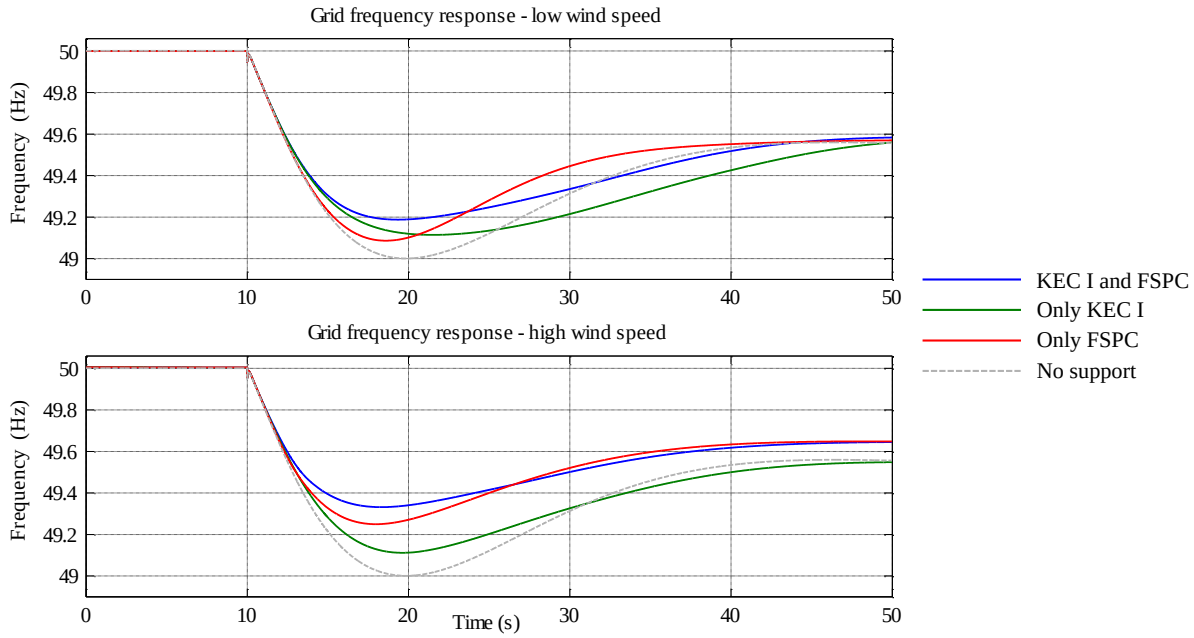

Figure 5-22: Frequency responses with combined frequency support by KEC I and FSPC for low wind (under nominal) and high wind (above nominal) speeds

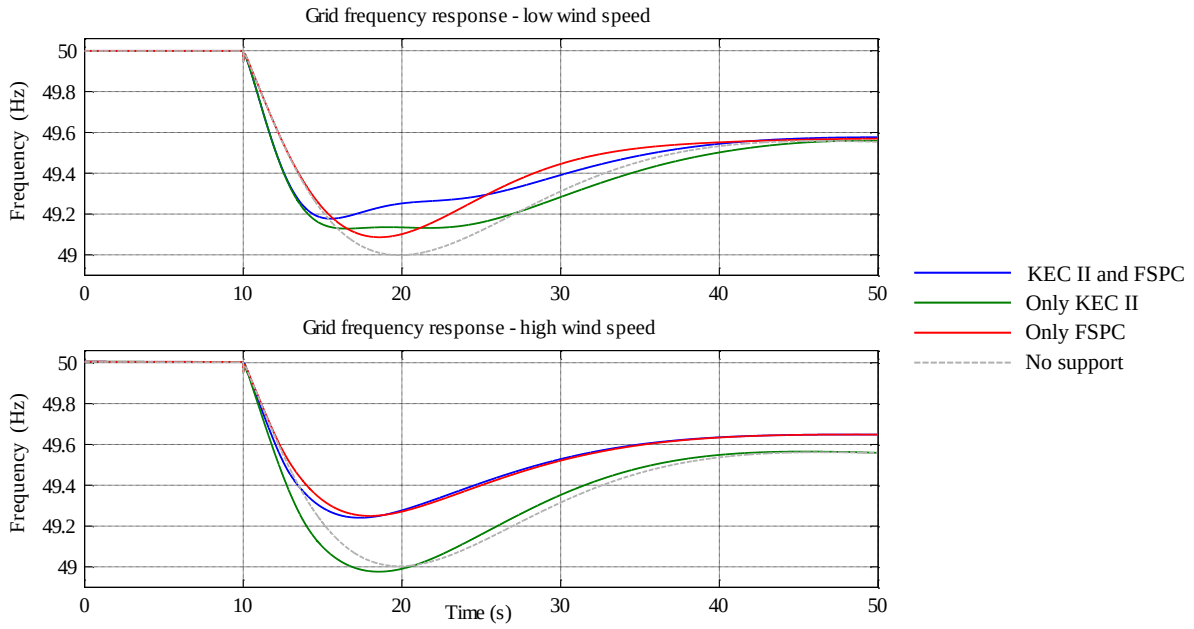

Figure 5-23: Frequency responses with combined frequency support by KEC II and FSPC for low wind (under nominal) and high wind (above nominal) speeds

5.3.4 Discussion on presented frequency support strategies

De-loading WTs to provide a primary reserve for the grid will be considered in some countries with high wind penetration in the grid. De-loading by additional pitch angle has minimum adverse effect in comparison with the over-speeding method. In FSPC strategy presented in section 5.3.1.2, the pitch angle deviation is adjusted according to the operating

point and once a frequency deviation is detected in the grid the pitch angle will be reduced to provide a frequency support to the grid. The time constant of the provided washout filter controls the duration of the frequency support by the WT. Accordingly, the active power (pitch angle) is ramped back to the original value.

If a fast inertial response support is required from the WTs which may be difficult to achieve by pitch actuators, the kinetic energy in the WT rotor can be extracted for fast but temporary frequency support. KEC I and KEC II methods were presented in sections 5.3.2.1 and 5.3.2.2, both strategies employ a lead-lag compensator that must be tuned properly. The main disadvantage of KEC I is that it requires adjusting the speed controller in the WT to avoid any adverse effects during the recovery (reacceleration) phase after the rotor speed drops. This problem is more present during under nominal speed operation for high wind power share in the grid. KEC II does not require any adjustments on the speed controller of the WT and shows a very good results for frequency support during low wind (under nominal) speed operation. For the case of high wind speed operation it was shown that the pitch controller will adversely interact with the control action of KEC II, this problem was solved by simply blocking the pitch control during the frequency support period. Additionally a slight change in the dynamic overload region of the WT power-speed characteristics can enhance significantly the performance of KEC II during high wind speed operation.

A combined strategy of FSPC and KEC provide further enhancement of the frequency response. Based solely on the results in Figure 5-22 and Figure 5-23 the combination of KEC I and FSPC offers the best option for frequency support, nevertheless, the fact that KEC II does not require any adjustments on the WT speed controller and provide more uniform behavior for different wind speeds might make the choice of the combined KEC II and FSPC strategy more attractive in practice.

Control parameter tuning in KEC methods is usually based on the assumption that the shape of the primary response of the grid frequency does not change significantly during different load flow scenarios and wind fluctuations. Such assumption is invalid in reality which makes the application of these methods more challenging in real grid with fluctuating wind speeds and variable wind power share. Additionally, the operating point of one single WT does not necessary correlate with the total wind power share in the grid, in other words a couple of WTs in a WF can be operating with lower wind speeds while the rest are operating with high wind speeds. If part of the WTs in the WF is operating with low wind speeds, their frequency support behavior could conflict with the other WTs operating with clearly higher wind speeds the WF. Therefore, the selectivity should be available to decide which WTs should participate

in the frequency support in order to optimize the overall contribution. Wake effect and wind variation during the primary frequency response phase are additional factors that should be considered for more accurate analysis. It can be concluded that due to the above mentioned uncertainties of the KEC strategies performance in real applications, such control methods do not offer the grid operator a 100% reliable solution for supporting the grid frequency.

6 Overfrequency limiting by VSC-HVDC connected offshore WTs

Overfrequency caused by a sudden loss of load or energy excess in a grid is a scenario that is not properly addressed in literature. Most of the studies on primary frequency response in electrical grids focus on the common case of loss of generation which causes a certain frequency drop. However in certain grid configurations, the case of overfrequency due to loss of load or surplus energy generation is a possible scenario that should be carefully investigated. Figure 6-1 shows the newly planned AC corridors to transfer the energy generated from the large offshore WFs in the northern sea of Germany to the load centers in the southern part. Any disturbance event that requires a disconnection in the transmission lines would mean that the northern part of the grid will be isolated from the southern part. As a result, a frequency rise will occur in the northern part due to the excess generation from the offshore WFs.

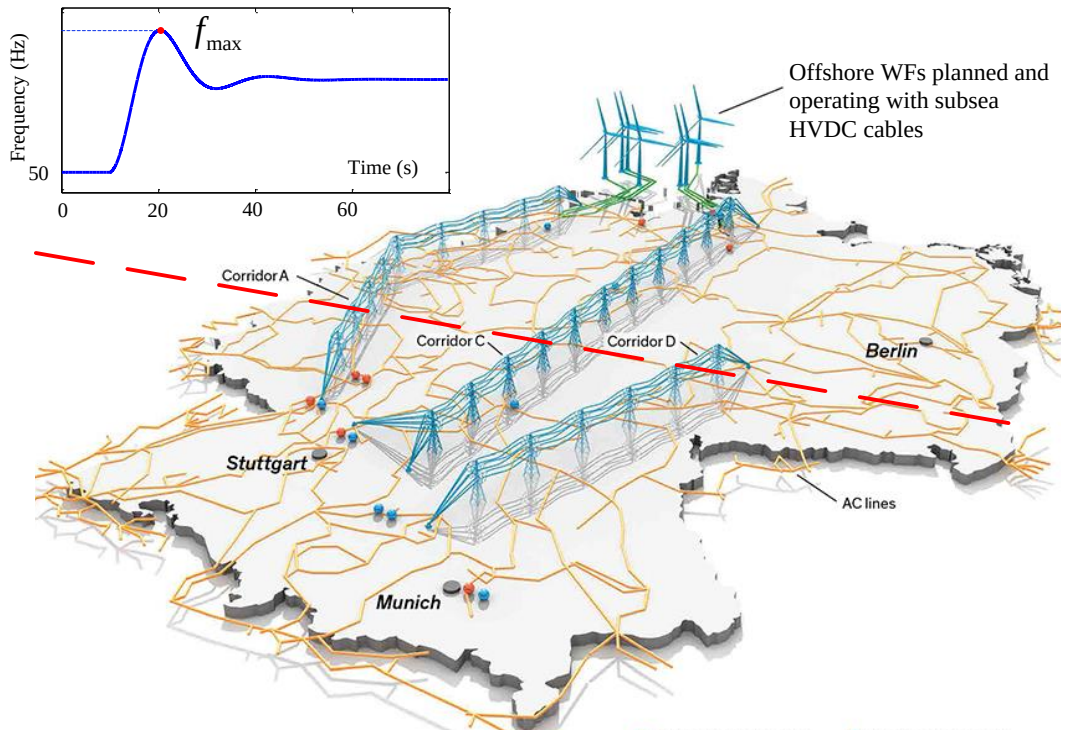

Figure 6-1: Planned HVDC transmission corridors in Germany to transfer the generated offshore wind power in the north to the main loads in south [52]

This chapter aims to answer the following questions:

- How can the offshore WF limit the frequency rise for this possible scenario?
- Are the offshore WF capable of reducing its output power fast enough to avoid high frequency overshoots?

- Can the KEC strategies discussed in section 5.3.2 be applied for overfrequency limiting?
- Can the VSC-HVDC connection offer any alternatives or enhancements for the Overfrequency limiting control?

6.1 Current grid requirements regarding overfrequency events

In Germany and other European countries special grid code requirements has been published for offshore grids. TenneT grid code [25] requires that all generating units must reduce, while in operation, at a frequency of more than 50.2 Hz the instantaneous active power with a gradient of 40% of the generators instantaneously available capacity per Hz [25]. Figure 6-2 shows the boundaries and the functional relationship between frequency and frequency-dependent active power reduction. No specific dynamic characteristics are defined for the WT response, and Figure 6-2 solely describes the steady-state characteristics. Besides, the active power reduction value is a function of the instantaneously available power value which changes with wind speed level.

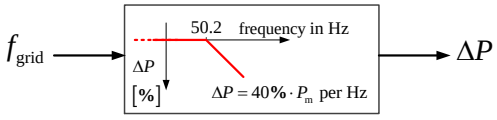

$$\Delta P = 20 P_m \frac{50.2\ \text{Hz} - f_{grid}}{50\ \text{Hz}} \quad \text{at } 50.2\ \text{Hz} < f_{grid} < 52.7\ \text{Hz}$$

P_m instantaneously available power

ΔP power reduction

f_{grid} grid frequency

For $47.5\ \text{Hz} < f_{grid} \leq 50.2\ \text{Hz}$ no restriction

At $f_{grid} \leq 47.5\ \text{Hz}$ and $f_{grid} \geq 52.7\ \text{Hz}$ disconnection from grid

Figure 6-2: Requirements for frequency-dependent active power reduction [11]

In some countries, where a high wind penetration is planned in a relatively weakly-coupled grid, new requirements regarding fast inertial support by WTs are introduced [53][54]. For overfrequency events no requirements are yet defined in the German grid regarding a fast power reduction targeting the limiting of the frequency overshoot. In 2014, the European Network of Transmission System Operators for Electricity (ENTSO) delivered a draft grid code on HVDC connections, linking two different synchronous areas and HVDC connected WFs [55]. The implementation requirements [56] for this grid code include new requirements regarding fast power response to frequency changes but did not provide specific implementation guidelines and performance parameters.

6.2 Active power reduction by WTs

Active power reduction in the WTs is realized typically by the pitch controller. The pitch actuator generally comes in two forms, hydraulic or electrical. The adjustment speed of the pitch actuator, which is defined in degrees per seconds, is limited to a specific value by the manufacturer to avoid any mechanical stresses. By limiting the adjustment speed, the rate of change of the active power is limited correspondingly. Pitch rate limits are usually defined individually for each direction of movement (increasing or decreasing active power). Technical aspects in general tend to compel the offshore WF generating units toward slower rate limit of active power reduction. Considering this, WF active power reduction is unlikely to be effective enough for limiting the dynamic overshoot during overfrequency in grids with high wind power penetration level.

The same test grid presented in section 5.2.3 is used here for the Overfrequency studies. In contrast to the event of under-frequency, the additional load (160 + j50) MVA is assumed to be already connected during steady-state conditions (50 Hz) to the grid and will be disconnected from the grid to cause an overfrequency response.

The FSPC strategy presented in section 5.3.1.2 can provide also frequency support action for overfrequency events.

In the WT speed and pitch control (Figure 5-5); the pitch angle rate limit defines the power rate limit of the WT. Figure 6-3 shows the impact of the two different power rate limits on the performance of the FSPC strategy. In the case of the higher rate limit (0.08 p.u./s), the active power reduction is fast enough to reduce the dynamic overshoot in the frequency. As the rate limit decreases, the active power reduction becomes slower and consequently the limiting effect on the dynamic overshoot of the frequency becomes weaker, as in the case for the rate limit 0.01 p.u./s. The frequency settles at the same steady-state level in both cases. For stronger overfrequency events with higher energy excess, the FSPC will not be able to reduce effectively the frequency overshoot. Additionally, as the wind power share in the grid increases, the total grid inertia will drop down. This will cause a fast RoCoF that cannot be handled only by the pitch control.

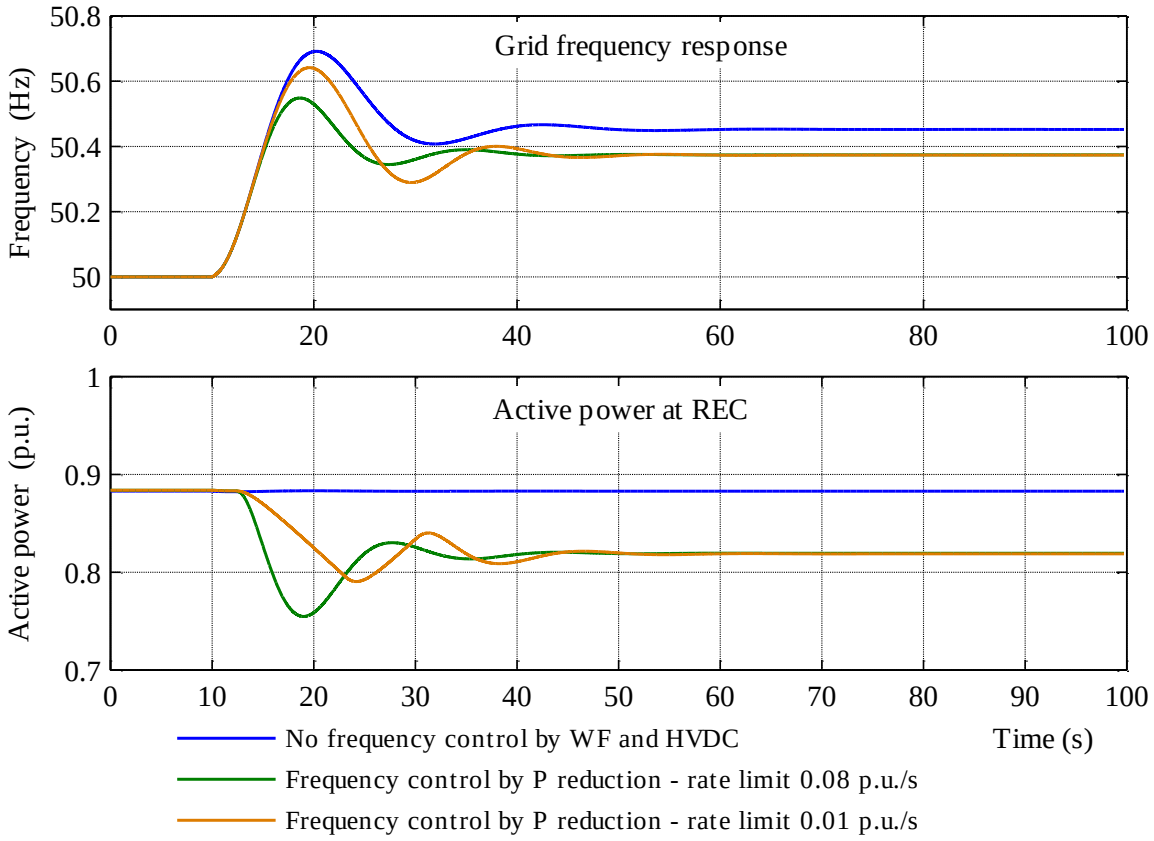

Figure 6-3: Performance of FSPC for overfrequency limiting by different active power rate limits

6.3 Utilizing KEC strategies for overfrequency limiting

6.3.1 KEC I for overfrequency limiting

By applying this scheme the rotor speed is accelerated initially to operate temporarily at a higher mechanical power setpoint. It follows that the rotor will be charged by extra kinetic energy causing a temporal drop in the output power. This control action limits the frequency overshoot during the first seconds of the primary response. The rotor speed is afterwards restored which means the extra kinetic energy will be discharged causing thereby a temporal increase in the output power which can be characterized as the recovery phase. The described behavior is illustrated in Figure 6-4.

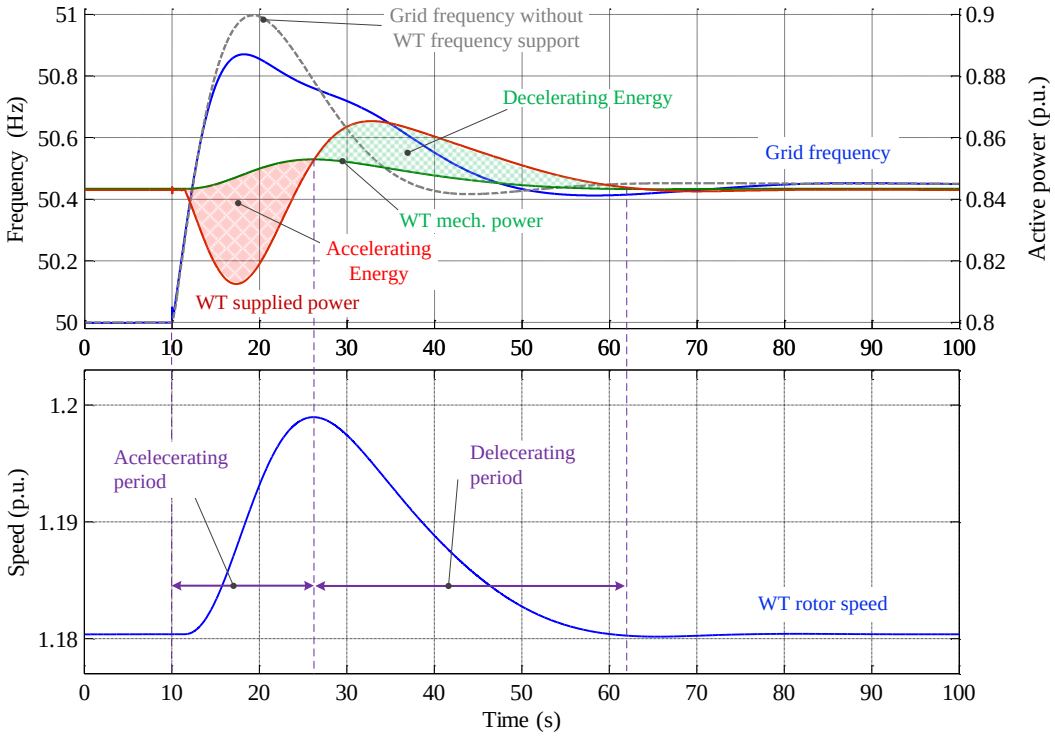

Figure 6-4: Performance of KEC I for an overfrequency event

6.3.2 KEC II for overfrequency limiting

KEC II strategy can be as well utilized for the limitation of the frequency overshoot as illustrated in Figure 6-5. When the frequency rises above the defined threshold, KEC II will initially increase the output power by dropping the rotor speed and releasing part of the stored kinetic energy. In the next phase the WT is controlled to deliver less power by accelerating the rotor and charging it with kinetic energy limiting therefore the frequency overshoot. The WT is afterwards controlled to operate normally at the optimal speed.

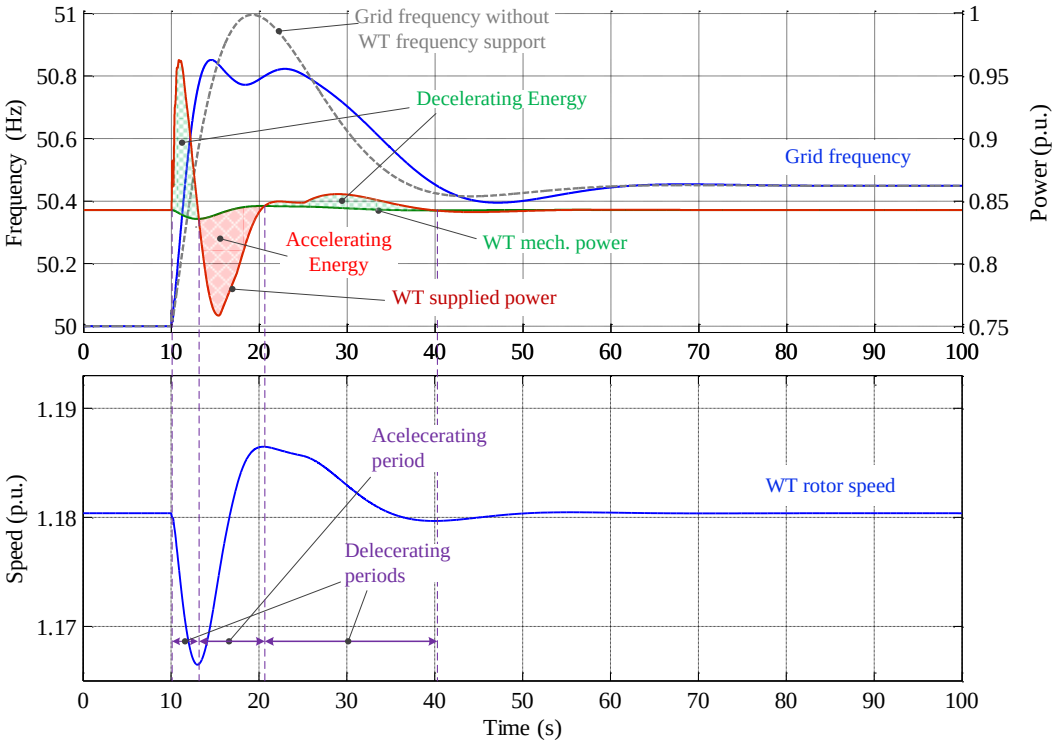

Figure 6-5: Performance of KEC II for an overfrequency event

In the results shown in Figure 6-4 and Figure 6-5, the controller parameters for KEC I and KEC II are tuned for a specific wind share level (20%) in the test grid and their performance cannot be reflected to all operating points.

The main drawbacks of the KEC strategies for underfrequency events which were addressed in [50][7] and [51] apply as well for overfrequency events and can be summarized in the following points:

- KEC parameters are tuned for limited rotor speed range for best possible results.
- Close coordination with the speed and pitch control is of a high importance (especially for KEC I) to avoid a second incursion.
- The higher the wind share and therefore the RoCoF the harder is to tune parameters of the KEC controller.
- Large wind speed variations within the offshore WF could weaken the overall KEC performance if no coordination exists between the WTs.

6.3.3 Overfrequency limiting by combined FSPC and KEC strategies

6.3.3.1 FSPC and KEC I for overfrequency limiting

The performance of the combined FSPC and KEC I strategies are compared against each single strategy presented in previous sections (6.2 and 6.3.1) for the same load switching

event that causes the overfrequency. FSPC and KEC I delivers in this case comparable results regarding the limitation of the frequency overshoot. The combined strategy offers a considerable enhancement of the frequency response as shown in Figure 6-6.

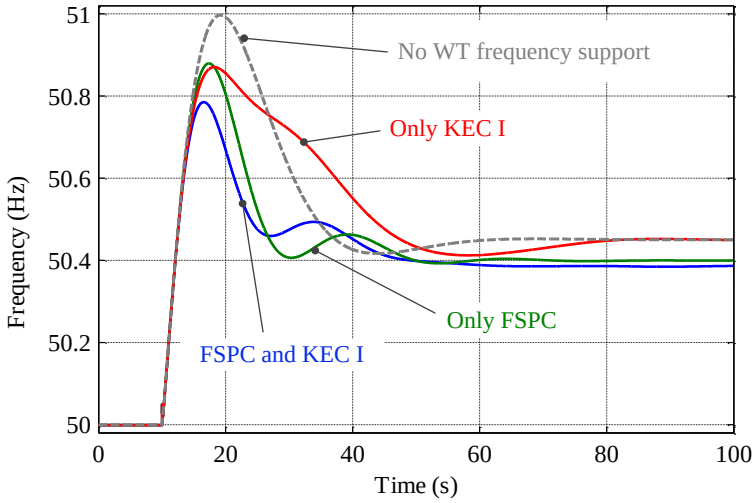

Figure 6-6: Results of KEC I and FSPC strategies for an overfrequency event

6.3.3.2 FSPC and KEC II for overfrequency limiting

Similar to the first case, the performance of the combined FSPC and KEC II strategies are tested against each single strategy. The combined control action here as well offers rather a slight but considerable enhancement for the overfrequency limiting performance as shown in Figure 6-7.

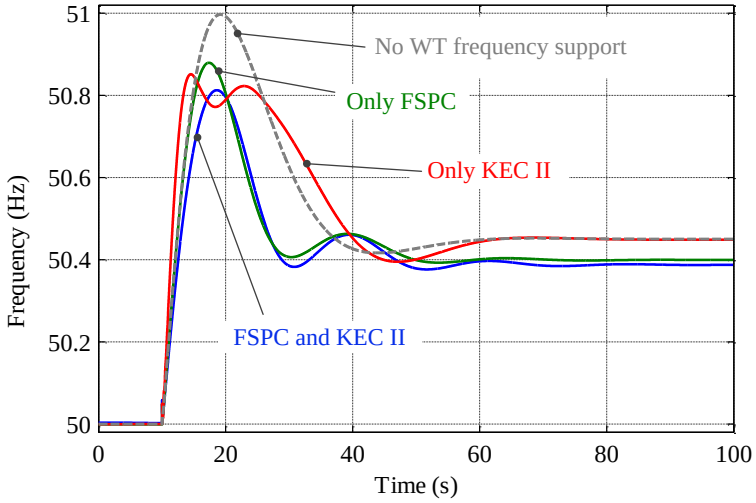

Figure 6-7: Results of KEC II and FSPC strategies for an overfrequency event

6.4 Overfrequency limiting by DC Chopper (OFLC)

For connecting offshore WFs via VSC-HVDC, a protection scheme should be implemented to minimize the effect of onshore side grid faults on the offshore WF. This topic has been discussed in [4] in details. A DC chopper is typically [12] [58][59] installed to isolate the offshore WF from AC onshore grid fault (Figure 6-8). When an AC onshore-side fault occurs, the DC voltage will start rising due to the surplus power that cannot be evacuated to the grid, the DC chopper will be activated and will limit the DC voltage rise by absorbing the energy coming from the offshore WFs. This solution is robust but rather costly due to the fact that the chopper resistance must have the full rating of the offshore WFs to be able to absorb the surplus energy during high wind speed levels.

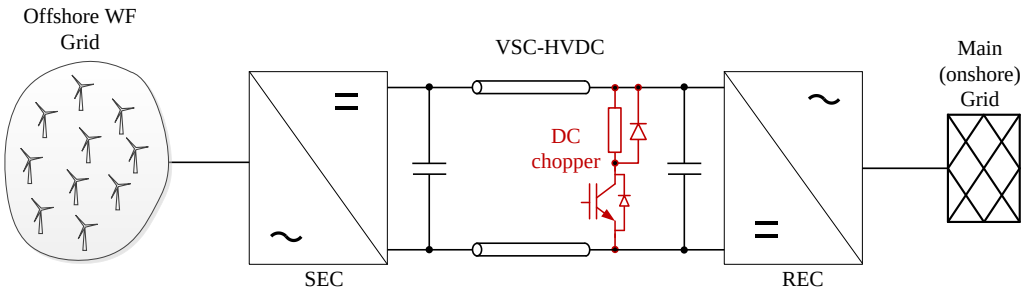

Figure 6-8: Simple configuration for VSC-HVDC connected Offshore WFs

The DC chopper power can be calculated using the relationship:

$$P_{CH} = \frac{V_{DC}^2}{R_{CH}} \tag{6.1}$$

To shield the offshore WFs from grid fault effects, the chopper has to be able to dissipate the whole power delivered from the WF. Thus, the braking resistance of a full-rated DC chopper is defined as:

$$R_{CH,full\_rated} = \frac{V_{DC,nom}^2}{P_{DC,nom}} \tag{6.2}$$

Where $P_{DC,nom}$ and $V_{DC,nom}$ are the nominal values of active power and DC voltage at the REC respectively. The energy dissipated by the chopper can be expressed as follows:

$$E_{CH} = \sum_{i=1}^{n} P_{CH} * T_{on,i} = \int P_{CH}.dt \tag{6.3}$$

Where *n* is the number of activation signals of the chopper. In eq. (6.3) it is assumed that the inductive effect in the chopper is negligible and the transient response in the chopper is very fast. Additionally, very small deviations in the DC voltage level during the OFLC operation

are neglected here.

One important aspect that should be considered in the control design is the maximum energy that can be absorbed and dissipated by the DC chopper, which represents the main limiting factor of this strategy. Typically in WTs with FSCG the DC chopper is designed to be able to dissipate the rated power for a period of 3-5 s, this ensures that the WT torque can stay constant during the FRT period and allows the WT generator and converters to withstand worst case scenarios of fault clearance or tripping. Since no relevant data is available in the literature, a similar dimensioning criterion of the DC chopper will be supposed for the VSC-HVDC. Thus it will be assumed that the HVDC chopper can dissipate the full rated power for a maximum period of 4 s (1 p.u. for 4 s). In the following sections it is assumed that 1 pu energy is equal to 1 p.u. power absorbed in 1 s:

$$E\ (\text{p.u.}) = p\ (\text{p.u.}) \cdot 1\ (\text{s}) \tag{6.4}$$

In this thesis it is proposed to extend the DC chopper functionality to limit the RoCoF and therefore the frequency overshoot by dissipating a defined amount of energy during the transient period of the primary frequency response using OFLC strategy. In the following two different OFLC controller layouts will be presented.

6.4.1 Indirect OFLC strategy integrated in the DC voltage controller

In this indirect strategy, an additional DC voltage reference $\Delta v_{\text{DC\_f}}$ is added to the DC voltage controller at the HVDC receiving end converter (REC) as shown in Figure 6-9. Once the grid frequency exceeds a specific value (here 50.2 Hz) as set in the deadband, the DC voltage controller will increase the DC voltage level to activate the normal chopper protection function. The value of the DC voltage rise and thus the chopper switching instances are controlled by a lead-lag compensator with a specific gain. The OFLC targets limiting the transient frequency overshoot during the primary frequency response. The washout filter defines the active period of the OFLC. Manual tuning by trial and error is applied for parameter estimation. One drawback of this strategy is the fact that the DC voltage should be increased in order to activate the chopper functionality to provide fast power limitation.

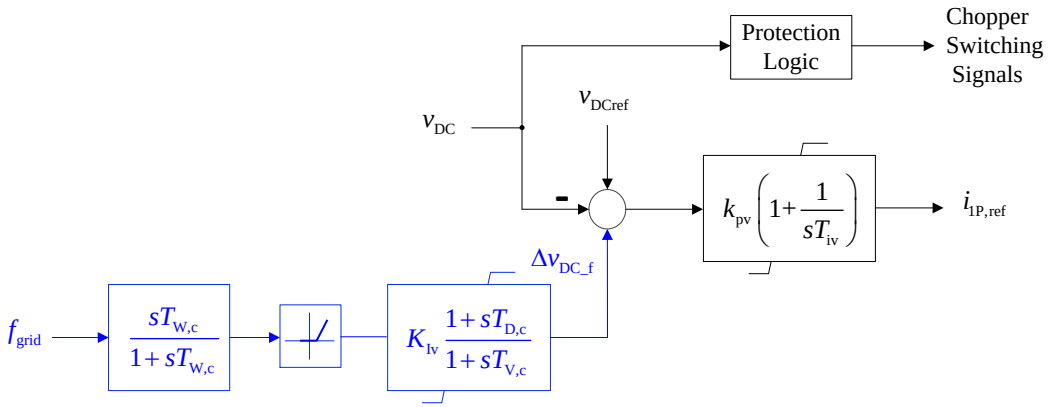

Figure 6-9: OFLC Strategy integrated in the DC voltage controller at the HVDC-REC

6.4.2 Direct OFLC Strategy

To avoid the targeted increase in the DC voltage level for activating the DC chopper, a separate control loop can be implemented for the OFLC to send directly the switching signals to the DC chopper control gate without modifying the DC voltage controller. The control concept is similar to the indirect OFLC, but instead of an additional voltage reference, the OFLC controller creates a control signal which is compared to a carrier signal with a predefined frequency to generate the chopper switching signals as illustrated in Figure 6-10.

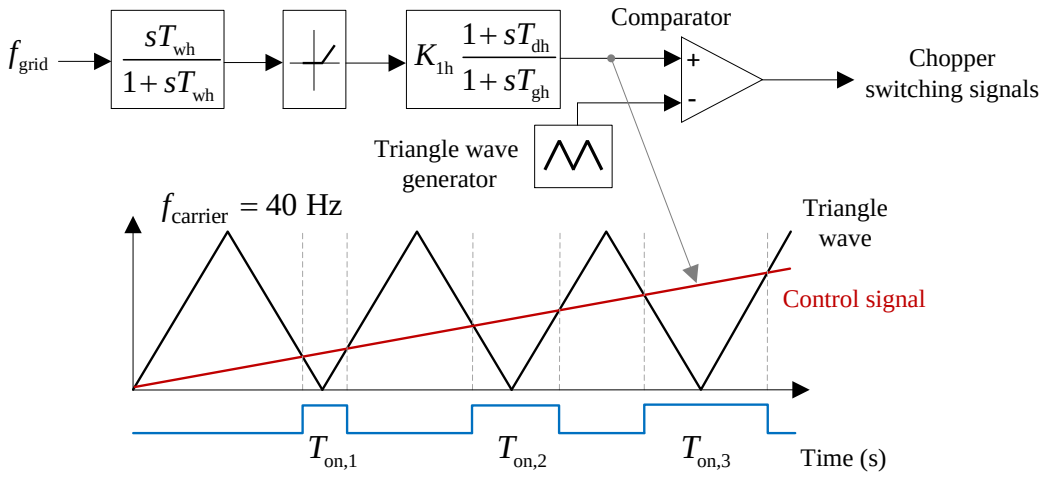

Figure 6-10: Direct OFLC Strategy at the HVDC-REC

A modulation frequency of 40 Hz is chosen for the triangle (modulator) wave for a sufficiently smooth active power reduction. The HVDC voltage is minimally affected during the chopper activation period, thus no undesired interactions with the chopper protection function can take place. The advantage of this direct OFLC is that no change on the DC voltage reference takes place and the DC chopper can be independently activated during an

overfrequency event without the need to increase deliberately the DC voltage level. Using a simple OR logic the DC chopper gate can receive the switching signals either from the default protection function or from the OFLC controller as illustrated in Figure 6-11.

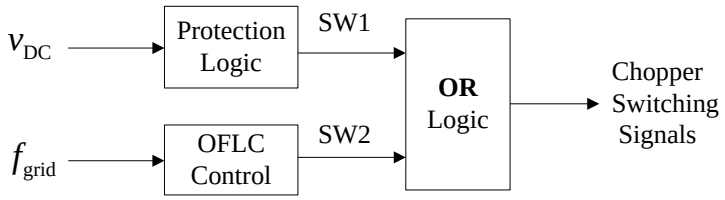

Figure 6-11: Direct OFLC Strategy in parallel with default chopper protection function

Figure 6-13 presents the performance of both OFLC methods. A load with same values in both cases is tripped after 10 s to cause the overfrequency event. A frequency deadband of 0.2 Hz is set in both cases. Both OFLC methods deliver comparable results regarding the overfrequency limiting performance. The direct OFLC method has a clear advantage of avoiding the need to increase the DC voltage level to a value of 1.1 p.u. in order to trigger the protection function of the DC chopper. The SEC active power is nearly unaffected by the OFLC operation, thus no adverse effects exist on the connected offshore WF. Therefore, in the next sections only the direct OFLC method is evaluated and compared to other strategies. At the end of the OFLC operation, the total energy dissipated by the chopper sums up to 3.5 p.u., which is equivalent to the dissipation of the rated power for the period of 3.5 s.
In the next sections only the direct OFLC method will be further analyzed and compared to other overfrequency limiting strategies.

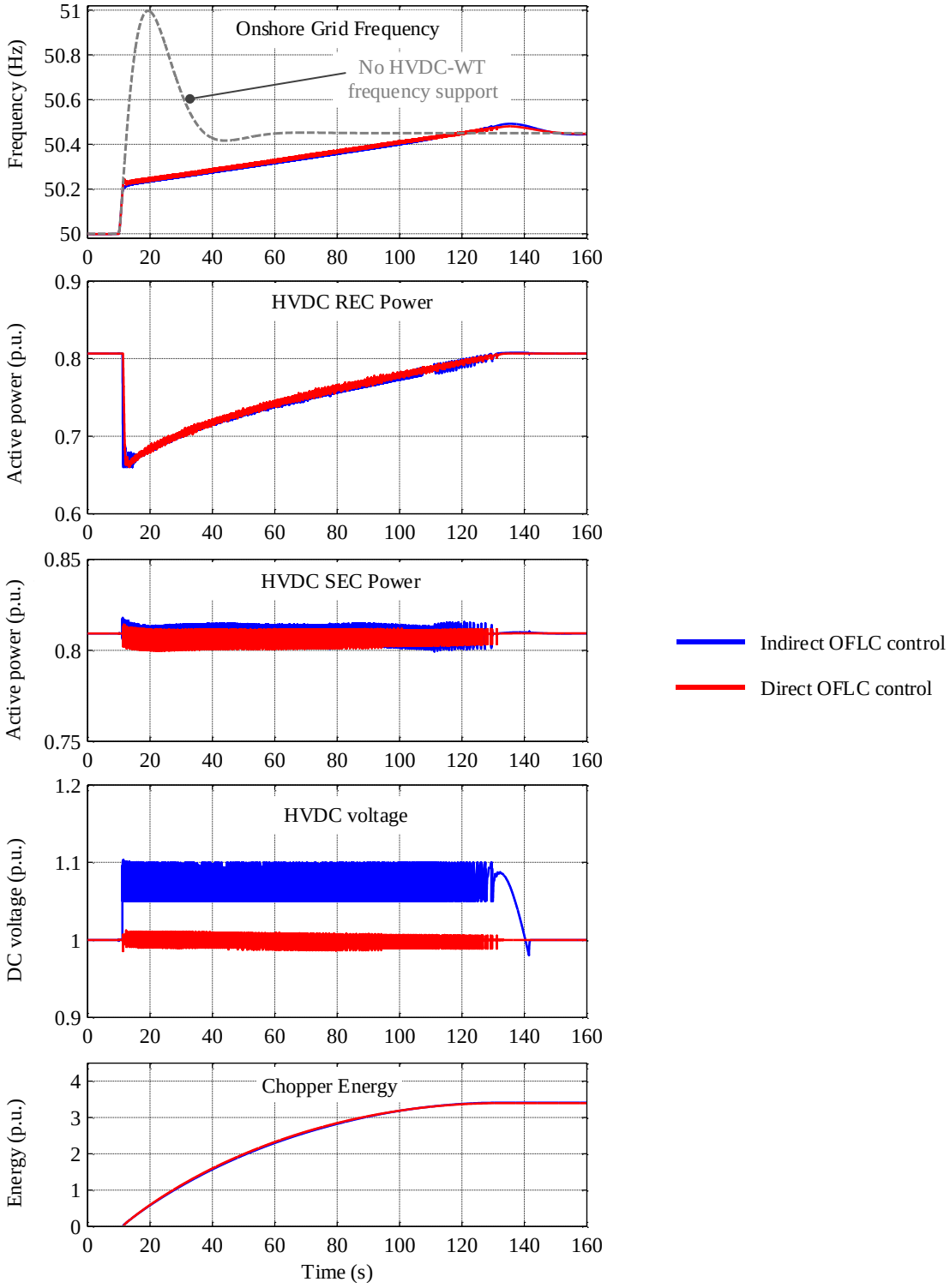

Figure 6-12: Performance of direct and indirect OFLC Strategies during an overfrequency event

6.4.2.1 Combined FSPC and OFLC strategies

OFLC and FSPC strategies can be combined to enhance the overfrequency limiting. As shown in Figure 6-13, the OFLC control limits effectively the RoCoF during the transient period, while the FSPC lower gradually the WF active power and lower the steady-state

frequency level of the primary frequency response. This combined strategy offers several advantages; on one hand the DC chopper will have to absorb less energy while the WTs can reduce their output power more slowly to avoid possible oscillations or mechanical stresses. Figure 6-13 shows that the energy absorption by the DC chopper decreases when the FSPC strategy is enabled; as a result, unnecessary over-dimensioning of the DC chopper can be avoided.

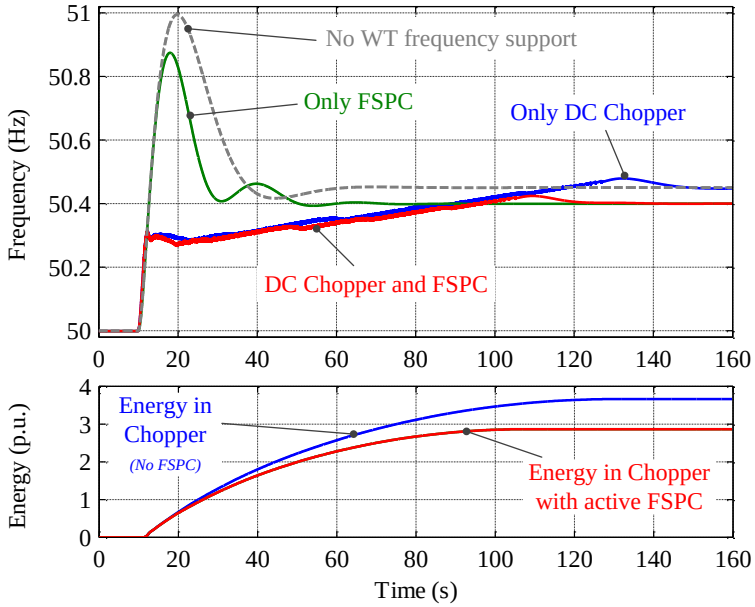

Figure 6-13: Comparison results for OFLC and FSPC strategies

Figure 6-14 summarizes the discussed control strategies for overfrequency limiting by the offshore WF with VSC-HVDC. The chopper control strategy shows the best results and can significantly limit the RoCoF during the primary frequency response. The best response is achieved by combining the chopper solution to limit the RoCoF as long as possible combined with output power reduction by the FSPC strategy. A possible combination of the chopper control and one of KEC strategies do not bring any improvement when compared to the frequency response with only chopper control.

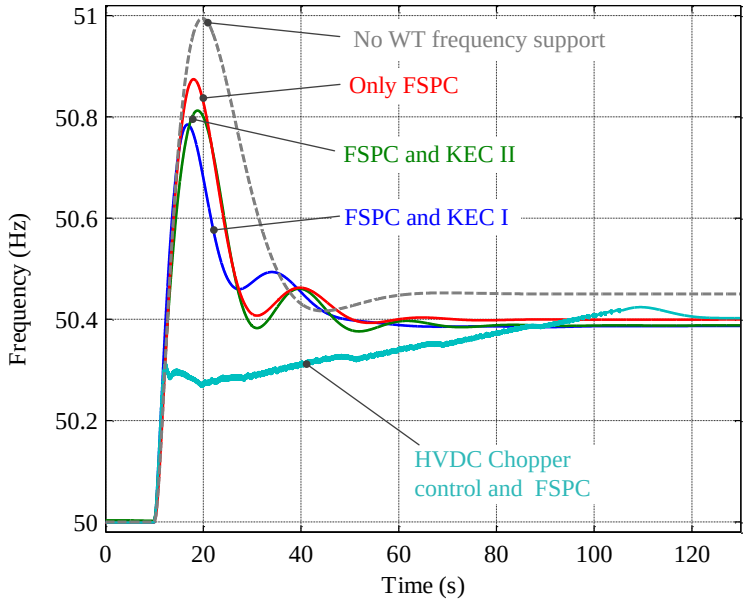

Figure 6-14: Comparison results for HVDC chopper with additional local FSCG-WT chopper control strategies

6.4.3 OFLC for offshore WFs with FSCG based WTs

A full-rated DC chopper is typically installed for FSCG based WTs. The DC chopper is designed to able to dissipated the maximum WT output power for a period of 3-5 s. OFLC strategy can therefore be applied for FSCG based WTs with AC or DC grid access.

In a configuration where FSCG based offshore WF is connected to the AC grid via a VSC-HVDC system (Figure 6-15), OFLC control can be applied for both the WTs and HVDC system resulting in a better overfrequency limitation. A robust communication link that sends the frequency measurement to the offshore WTs is prerequisite for this strategy. In general, the total time delay of the communication link and the measuring filter of the onshore grid frequency, that could add up to a 100 ms, does not adversely affect the performance of the proposed frequency control strategies by the offshore WTs.

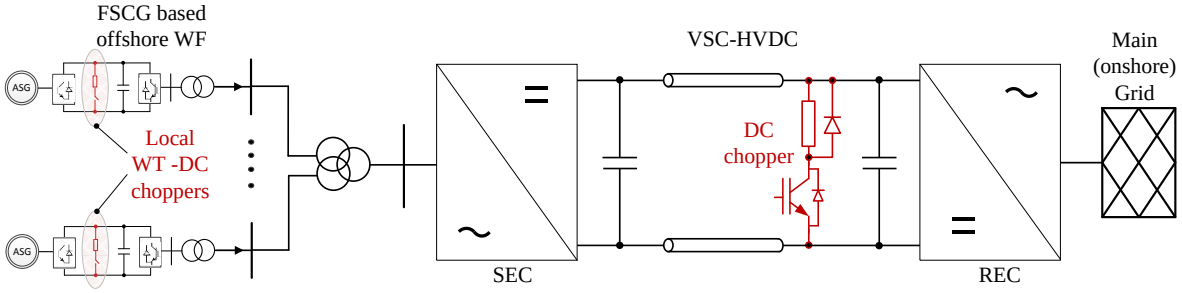

Figure 6-15: OFLC for HVDC with FSCG based offshore WF

Figure 6-16 compares between two simulation cases. In case 1 only the overfrequency

limiting control for the HVDC chopper is enabled. In case 2 each WT in the offshore WF receives the 'onshore' grid frequency measurements and activates its own chopper to participate in the overfrequency limiting control. The results indicate that applying the chopper control strategy locally for each FSCG based WT enhances the transient part of the primary frequency response and reduces the total energy absorption by the HVDC chopper.

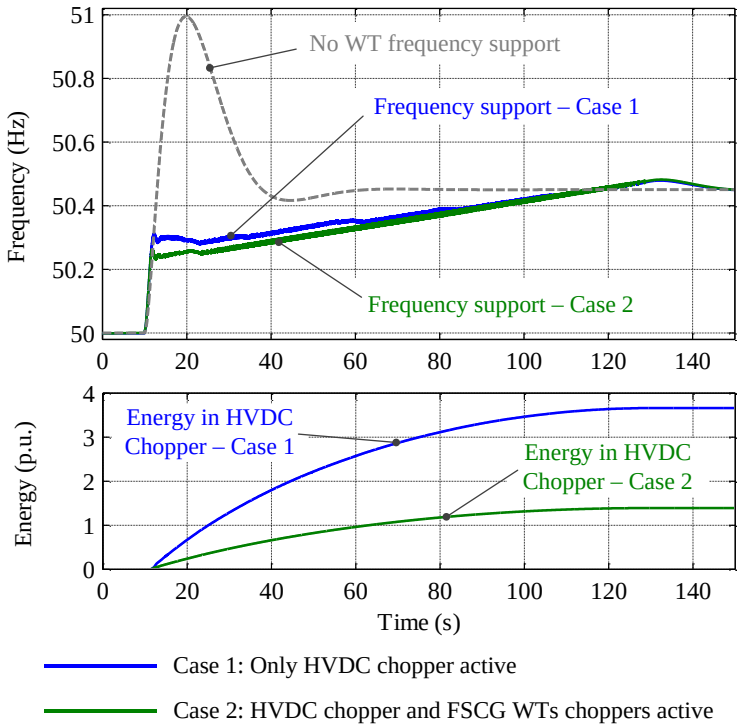

Figure 6-16: Comparison results for HVDC chopper with additional local FSCG-WT chopper control strategies

For offshore WFs with FSCG based WTs, the controlled voltage drop method [4] can be applied for a safe FRT operation during onshore faults. The basic idea is to replicate the fault condition at the offshore grid in a fast controlled manner, avoiding consequently the overvoltage in the HVDC link and the need for a DC chopper. In this case, the overfrequency limiting is performed only by the local DC choppers at each FSCG based WT. The onshore frequency increase can be either replicated at the offshore grid or sent through communication link to the offshore WF, the robust communication is a perquisite for the latter option.

To evaluate the performance of the OFLC strategy for low wind case, the overfrequency event will be tested when the offshore WF is running with 50% generation capability and compared to the case with full generation capacity. Thus at low wind conditions with a 50% generation , the offshore WF power share is 10%, while at high speed wind conditions the wind power share increases to 20%. Figure 6-17 shows the simulation result of this case. The frequency overshoot in both cases with no frequency support from the offshore WF is nearly identical

since no extra inertia source is added to the power system with unchanged total power generation.

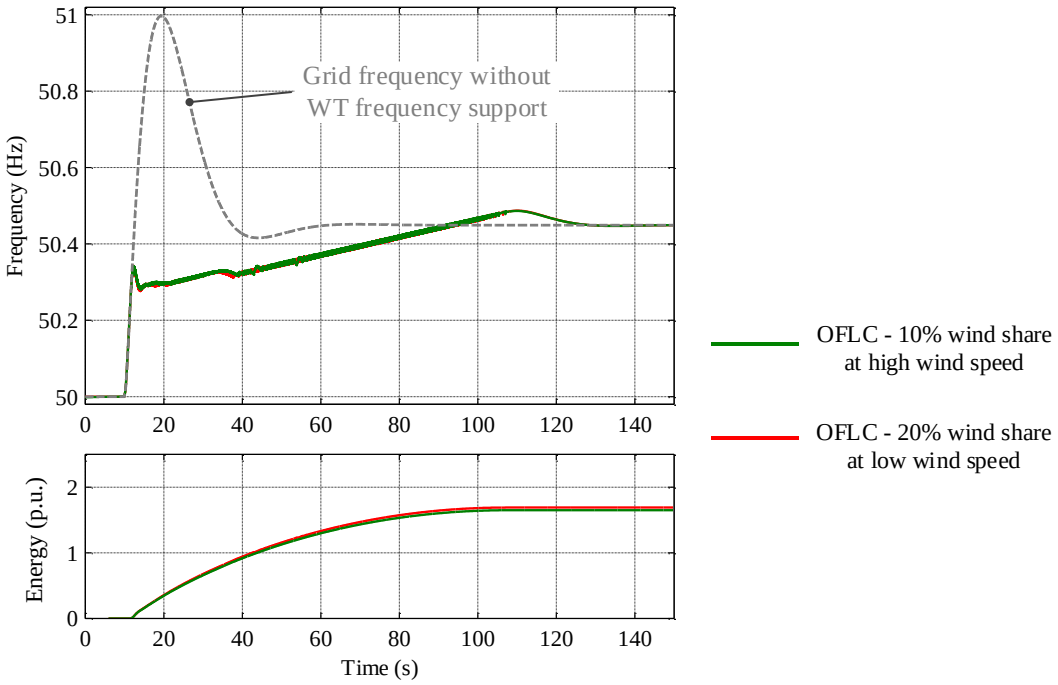

Figure 6-17: Comparison results for low and high wind speed and using OFLC strategy for local FSCG-WT chopper control strategies

6.4.4 OFLC for offshore WFs with DFIG based WTs

The DC chopper is installed typically in DFIG based WTs and FSCG based WTs. In DFIG system, the chopper is rated to the nominal DFIG rotor power which is limited to 0.3 p.u.. This means that DC chopper in DFIG based WTs cannot provide a significant power limitation and cannot provide the same contribution to overfrequency limiting as the case for FSCG based WTs. Thus the maximum theoretical energy that can be dissipated by the DC chopper in a DFIG based WT can be expressed as:

$$E_{\mathrm{CH}} = |s_{\max}| \cdot P_{\mathrm{nom}} \cdot t_{\max} \tag{6.5}$$

Where P_{nom} is the nominal WT power and $t_{\max}$ the maximum energy dissipation time and $s_{\max}$ is the maximum slip at which the chopper power is rated. Hence, if the DC chopper is designed to dissipate the maximum slip (rotor) power ($p_{\mathrm{r,max}} = 0.3$ p.u.) for a period of 3.5 s, the yielding energy can be calculated in p.u. as:

$$E_{\mathrm{CH,pu}} = 0.3*1*3.5 = 1.05 \text{ p.u.} \tag{6.6}$$

An important issue that must be taken into account is the influence of the DC chopper

operation on stator power when applying OFLC during overfrequency events. Since the MSC controls typically the total power of the DFIG at the AC bus as described in section 2.2.2.1, switching the DC chopper during no-fault condition will interfere with the power control. As a result, the stator power and thus the electrical torque will be affected by the power dissipated in the chopper. To minimize this adverse effect the measured chopper power must be considered in calculating the reference stator power from the WT power reference as shown in Figure 6-18.

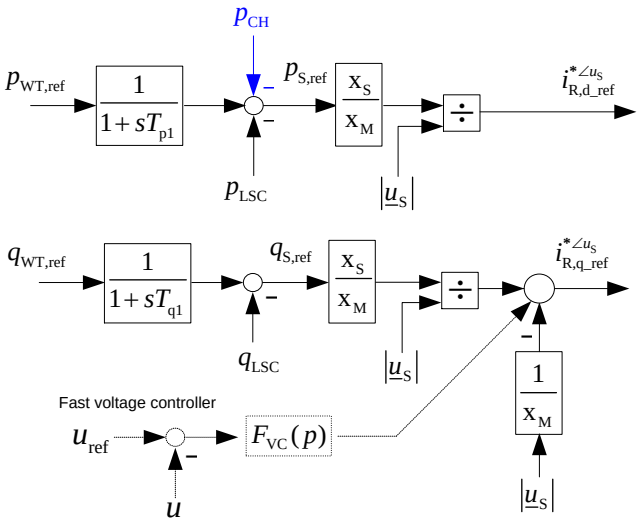

Figure 6-18: DFIG-WT power control at MSC with added chopper power measurement

In Figure 6-19, simulation results of an overfrequency event with OFLC by DFIG based WTs shows that the overfrequency limiting is more stable when considering the measured value of the chopper power in the MSC control. The interaction between the OFLC and power controller is minimized as seen in the stator power and generator torque results. As a result of the modified MSC control, the rotor speed will stay nearly constant during the overfrequency limiting period. Although the energy consumption for the case without DFIG control modification is higher as observed in the same figure; the frequency overshoot is higher due to the adverse interaction between both controllers.

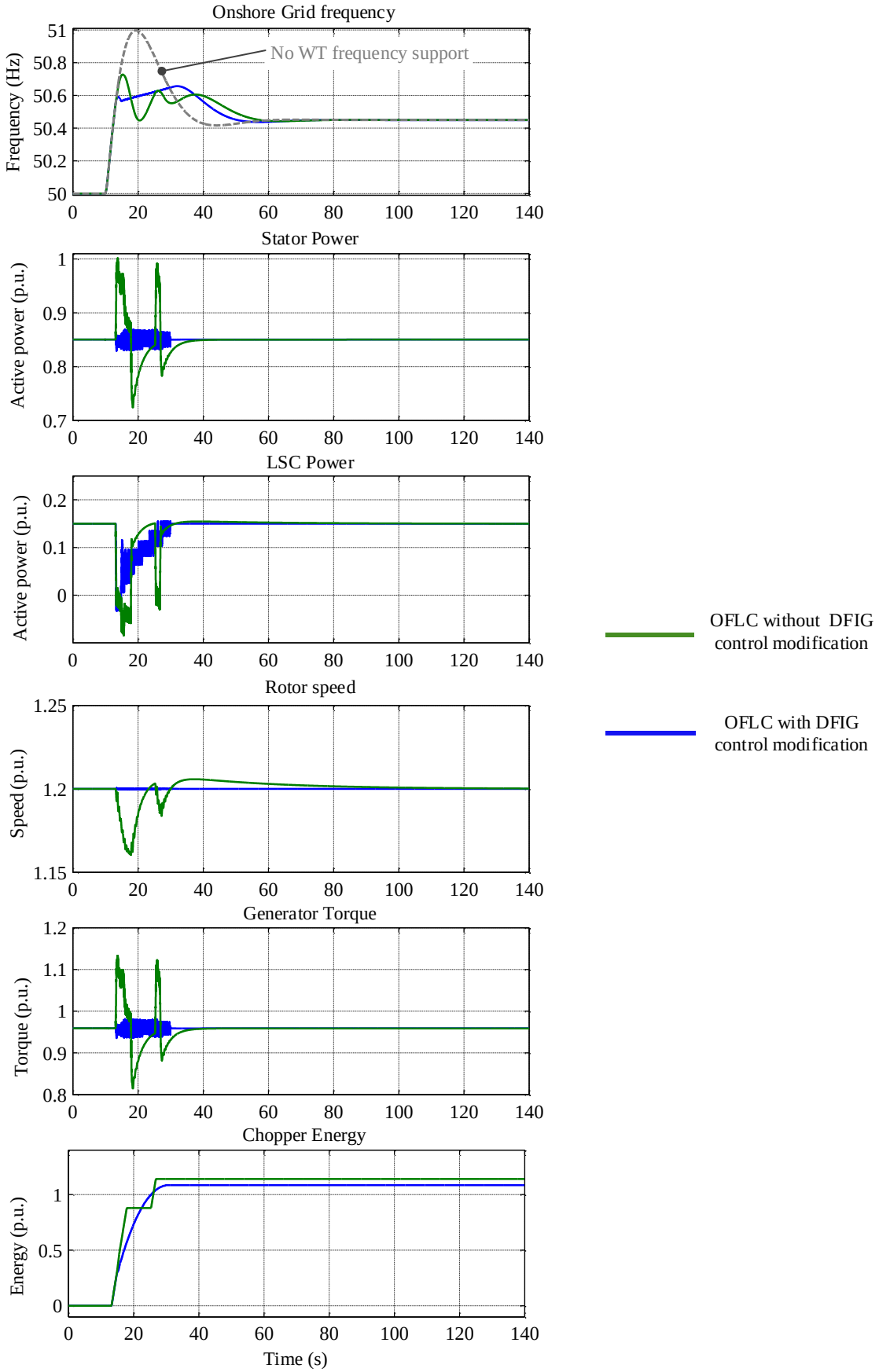

Figure 6-19: OFLC for DFIG based WT with MSC control modification

6.4.5 OFLC control for grids with high offshore wind share

The available overall chopper rating that can be potentially used for the proposed OFLC scheme increases with the installed wind power capacity. As a result, the proposed solution, if implemented, will inherently catch up with the requirements of the grid in terms of responding to dynamic frequency rise in networks with large wind share.

For a clear comparison, the primary frequency response without OFLC for the three cases is shown in Figure 6-20. The load events are adjusted for the 50% and 70% wind shares in order to produce a 51 Hz maximum frequency overshoot similar to the 20% wind share case. As discussed in section 5.2.4, the hydro governor action gets stronger as the frequency sensitivity to an active power change increases with the increase of wind power share. Thus the settling frequency as observed is closer to the nominal frequency in the 70% wind power share case compared to the 50% or 20% cases.

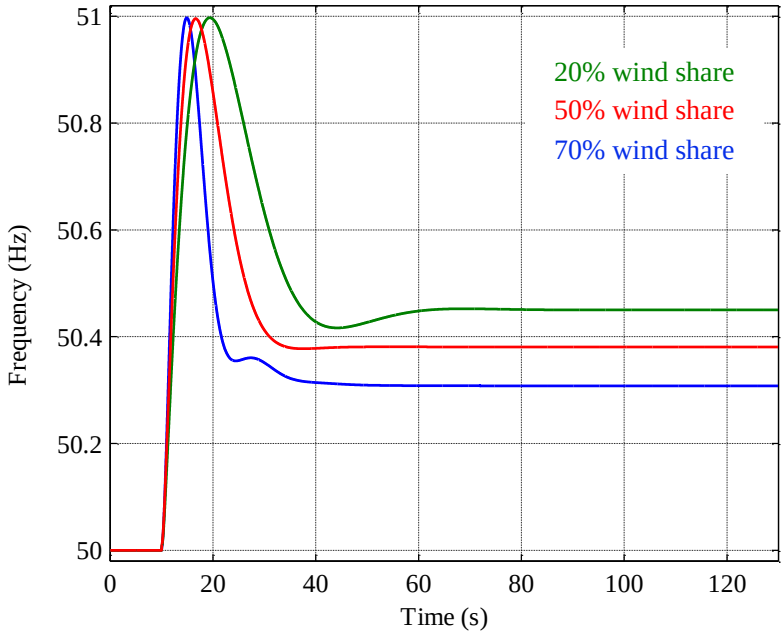

Figure 6-20: Primary frequency response with 51 Hz maximum frequency for different wind shares without frequency support from HVDC connected offshore WF

To study the effect of the wind power share on the performance of the OFLC strategy, the 20% wind share is used as a basis for the comparison. The parameters of the OFLC is tuned for the 20% wind share case and kept unchanged while testing comparable frequency events for 50% and 70% wind shares. The performance of the RoCoF limitation is nearly the same for all cases as shown in Figure 6-21. The limitation effect of the RoCoF increases slightly with the increase of wind power share. On the other hand, the duration of the transient period reduces clearly as the wind power share increases. As the frequency sensitivity to active

power change increases with higher wind power share, it can be observed that the ripple caused by the chopper switching becomes more intensified during the transient period.

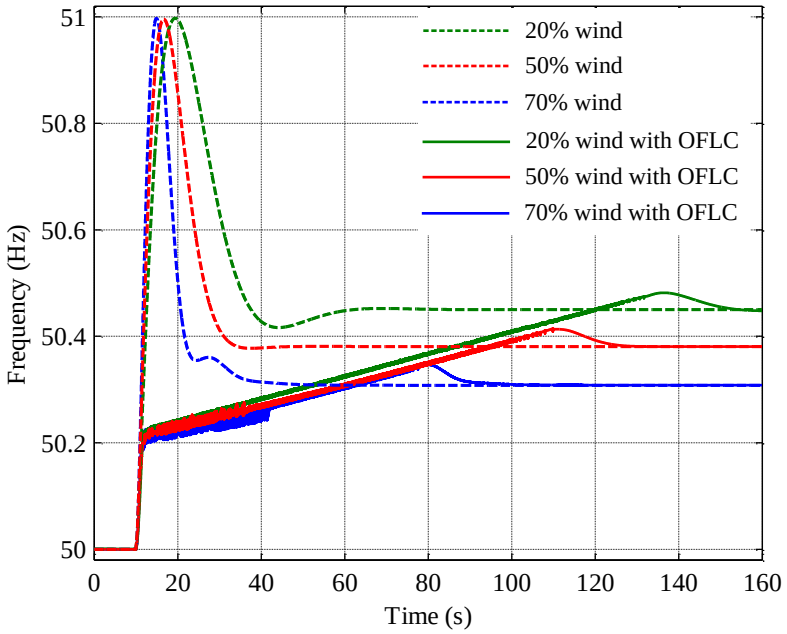

Figure 6-21: Primary frequency response with 51 Hz maximum frequency for different wind shares with frequency support by OFLC the VSC-HVDC

6.4.6 Multi-level HVDC chopper

Modern VSC-HVDC with multi-level converter topology features a multi-level DC switching chopper which offers different power dissipation levels [20]. In this arrangement, the DC chopper resistance is divided into a specific number of independently controlled switchable resistances in which offers smooth DC voltage and current control rather than having only a single switchable DC chopper resistor. The module based DC chopper offers scalability, redundancy and low maintenance requirement [60]. It can be also used in general as a protection function in case of emergency conditions which requires fast power reduction. Since average-based modeling approach is considered for VSC-HVDC in the conducted studies in this thesis, specific control features of the multi-level DC chopper topology are not investigated.

6.5 Discussion of simulation results

The chopper control strategy has the advantage of offering a defined amount of energy dissipation independent of the actual wind power prior to the overfrequency event. Furthermore, badly tuned chopper control leads only to less limitation of the overfrequency and will not adversely interact with the WT controllers as the case with KEC strategies. Only

in the case of a very high wind share with HVDC connection (above 70% of total power generation), the frequency of the DC chopper switching must set carefully to avoid causing any frequency oscillation during the transient period of the primary frequency response.

The FSPC method provides power reduction by increasing the pitch angle which is typically limited to a certain rate to avoid mechanical stresses, thus FSPC will have limited ability to provide fast frequency control in low-inertia grids with high RoCoF. Two KEC methods are utilized and evaluated for the overfrequency limiting purpose. By a certain control sequence the kinetic energy in the rotor can be controlled in a way to limit the frequency overshoot. Both methods KEC I and KEC II are able to limit the frequency overshoot, the main concerns about applying these strategies are the strong dependency on the wind speed level and the difficulty of tuning the control parameter for a grid with high wind share. FSPC and KEC strategies can be combined for an improved frequency response.

The strategy employing the DC chopper in the HVDC system and the FSCG based WTs offers an attractive alternative to the previous strategies and provides the best performance regarding the limitation of the transient overfrequency. One important aspect here is that this solution is temporary and can be applied for certain period of time corresponding to the maximum energy absorption capability of the DC chopper. Proper control settings can avoid extra costs due to over-dimensioning the DC chopper.

7 Summary and Conclusion

The main dynamic modeling and control aspects for integrating large offshore WFs via VSC-HVDC system were investigated in this thesis. Special emphasis was given to the control strategies at each HVDC converter station taking into account the nature of the interconnected AC networks. Besides establishing the voltage magnitude and frequency of the offshore grid, the offshore HVDC-SEC controller should be carefully designed to avoid adverse interactions with offshore WF controllers. A coordinated control strategy was proposed in this thesis to enhance the stability of the offshore grid and consequently the availability of the offshore wind power.

The AC voltage -reactive power control strategy for the onshore HVDC-REC depends mainly on the grid operator requirements. Slow and fast voltage control loops can be implemented to fulfill both steady-state and dynamic requirements of the grid code. A review of the existing REC and SEC control strategies has been done and enhancements regarding the dynamic performance of the offshore grid were proposed and verified through EMT time-domain simulations. The focus in this thesis was on offshore WFs with DFIG based WT technology.

An essential target for designing the offshore grid is minimizing the high offshore installation costs, which results in the absence of n-1 criterion at certain locations in the offshore WF and the HVDC link. Offshore AC cables suffer in general less fault conditions in comparison with overhead-lines, and these are usually caused by a permanent mechanical damage in the cable. This fact makes the FRT operation for offshore faults more challenging than onshore "overhead lines" grid faults. Additionally, the short-circuit contribution of the offshore WFs depends on the type of connected offshore WF with its converters control design. DFIG based WTs provides a higher short-circuit current due to the direct grid connection of the stator circuit in comparison to FSCG based WT. These aspects determine the main control and protection philosophy at the offshore grid.

Different control strategies were presented for the offshore HVDC-SEC in this work. Voltage and frequency control can be combined with fast inner current controllers to allow a robust current limitation during offshore grid faults and avoid consequently blocking the IGBT valves of the offshore SEC. Alternative angle control strategy is proposed for the HVDC-SEC which allows fast and smooth offshore frequency control combined with an inner current control loop. The offshore frequency can be controlled to replicate the onshore frequency to provide fast frequency support by the offshore WTs in case no robust communication links exist in the HVDC transmissions system.

In an offshore grid dominated by power electronics based converters, controllers interaction during normal operation is a vital aspect that should have a high priority when designing the HVDC-SEC control. Improperly tuned current controller can cause adverse interactions with the WTs controllers that can lead to unstable resonant interactions in the offshore grid. In this scope, a new control strategy with indirect current limitation has been introduced for the HVDC-SEC. In this strategy it was proposed, instead of using a current controller, to decrease the AC voltage reference at the offshore grid upon fault detection limiting thereby the converter short-circuit current contribution. The voltage reference can be ramped up after successful fault clearance to avoid blocking the IGBTs due to a second high current peak. The possibility for adverse control interactions with the WT converters is significantly lower, however, it cannot provide fast and robust current limitation during very low impedance faults which forces the protection system to block the IGBTs above a certain current peak.

An important aspect regarding FRT capability for the HVDC-SEC is related to the offshore grid topology and the ability of the protection relays to isolate the faulty part to allow the rest of the offshore WF to keep feeding in its generated power. For real applications and in an early planning stage, simulations studies must be conducted with detailed models of the real WTs with its converters filters and dynamic controllers along with offshore AC cables and transformers models to determine the most suitable control strategy for the offshore HVDC-SEC. Since no standards exist for WT converter controllers and the short-circuit behavior of WTs, the outcome of many evaluation studies on possible control interactions cannot be generalized to all offshore WFs even for WFs with similar WT types.

As the wind power share in modern power system increases, wind generation units are required to participate effectively in the primary frequency support during underfrequency or overfrequency events caused by temporal energy imbalances. Fast frequency control methods were investigated in this thesis to enable the offshore WFs to provide a frequency support equivalent to the inertial support provided by the synchronous generators. Improvements on the existing frequency support by pitch control strategy (FSPC) have been proposed to ensure consistent performance for low and high wind speed cases. A thorough investigation of the kinetic energy control (KEC) methods showed that the performance of these methods rely heavily on the available wind speed level, actual wind power share and its controller parameter tuning. Although tuning of the KEC control parameters targets the best outcome for widest possible range of the WT rotor speed, the assumption that the RoCoF and the underfrequency profile is well known is not realistic in most power systems. Furthermore the thesis considered an aggregated WF without considering wind speed variations within the

offshore WF. The latter aspect must be considered in depth in future research with the focus on developing a coordinated control strategy to optimize the KEC response for the whole WF.
The new concerns regarding overfrequency events that might take place in the northern part of the German grid due to energy generation surplus coming from the offshore WFs were discussed in this work. To avoid high frequency overshoots that may trigger protection schemes which lead to major tripping of WFs, fast overfrequency limiting strategies were given a special emphasis. In this thesis a new method with the acronym OFLC was proposed to limit the overfrequency by utilizing the DC chopper which is typically installed in HVDC systems for offshore applications. A dedicated OFLC control was designed to target limiting the frequency overshoot during the first seconds of the primary frequency response period. The capability limit of the energy dissipation by the DC chopper was investigated as a limiting factor for this strategy. With an appropriate control design no over-sizing of the DC chopper and thus no additional costs would be required. The proposed OFLC strategy showed a superior performance over other strategies in terms of fast limiting of the RoCoF in the transient period and provided in combination with the FSPC strategy the best overfrequency limiting performance. The OFLC strategy was also tested for full rated DC choppers in the FSCG based WT and provided similarly good performance. For an offshore WF with FSCG based WTs and HVDC connection, the proposed strategy can be applied on the HVDC chopper and local WT DC choppers simultaneously to obtain an improved overfrequency limitation. For DFIG based WTs it was shown that the DC chopper can contribute effectively to the overfrequency limiting despite being only rated up to 30% of the nominal WT power. However, DC chopper switching during no-fault conditions can interact with the MSC power controller which is adversely reflected on the generator torque and rotor speed. Therefore it was proposed to include the measured DC chopper power in the MSC control to minimize the interaction effect and keep the stator power and thus the rotor speed nearly constant during the utilization period of the DC chopper for limiting the onshore overfrequency.
A coordinated control that optimize the utilization of the energy dissipation capability of all participating DC choppers can extend the RoCoF limitation period and allow smoother power reduction of the WT units in the primary and secondary frequency response periods. An alternative controller design for the proposed OFLC method can be investigated in a future work to employ an online optimization method for enhancing the overfrequency limiting performance with minimum energy dissipation according to the actual network configuration and the nature of the overfrequency event.
A future solution incorporating an energy storage system could replace the DC chopper to

provide frequency control for both over and underfrequency events. The energy storage system should handle as well the original functionality of the DC chopper during grid faults. This solution is not considered feasible as long as no real breakthrough occurs in the energy storage technology regarding cost and expected operation lifetime issues.

8 References

[1] Tennet offshore WF projects: Online, available: http://www.tennet.eu/de/netz-und-projekte/offshore-projekte.html.

[2] M. Behnke, A. Ellis, Y. Kazachkov, T. McCoy, E. Muljadi, W. Price, and J. Sanchez - Gasca, "Development and validation ofWECC variable speed wind turbine dynamic models for grid integration studies," in AWEA WindPower Conference, 2007.

[3] Kretschmann J.; Wrede H.; Müller-Engelhardt S.; Erlich I.; "Enhanced Reduced Order Model of Wind Turbines with DFIG for Power System Stability Studies," Power and Energy Conference, 2006. PECon '06. IEEE International, 28-29 Nov. 2006.

[4] C. Feltes, "Advanced Fault Ride-through Control of DFIG Based Wind Turbines Including Grid Connection Via VSC-HVDC," Ph.D. dissertation, Dep. Elec. Eng., Uni. Duisburg Essen, Germany, 2012.

[5] M. Suwan T.Neumann, C. Feltes; I. Erlich, „Educational experimental rig for Doubly-Fed Induction Generator based wind turbine," IEEE PES General meeting 2012, 22-26 July, San Diego, USA.

[6] J. Fortmann, S. Engelhardt, J. Kretschmann, C. Feltes, Tobias Neumann, Istvan Erlich, „Generic Simulation Model for DFIG and Full Size Converter based Wind Turbines," 9th International Workshop on Large-Scale Integration of Wind Power into Power Systems Oct. 2010, Quebec City, Quebec, Canada.

[7] M. Wilch, "Aspekte der Netzeinbindung von Windenergieanlagen," Ph.D. dissertation, Dep. Elec. Eng., Uni. Duisburg Essen, Germany, 2013.

[8] J. Slootweg, "Wind Power - Modeling and Impact on Power System Dynamics", Dessertation, DELFT University, 2003.

[9] Chan-Ki Kim, V. K. Sood, G. Jang, S. Lim, S. Lee, "HVDC Transmission: Power Conversion Applications in Power Systems," IEEE Press, John Wiley & Sons (Asia) Pte Ltd, 2009.

[10] ABB, "VSC-HVDC Transmission with Cascaded Two-Level Converters", CIGRE 2010. Available, online: http://www.abb.de/industries/us/9AAF400196.aspx.

[11] ABB, "Technical description of HVDC Light technology", rev. 7, 2013, [online], Available: http://www.abb.com.

[12] V. Hussennether, D. Worthington, B. Hühnerbein, "Projects BorWin2 and HelWin1 Large Scale Multilevel Voltage-Sourced Converter Technology for Bundling of Offshore Windpower", CIGRE 2012.

[13] S. P. Teeuwsen, "Simplified Dynamic Model of a Voltage-Sourced Converter with Modular Multilevel Converter design," IEEEIPES -Power Systems Conference and Exposition, Mar. 2009.

[14] M. Dommaschk, "Modularer Multilevelstromrichter für Anwendung in der Hochspannungsgleichstromübertragung, " Ph.D. dissertation, Dep. Elec. Eng., Uni. Chemnitz, Germany, 2013.

[15] ABB: "Recent advancements in HVDC VSC systems HVDC and Power Electronics technology and development," CIGE 2015. Online, available: https://library.e.abb.com/public/e88c538bbd394c8baed8fe032573c082/Recent%20advancements%20in%20HVDC%20VSC%20systems.pdf

[16] Siemens [2011]: HVDC Plus – Basics and Principles of Operation. Available, online: http://www.energy.siemens.com/hq/pool/hq/power-transmission/HVDC/HVDC_Plus_Basic%20and%20Principals.pdf

[17] Grain P. Adam, Barry W. Williams," Half- and Full-Bridge Modular Multilevel Converter Models for Simulations of Full-Scale HVDC Links and Multiterminal DC Grids," IEEE Journal of Emerging and Selected Topics in Power Electronics (Volume:2 , Issue: 4). Dec. 2014.

[18] V. Staudt, M. Jäger ; Axel Rothstein ; A. Steimel," Short-circuit protection in DC ship grids based on MMC with full-bridge modules," Electrical Systems for Aircraft, Railway, Ship Propulsion and Road Vehicles (ESARS), 2015 International Conference.

[19] T. Haileselassie, "Control, Dynamics and Operation of Multi-terminal VSC-HVDC Transmission Systems," PhD dissertation, Norwegian University of Science and Technology, Dec. 2012.

[20] K. Friedrich, "Modern HVDC PLUS application of VSC in Modular Multilevel Converter Topology," 2010, [online], Available: http://www.ptd.siemens.de/Paper_ISIE2010_Fd.pdf.

[21] Stijn Cole, "Steady-State And Dynamic Modeling Of Vsc Hvdc Systems For Power System Simulation," PhD. dissertation, KU Leuven, Spetember 2010.

[22] S. Engelhardt, J. Kretschmann, J. Fortmann, F. Shewarega, I. Erlich, C. Feltes, " Negative Sequence Control of DFG based Wind Turbines," IEEE PES General Meeting 2011, San Diego, USA.

[23] S. Engelhardt, " Direkte Leistungsregelung einer Windenergieanlage mit doppelt gespeister Asynchronmaschine," Ph.D. dissertation, Dep. Elec. Eng., Uni. Duisburg Essen, Germany, 2013.

[24] M. Sujod, "Advanced Converter Control Techniques for Improving the Performances of DFIG based Wind Turbines," Ph.D. dissertation, Dep. Elec. Eng., Uni. Duisburg Essen, Germany, 2014.

[25] Tennet: Requirements for Offshore Grid Connections in the Grid of TenneT TSO GmbH. Available, online:
http://www.tennet.eu/de/fileadmin/downloads/Kunden/tennet_tso_gmbh-asn-eng_21122012_final.pdf

[26] H.Saad,J.Peralta,S.Dennetiere,J.Mahseredjian,J.Jatskevich,J. A. Martinez, A. Davoudi, M. Saeedifard, V. Sood, X. Wang, J. Cano,and A. Mehrizi-Sani, "Dynamic averaged and simplified models for MMC-based HVDC transmission systems," IEEE Trans. Power Del., vol. 28, no. 3, pp. 1723–1730, Jul. 2013.

[27] C. Hahn, M. Burkhardt, M. Luther and O. Ruhle, "Generic Modeling of a Self-Commutated Multilevel VSC HVDC System for Power System Stability Studies," Applied Power Electronics Conference and Exposition (APEC), 2015 IEEE.

[28] C. Feltes, R. van de Sandt, F. Koch, F. Shewarega, I. Erlich, „Neutral Grounding in Wind Farm Medium Voltage Collector Grids," Power Systems Conference and Exposition (PSCE), 20-23 March 2011, Phoenix, AZ.

[29] M. Esken, C. Feltes, "Electrical protection system at Nordsee Ost offshore wind", available, online:
http://wiki-cleantech.com/wind-energy/electrical-protection-system-at-nordsee-ost-follow-utility-approach-to-get-maximum-operational-flexibility-and-reliability-for-an-offshore-power-plant.

[30] C. Feltes, S. Engelhardt, J. Kretschmann, J. Fortmann, I. Erlich, „Dynamic Performance Evaluation of DFIG-based Wind Turbines regarding new German Grid Code Requirements ," IEEE PES GM 2010, Minneapolis, MN, USA.

[31] Tennet: Requirements Grid code – High and extra high voltage-. Available, online:
http://www.tennet.eu/de/fileadmin/downloads/Kunden/tennet-NAR2015eng.pdf.

[32] VDE, "E VDE-AR-N 4120:2012-11 Technische Bedingungen für den Anschluss und Betrieb von Kundenanlagen an das Hochspannungsnetz."

[33] I. Erlich, T. Neumann, F. Shewarega, P. Schegner, and J. Meyer, "Wind Turbine Negative Sequence Current Control and its Effect on Power System Protection," in *IEEE PES General Meeting*, 2013.

[34] Wijnhoven, T., Deconinck, G. ; Neumann, T. ; Erlich, I., „Control aspects of the dynamic negative sequence current injection of type 4 wind turbines," IEEE PES General Meeting, July 2014, National Harbor, MD, USA.

Altın, M.; Göksu, O.; Teodorescu, R.; Rodriguez, P., "Overview of recent grid codes for wind power integration," IEEE OPTIM 2012, Brasov, Romania.

[35] ENTSO-E: ENTSO-E Network Code for Requirements for Grid Connection Applicable to all Generators. March 2013, available, Online: http://networkcodes.entsoe.eu/connection-codes/requirements-for-generators/

[36] L. Harnefors, M. Bongiorno, and S. Lundberg, "Input-admittance calculation and shaping for controlled voltage-source converters," IEEE Trans. Ind. Electron., vol. 54, no. 6, pp. 3323-3334, Dec. 2007.

[37] Wang, Xiongfei; Blaabjerg, Frede; Chen, Zhe; Wu, Weimin," Modeling and analysis of harmonic resonance in a power electronics based AC power System," Proceedings of the 2013 IEEE Energy Conversion Congress and Exposition (ECCE). (pp. 5229-5236).

[38] Pipelzadeh, Y., Chaudhuri, B., Green, T.C., "Inertial response from remote offshore wind farms connected through VSC-HVDC links: A Communication-less scheme," IEEE PES General Meeting, July-2012, San Diego, USA.

[39] T. M. Haileselassie, R. E. Torres-Olguin, T. K. Vrana, K. Uhlen, and T. Undeland, " Main Grid Frequency Support Strategy for VSC-HVDC Connected Wind Farms with Variable Speed Wind Turbines," PowerTech, 2011 IEEE Trondheim, 19-23 June 2011.

[40] C. Feltes and I. Erlich, "Variable Frequency Operation of DFIG based Wind Farms connected to the Grid through VSC-HVDC Link," IEEE PES GM 2007, 24-28 June, Tampa, FL.

[41] NERC: "Balancing and frequency control". Jan, 2011. [Online]. Available: http://www.nerc.com/docs/oc/rs/NERC%20Balancing%20and%20Frequency%20Control%20040520111.pdf.

[42] RogÉrio G. de Almeida ; J. A. Pecas Lopes, "Participation of Doubly Fed Induction Wind Generators in System Frequency Regulation," IEEE Transactions on Power Systems (Volume: 22, Issue: 3, Aug. 2007).

[43] Hanne Støylen, Kjetil Uhlen ; Atle Rygg Årdal, "Laboratory Demonstration of Inertial Response from VSC-HVDC connected Wind Farms," AC and DC Power Transmission, 11th IET International Conference, Birmingham, Feb 2015.

[44] J. Machowski, J. W. Bialek and J. R. Bumby, Power System Dynamics Stability and Control, 2nd ed., John Wiley \& Sons, Ltd., 2012.

[45] Y. Pipelzadeh, B. Chaudhur and T.C. Green, "Inertial Response from Remote Offshore Wind Farms Connected Through VSC-HVDC Links: A Communication-less Scheme," IEEE PES General Meeting, 22-26 July 2012.

[46] Adri Junyent-Ferr; Yousef Pipelzadeh ; Tim C. Green, "Blending HVDC-Link Energy Storage and Offshore Wind Turbine Inertia for Fast Frequency Response," IEEE Transactions on Sustainable Energy (Volume:6 , Issue: 3), July 2015.

[47] P. Kundur, Power system stability and control, ser. The EPRI power system engineering series. New York; London: McGraw-Hill, 1994.

[48] I. Erlich and M. Wilch, "Primary frequency control by wind turbines," IEEE PES General Meeting, 25-29 July 2010.

[49] K. Clark, N. Miller, and J. Sanchez-Gasca, "Modeling of GE wind turbine-generators for grid studies," Version 4.5, GE Energy, April 2010.

[50] N. Miller, K. Clark, and Shao, M., "Frequency responsive wind plant controls: Impacts on grid performance," IEEE PES General Meeting, 24-29 July 2011.

[51] Lisa Ruttledge, Nicholas W. Miller, Jonathan O'Sullivan, Damian Flynn, "Frequency Response of Power Systems with Variable Speed Wind Turbines ", IEEE Transactions on Sustainable Energy, Vol. 3, No. 4, October 2012.

[52] IEEE Spectrum: Germany Takes the Lead in HVDC. Online: http://spectrum.ieee.org/energy/renewables/germany-takes-the-lead-in-hvdc

[53] Pelletier, M.A., Phethean, M.E. ; Nutt, S., „Grid code requirements for artificial inertia control systems in the New Zealand power system", IEEE PES General Meeting, 22-26 July 2012.

[54] Transmission Provider Technical Requirements for the Connection of Power Plants to the Hydro-Québec Transmission System, Hydro-Québec TransÉnergie,February2009, http://www.hydroquebec.com/transenergie/fr/commerce/pdf/exigence_raccordement_fev_09_en.pdf.

[55] ENTSO-E Draft Network Code on High Voltage Direct Current Connections and DC connected Power Park Modules, 30 April 2014, [online], available: https://www.entsoe.eu.

[56] Implementation Guideline for Network Code "Requirements for Grid Connection Applicable to all Generators", 16 October 2013, [online], available: https://www.entsoe.eu.

[57] J. Zhu, C. D. Booth, G. P. Adam, A. J. Roscoe, and C. G. Bright, "Inertia emulation control strategy for VSC-HVDC transmission systems," IEEE Transactions on Power Systems, vol. 28, no. 2, pp. 1277–1287, 2013.

[58] Stendius, L., Sandeberg, P," Large scale offshore wind power energy evacuation by HVDC Light", European Wind Energy Conference EWEC 2008, [online], available: http://www.abb.com.

[59] Y. Jiang-Häfner, R. Ottersten," HVDC with Voltage Source Converters – A Desirable Solution for Connecting Renewable Energies", online, available: http://www.abb.com.

[60] J. Strauss, Siemens AG," MMC Design Aspects and Applications ", online, available: http://www.ptd.siemens.de/CIGRE_MMC_DesignAspects.pdf.

Publications and R&D project Reports

A. Mohammad Suwan and Istvan Erlich, „Overfrequency Limiting Control by VSC-HVDC Connected Offshore WFs“, IEEE PES general meeting conference, Denver, USA, July 2015.

B. Istvan. Erlich, F. Shwearega and Mohammad Suwan, „Coordinated Voltage – Reactive Power Control in Networks with Embedded VSC HVDC Lines“, 9th IFAC Symposium on Control of Power and Energy Systems (CPES) – December 2015, New Delhi, India.

C. Mohammad Suwan and Istvan Erlich, „Frequency Control by HVDC connected Offshore Wind Farms for Overfrequency Limitation“, IEEE Energycon, Leuven, Belguim, April 2016.

D. Mohammad Suwan, T. Neumann, C. Feltes and Istvan Erlich,“ Educational experimental rig for Doubly-Fed Induction Generator based wind turbine“, IEEE PES general meeting conference, San Diego, USA, July 2012.

E. Mohammad Suwan and Istvan Erlich, „Modeling of VSC-HVDC connected Offshore Wind Farms for RMS-type Stability Studies“, Dresdener Kreis, Leipzig, Germany, March 2014.

F. Mohammad Suwan, „Modeling of Protection Systems for Offshore WF with VSC-HVDC grid connection“, final report, Research project funded by federal ministry for envirnoment and nature conservation (BMU) and cooperation with Senvion – Germany, October 2014.

G. Mohammad Suwan, „Design and Development of VSC-HVDC Transmission System for Integrating Large Offshore Wind Farms to the Grid“, final report, Research project, RWE Innogy – Germany, April 2014.

A. Appendix

A.1 Basics of space vectors

Three-phase time-dependent quantities can be represented as complex rotating space vector in an arbitrary chosen reference frame. Assuming a fixed frequency ω, the three-phase quantities can be transformed into a complex state vector as following:

$$\underline{u} = u_{\mathrm{a}} + \mathrm{j}\frac{\sqrt{3}}{2}\left(u_{\mathrm{b}} - u_{\mathrm{c}}\right) u_{\beta} = u_{\alpha} + \mathrm{j}u_{\beta} \tag{A.1}$$

Typically no zero sequence voltage is induced through the converter transformer. Hence equation (A.1) applies also for steady-state unbalanced conditions. In this work a number of annotations are used to represent different reference frames. In a stationary reference frame, the complex space vector can be written as:

$$\underline{u}^{\angle 0} = u_{\alpha} + \mathrm{j}u_{\beta} \tag{A.2}$$

The positive sequence space vector is given the subscript "1":

$$\underline{u}_1^{\angle 0} = u_{1\alpha} + \mathrm{j}u_{1\beta} \tag{A.3}$$

While the negative sequence vector is given the subscript "2":

$$\underline{u}_2^{\angle 0} = u_{2\alpha} + \mathrm{j}u_{2\beta} \tag{A.4}$$

IN a vector control approach the complex vectors are aligned to a synchronous rotating system representing the fundamental frequency ω. In this reference frame the space vector is fixed and its components become DC quantities (dq-components) [4]. This dq-transformation allows a developing fast and reliable voltage and current control with simple PI-controllers. The space vector is represented in the rotating reference frame as:

$$\underline{u}^{\angle \omega} = \underline{u}^{\angle 0} e^{-\mathrm{j}\omega t} = u_{\mathrm{d}}^{\angle \omega} + \mathrm{j}u_{\mathrm{q}}^{\angle \omega} \tag{A.5}$$

The space vector in an unbalanced system will be composed of positive and negative sequence complements as following:

$$\begin{aligned}
&\underline{u}^{\angle 0} = u_{\alpha} + \mathrm{j}u_{\beta} = \frac{2}{3}\left(u_{\mathrm{a}} + \underline{a}\, u_{\mathrm{b}} + \underline{a}^2 u_{\mathrm{c}}\right) \\
&= \frac{1}{3}\left(\underline{u}_{\mathrm{a}}^{\angle 0} + \left(\underline{u}_{\mathrm{a}}^{\angle 0}\right)^* + \underline{a}\,\left(\underline{u}_{\mathrm{b}}^{\angle 0} + \left(\underline{u}_{\mathrm{b}}^{\angle 0}\right)^*\right) + \underline{a}^2\left(\underline{u}_{\mathrm{c}}^{\angle 0} + \left(\underline{u}_{\mathrm{c}}^{\angle 0}\right)^*\right)\right) \\
&= \frac{1}{3}\left(\underline{u}_{\mathrm{a}}^{\angle 0} + \underline{a}\, \underline{u}_{\mathrm{b}}^{\angle 0} + \underline{a}^2 \underline{u}_{\mathrm{c}}^{\angle 0}\right) + \frac{1}{3}\left(\left(\underline{u}_{\mathrm{a}}^{\angle 0}\right)^* + \underline{a}\,\left(\underline{u}_{\mathrm{b}}^{\angle 0}\right)^* + \underline{a}^2\left(\underline{u}_{\mathrm{c}}^{\angle 0}\right)^*\right) \\
&= \underline{u}_1^{\angle 0} + \left(\underline{u}_2^{\angle 0}\right)^* = \underline{u}_1^{\angle \omega} e^{j\omega t} + \left(\underline{u}_2^{\angle \omega}\right)^* e^{-j\omega t} = \left(\underline{u}_1^{\angle \omega} + \left(\underline{u}_2^{\angle \omega}\right)^* e^{-j2\omega t}\right) e^{j\omega t}
\end{aligned} \tag{A.6}$$

Equation (A.6) shows that the negative sequence is rotating in the inverse direction of the positive sequence with the same network frequency. In the rotating positive sequence reference frame, the negative sequence will have a rotating component with double the network frequency (2ω).

The instantaneous positive and negative sequence complex powers in the three-phase system are calculated using the space vector representation as following:

$$\underline{s}_1 = \underline{u}_1^{\angle} \cdot \underline{i}_1^{*\angle} = p_1 + \mathrm{j}q_1 = u_{1\mathrm{d}}^{\angle} i_{1\mathrm{d}}^{\angle} + u_{1\mathrm{q}}^{\angle} i_{1\mathrm{q}}^{\angle} + \mathrm{j}(u_{1\mathrm{q}}^{\angle} i_{1\mathrm{d}}^{\angle} - u_{1\mathrm{d}}^{\angle} i_{1\mathrm{q}}^{\angle}) \tag{A.7}$$

$$\underline{s}_2 = \underline{u}_2^{\angle} \cdot \underline{i}_2^{*\angle} = p_2 + \mathrm{j}q_2 = u_{2\mathrm{d}}^{\angle} i_{2\mathrm{d}}^{\angle} + u_{2\mathrm{q}}^{\angle} i_{2\mathrm{q}}^{\angle} + \mathrm{j}(u_{2\mathrm{q}}^{\angle} i_{2\mathrm{d}}^{\angle} - u_{2\mathrm{d}}^{\angle} i_{2\mathrm{q}}^{\angle}) \tag{A.8}$$

A.2 Per unit system for VSC-HVDC

AC-side Quantities

The p.u. system for the main AC quantities is derived from the rated line-to-line AC voltage U_r and the rated HVDC power P_r (SI units) as following:

Phase voltage: $u = \dfrac{\sqrt{3}\hat{u}_{\mathrm{SI}}}{\sqrt{2}U_\mathrm{r}}$

Power: $p = \dfrac{P}{P_\mathrm{r}}$

Current: $i = \dfrac{I \cdot \sqrt{3}U}{S_\mathrm{r}}$

Impedance: $z = \dfrac{Z \cdot S_\mathrm{r}}{U_\mathrm{r}^2}$

Reactance: $x = \dfrac{X \cdot S_\mathrm{r}}{U_\mathrm{r}^2}$

Resistance: $r = \dfrac{R \cdot S_\mathrm{r}}{U_\mathrm{r}^2}$

Angular speed: $\omega = \dfrac{\omega_{\mathrm{SI}}}{\omega_\mathrm{r}}$

Inductance: $l = \dfrac{L \cdot \omega_\mathrm{r} S_\mathrm{r}}{U_\mathrm{r}^2}$

Capacitance: $c = \dfrac{C \cdot \omega_\mathrm{r} \cdot U_\mathrm{r}^2}{S_\mathrm{r}}$

DC-side Quantities

The p.u. system for the DC quantities is derived from the rated DC voltage of the HVDC. At

the rated AC voltage with unity modulation index, the rated DC voltage is expressed as:

$$U_{\mathrm{r,DC}} = \frac{2\sqrt{2}\cdot U_{\mathrm{r}}}{\sqrt{3}} \tag{A.9}$$

With the same rated HVDC power P_{r}, the following p.u. system is derived:

DC voltage: $u_{\mathrm{DC}} = \dfrac{U_{\mathrm{DC}}}{U_{\mathrm{r,DC}}}$

DC current: $i_{\mathrm{DC}} = \dfrac{I_{\mathrm{DC}} \cdot U_{\mathrm{r,DC}}}{P_{\mathrm{r}}}$

DC capacitance: $c_{\mathrm{DC}} = \dfrac{C_{\mathrm{DC}} \cdot \omega_{\mathrm{r}} U_{\mathrm{r,DC}}^2}{P_{\mathrm{r}}}$

DC inductance: $l_{\mathrm{DC}} = \dfrac{L_{\mathrm{DC}} \cdot P_{\mathrm{r}}}{\omega_{\mathrm{r}} U_{\mathrm{r,DC}}^2}$

DC inductance: $r_{\mathrm{DC}} = \dfrac{R_{\mathrm{DC}} \cdot P_{\mathrm{r}}}{U_{\mathrm{r,DC}}^2}$

A.3 Measurement quantities for dynamic simulations

The symbols of the measured quantities used in chapter 4 are defined as following:

p_{SEC} / q_{SEC}	Instantaneous SEC active/reactive power at the offshore PCC of the HVDC
p_{REC} / q_{REC}	Instantaneous REC active/reactive power at the onshore PCC of the HVDC
$v_{\mathrm{DC,SEC}}$	DC voltage at the offshore HVDC-SEC
$v_{\mathrm{DC,REC}}$	DC voltage at the onshore HVDC-REC
u_{G}	AC voltage at the offshore PCC of the HVDC-SEC
$u_{\mathrm{G,ref}}$	AC voltage reference at the offshore PCC of the HVDC-SEC
$\lvert u_{\mathrm{G,1}} \rvert$	Positive sequence magnitude of the offshore AC voltage
$\lvert u_{\mathrm{G,2}} \rvert$	Negative sequence magnitude of the offshore AC voltage
i_{G1P}	Offshore SEC positive sequence active current
i_{G1Q}	Offshore SEC positive sequence reactive current

A.4 Test grid for Frequency studies with Different wind power shares

The share of power generation for the test grid shown in *Figure 5-2: Test grid for frequency stability studies*

in section 5.2.3 is shown in the following three tables. It should be mentioned that for 50% wind share, thermal plant B is disconnected from the grid. At 70% wind share, the hydro plant is the only active conventional unit in the test grid.

Table A-1: Active power distribution for the scenario with 20% wind power

Power plant	Active power output	share of total generation	Reserve power
Thermal plant A	800 MW	20 %	0 MW
Thermal plant B	1200 MW	30 %	0 MW
Hydro plant	1200 MW	30 %	200 MW
Offshore WF	**800** MW	20 %	0 MW
Total	4000 MW		200 MW

Table A-2: Active power distribution for the scenario with 50% wind power

Power plant	Active power output	share of total generation	Reserve power
Thermal plant A	800 MW	20 %	0 MW
Thermal plant B	0 MW - Tripped	0 %	0 MW
Hydro plant	1200 MW	30 %	200 MW
Offshore WF	**2000** MW	50 %	0 MW
Total	4000 MW		200 MW

Table A-3: Active power distribution for the scenario with 70% wind power

Power plant	Active power output	share of total generation	Reserve power
Thermal plant A	0 MW - Tripped	0 %	0 MW
Thermal plant B	0 MW - Tripped	0 %	0 MW
Hydro plant	1200 MW	30 %	200 MW
Offshore WF	**2700** MW	70 %	0 MW
Total	4000 MW		200

A.5 VSC-HVDC components parameters

The AC and DC main components of the VSC-HVDC system are modeled in this thesis based on the HVDC light technology by ABB [11]. HVDC light modules cover the range of 100 to 1200 MW transfer capacity. Different offshore WF capacities were used in this thesis to represent different wind power shares in the grid, thus the HVDC components rating where adjusted accordingly with the help of the HVDC light modules specifications.

Table The following table summarizes the main HVDC parameters used to model a 20% of wind power share which is equal to 800 MW. The main parameters are basically based on the HVDC light M8 module data [11].

Nominal active power	800 MW
Nominal DC Voltage (pole to ground)	± 320 kV
Nominal frequency	50 Hz
HVDC cables length	100 km
Nominal AC voltage – Converter bus	400 kV
Total transmission losses	2.2 %
Total DC capacitors time constant	0.002 s
DC Cable capacitance	0.5 µF/km
DC Cable inductance	0.0012 mH/km
DC Cable resistance	0.006 Ω/km
Converter - AC line reactance	0.15 p.u.
Converter transformer uk%	12 %
Converter maximum current	1.1 p.u.
Converter maximum voltage	1.12 p.u.

A.6 HVAC Offshore Grid Parameters

The following parameters are used in the dynamic simulations conducted in chapter 4 for the test network described in section 4.1.2.

A.6.1 MVAC copper cable 3x800 mm2/36 kV

Cable Length WF-A	5 km
Cable Length WF-B	5 km
Cable nominal voltage	36 kV
Cable rated current	0.8 kA
Cable resistance	0.07 Ohm/km
Cable reactance	0.09 Ohm/km

A.6.2 HVAC copper cable 3x400 mm2/155 kV

Cable Length WF-A	5 km
Cable Length WF-B	5 km
Cable nominal voltage	155 kV
Cable rated current	0.65 kA
Cable resistance	0.07 Ohm/km
Cable reactance	0.12 Ohm/km

A.6.3 HV-MV Three-Winding Transformer D5-D5-YN

Nominal Powers and Voltages

U_{1n} = 155000 V	S_{1n} = 400 MVA
U_{2n} = 33000 V	S_{2n} = 200 MVA
U_{3n} = 33000 V	S_{3n} = 200 MVA

Relative Short-circuit Voltages uk[%]

u_{k12}[%] = 14 %	referred to S_{2n}
u_{k13}[%] = 27 %	referred to S_{3n}
u_{k23}[%] = 14 %	referred to S_{3n}

A.7 DFIG based WT Parameters

Nominal Power	P_{nom}	5 MW
Rated frequency	f_{nom}	50 Hz
Rated voltage	u_{nom}	690 V
Stator resistance	r_{S}	0.015 p.u.
Stator reactance	x_{S}	0.12 p.u.
Magnetizing reactance	x_{M}	3.5 p.u.
Rotor resistance	r_{R}	0.015 p.u.
Rotor reactance	x_{R}	0.1 p.u.
Nominal speed	n_{nom}	1500 rpm
Generator inertia	H_{G}	1.3 p.u.
Shaft stiffness	k_{sh}	450 p.u./rad
Shaft damping	d_{sh}	3.15 p.u.
MSC maximum current	$i_{\text{MSC,max}}$	1.3 p.u.
MSC maximum voltage	$u_{\text{MSC,max}}$	0.45 p.u.
LSC inductance	l_{LSC}	0.15 p.u.
LSC resistance	r_{LSC}	0.45 p.u.
LSC maximum current	$i_{\text{LSC,max}}$	0.4 p.u.
LSC maximum voltage	$u_{\text{LSC,max}}$	1.14 p.u.